SLAC-R-637

Synchrotron Radiation

Helmut Wiedemann

Stanford Linear Accelerator Center, Stanford University, Stanford, CA 94309

Work supported by Department of Energy contract DE–AC03–76SF00515.

To my family and students

Preface

This book covers the physical aspects of synchrotron radiation generation and is designed as a textbook and reference for graduate students, teachers and scientists utilizing synchrotron radiation. It is my hope that this text may help especially students and young researchers entering this exciting field to gain insight into the characteristics of synchrotron radiation.

Discovered in 1945, synchrotron radiation has become the source of photons from the infrared to hard x-rays for a large community of researchers in basic and applied sciences. This process was particularly supported by the development of electron accelerators for basic research in high energy physics. Specifically, the development of the storage ring and associated technologies resulted in the availability of high brightness photon beams far exceeding other sources.

In this text, the physics of synchrotron radiation for a variety of magnets is derived from first principles resulting in useful formulas for the practitioner. Since the characteristics and quality of synchrotron radiation are intimately connected with the accelerator and electron beam producing this radiation, a short overview of relevant accelerator physics is included.

In the first four chapters radiation phenomena in general and synchrotron radiation in particular are introduced based on more visual and basic physical concepts. Where exact formulas are required, we borrow results from rigorous derivations in Chaps. 9 and 10. This way the physics of synchrotron radiation can be discussed without extensive deviations into mathematical manipulations, which can be quite elaborate although straightforward. The consequence for the reade, of this dual approach to synchrotron radiation is that, here and there, one will find some repetitive discussions, which the author hopes will provide easier reading and continuity in the train of thought.

Chapters 5 to 8 give an overview of beam dynamics in storage rings and guidance for the optimization of a storage ring for synchrotron radiation production. The theory of synchrotron radiation is derived rigorously in Chap. 9 and that of undulator or insertion device radiation in Chap. 10. Finally, in Chap. 11 the physics of a free electron laser is discussed.

Each chapter includes a set of exercises. For those exercises which are marked with the argument (S), solutions are provided in Appendix A. In support of the practitioner utilizing synchrotron radiation most relevant for-

mulas together with useful mathematical and physical formulas and constants are compiled in Appendices B - D.

The author would like to thank the editorial staff at Springer Verlag and especially Drs. H. Lotsch and C. Ascheron for suggesting the writing of this book. The trained eyes of Dr. A. Lahee and Mrs. Dimler contributed much to minimize typographical errors and to greatly improve the overall appearance of the book. Special thanks goes to Professors J. Dorfan and K. Hodgson at Stanford University for granting a sabbatical and to Professor T. Vilaithong at the Chiang Mai University in Thailand for providing a quiet and peaceful environment during the final stages of writing this book.

Chiang Mai, *Helmut Wiedemann*
December 2, 2001

Contents

1. Charges and Fields 1
1.1 Radiation from Moving Charges 1
1.1.1 Why do Charged Particles Radiate? 2
1.1.2 Spontaneous Synchrotron Radiation 2
1.1.3 Stimulated Radiation 4
1.1.4 Electron Beam 5
1.2 Maxwell's Equations 6
1.2.1 Conversion from cgs to MKS Units 6
1.2.2 Lorentz Force 8
1.3 The Lorentz Transformations 10
1.3.1 Lorentz Transformation of Coordinates 11
1.3.2 Energy and Momentum 13
Exercises 14

2. Fundamental Processes 17
2.1 Conservation Laws and Radiation 17
2.1.1 Cherenkov Radiation 18
2.1.2 Compton Radiation 19
2.2 The Poynting Vector 20
2.3 Electromagnetic Radiation 21
2.3.1 Coulomb Regime 22
2.3.2 Radiation Regime 23
2.4 Spatial and Spectral Properties of Radiation 26
Exercises 28

3. Overview of Synchrotron Radiation 31
3.1 Radiation Power 32
3.2 Spectrum 36
3.3 Spatial Photon Distribution 41
3.4 Fraunhofer Diffraction 42
3.5 Spatial Coherence 45
3.6 Temporal Coherence 47
3.7 Spectral Brightness 50
3.7.1 Matching 51

Exercises . . . 53

4. Radiation Sources . . . 55
4.1 Bending Magnet Radiation . . . 55
4.2 Superbends . . . 56
4.3 Wavelength Shifter . . . 57
4.4 Wiggler Magnet Radiation . . . 58
4.5 Undulator Radiation . . . 62
4.6 Back Scattered Photons . . . 68
4.6.1 Photon Flux . . . 68
Exercises . . . 70

5. Accelerator Physics . . . 73
Exercises . . . 76

6. Particle Beam Optics . . . 77
6.1 Deflection in Bending Magnets . . . 77
6.2 Beam Focusing . . . 79
6.2.1 Principle of Focusing . . . 80
6.2.2 Quadrupol Magnet . . . 80
6.3 Equation of Motion . . . 82
6.3.1 Solutions of the Equations of Motion . . . 84
6.3.2 Matrix Formalism . . . 84
6.3.3 FODO Lattice . . . 85
6.4 Betatron Function . . . 86
6.4.1 Betatron Phase and Tune . . . 87
6.4.2 Beam Envelope . . . 88
6.5 Phase Ellipse . . . 88
6.6 Beam Emittance . . . 89
6.6.1 Variation of the Phase Ellipse . . . 90
6.6.2 Transformation of Phase Ellipse . . . 91
6.7 Dispersion Function . . . 92
6.8 Periodic Lattice Functions . . . 93
6.8.1 Periodic Betatron Function in a FODO Lattice . . . 93
6.8.2 Periodic Dispersion or η-Function . . . 95
6.8.3 Beam Size . . . 95
Exercises . . . 96

7. Radiation Effects . . . 99
7.1 Synchrotron Oscillations . . . 99
7.1.1 Longitudinal Phase Space Motion . . . 103
7.2 Damping . . . 104
7.3 Quantum Effects . . . 105
7.4 Equilibrium Beam Parameters . . . 106
7.4.1 Equilibrium Energy Spread . . . 106

7.4.2 Bunch Length . . . 107
7.4.3 Horizontal Beam Emittance . . . 108
7.4.4 Vertical Beam Emittance . . . 109
7.5 Transverse Beam Parameters . . . 110
7.5.1 Beam Sizes . . . 111
7.5.2 Beam Divergence . . . 112
7.6 Beam Emittance and Wiggler Magnets . . . 112
7.6.1 Damping Wigglers . . . 115
7.6.2 Variation of the Damping Distribution . . . 117
7.6.3 Can we Eliminate the Beam Energy Spread? . . . 119
7.7 Photon Source Parameters . . . 121
Exercises . . . 122

8. Storage Ring Design as a Synchrotron Light Source . . . 125
8.1 Storage Ring Lattices . . . 126
8.1.1 FODO Lattice . . . 126
8.2 Optimization of a Storage Ring Lattice . . . 127
8.2.1 Minimum Beam Emittance . . . 128
8.2.2 The Double Bend Achromat (dba) Lattice . . . 131
8.2.3 The Triple Bend Achromat (tba) Lattice . . . 134
8.2.4 Limiting Effects . . . 134

9. Theory of Synchrotron Radiation . . . 137
9.1 Radiation Field . . . 137
9.2 Total Radiation Power and Energy Loss . . . 144
9.2.1 Transition Radiation . . . 144
9.2.2 Synchrotron Radiation Power . . . 147
9.3 Radiation Lobes . . . 150
9.4 Synchrotron Radiation Spectrum . . . 155
9.5 Radiation Field in the Frequency Domain . . . 155
9.5.1 Spectral Distribution in Space and Polarization . . . 160
9.5.2 Spectral and Spatial Photon Flux . . . 163
9.5.3 Harmonic Representation . . . 165
9.6 Spatial Radiation Power Distribution . . . 165
9.6.1 Asymptotic Solutions . . . 167
9.7 Angle-Integrated Spectrum . . . 168
9.7.1 Statistical Radiation Parameters . . . 174
Exercises . . . 176

10. Insertion Device Radiation . . . 177
10.1 Periodic Magnetic Field . . . 178
10.1.1 Periodic Field Configuration . . . 179
10.1.2 Particle Dynamics in a Periodic Field Magnet . . . 182
10.1.3 Focusing in a Wiggler Magnet . . . 183

10.1.4 Hard Edge Wiggler Model ... 186
10.2 Undulator Radiation ... 187
10.2.1 Fundamental Wavelength ... 188
10.2.2 Radiation Power ... 189
10.2.3 Spatial and Spectral Distribution ... 190
10.2.4 Line Spectrum ... 203
10.2.5 Spectral Undulator Brightness ... 207
10.3 Elliptical Polarization ... 208
10.3.1 Elliptical Polarization from Bending Magnet Radiation 208
10.3.2 Elliptical Polarization from Periodic Insertion Devices . 211
Exercises ... 214

11. Free Electron Lasers ... 217
11.1 Small Gain FEL ... 220
11.1.1 Energy Transfer ... 220
11.1.2 Equation of Motion ... 222
11.1.3 FEL-Gain ... 225
Exercises ... 230

A. Solutions to Exercises ... 231

B. Mathematical Constants and Formulas ... 243
B.1 Constants ... 243
B.2 Series Expansions ... 243
B.3 Multiple Vector Products ... 244
B.4 Differential Vector Expressions ... 244
B.5 Theorems ... 245
B.6 Coordinate Systems ... 245
B.7 Gaussian Distribution ... 247
B.8 Miscelaneous Mathematical Formulas ... 248

C. Physical Formulas and Parameters ... 251
C.1 Constants ... 251
C.2 Unit Conversion ... 252
C.3 Relations of Fundamental Parameters ... 253
C.4 Energy Conversion ... 253
C.5 Maxwell's Equations ... 253
C.5.1 Lorentz Force ... 253
C.6 Wave and Field Equations ... 254
C.7 Relativistic Relations ... 254
C.8 Four-Vectors ... 255

D. Electromagnetic Radiation 257
D.1 Radiation Constants 257
D.2 Bending Magnet Radiation 258
D.3 Periodic Insertion Devices 261
D.3.1 Insertion Device Parameter 261
D.3.2 Field Scaling for Hybrid Wiggler Magnets 262
D.3.3 Particle Beam Parameter 262
D.4 Undulator Radiation 263
D.5 Photon Beam Brightness 265
D.5.1 Effective Source Parameter 265

References 267

Index 269

1. Charges and Fields

Ever since J.C. Maxwell formulated his unifying electromagnetic theory in 1873, the phenomenon of electromagnetic radiation has fascinated the minds of theorists as well as experimentalists. The idea of displacement currents was as radical as it was important to describe electromagnetic waves. It was only fourteen years later when G. Hertz in 1887 succeeded to generate, emit and receive again electromagnetic waves, thus, proving experimentally the existence of such waves as predicted by Maxwell's equations. The sources of the radiation are oscillating electric charges and currents in a system of metallic wires. In this text, we discuss the generation of electromagnetic radiation emitted by free electrons from first principles involving energy and momentum conservation as well as Maxwell's equations.

1.1 Radiation from Moving Charges

Analytical formulation of the emission of electromagnetic radiation posed a considerable challenge. Due to the finite speed of light one cannot make a snapshot to correlate the radiation field at the observer with the position of radiating charges. Rather, the radiation field depends on the position of the radiating charges some time earlier, at the retarded time, when the radiation was emitted. Already 1867 L. Lorenz included this situation into his formulation of the theory of electromagnetic fields and introduced the concept of retarded potentials. He did, however, not offer a solution to the retarded potentials of a point charge. Liénard [1] in 1898 and independently in 1900 Wiechert [2] derived for the first time expressions for retarded potentials of point charges like electrons. These potentials are now called the Liénard-Wiechert potentials relating the scalar and vector potential of electromagnetic fields at the observation point to the location of the emitting charges and currents at the time of emission. Using these potentials, Liénard was able to calculate the energy lost by electrons while circulating in a homogenous magnetic field.

In 1907 [3, 4] and 1912 [5] Schott formulated and published his classical theory of radiation from an orbiting electron. He was primarily interested in the spectral distribution of radiation and hoped to find an explanation for atomic radiation spectra. Verifying Liénard's conclusion on the energy

loss, he derived the angular and spectral distribution and the polarization of radiation. Since this classical approach to explain atomic spectra was destined to fail, his paper was forgotten and only forty years later were many of his findings rediscovered.

1.1.1 Why do Charged Particles Radiate?

Before we dive into the theory of electromagnetic radiation in more detail we may first ask ourselves why do charged particles radiate at all? Emission of electromagnetic radiation from charged particle beams (microwaves or synchrotron radiation) is a direct consequence of the finite velocity of light. A charged particle in uniform motion through vacuum is the source of electric field lines emanating from the charge radially out to infinity. While the charged particle is at rest or moving uniformly these field lines also are at rest or in uniform motion together with the particle. Now, we consider a particle being suddenly accelerated for a short time. That means the field lines should also be accelerated. The fact that the particle has been accelerated is, however, still known only within the event horizon in a limited area close to the particle. The signal of acceleration travels away from the source (particle) only at the finite speed of light. Field lines close to the charged particle are directed radially toward the particle, but far away, the field lines still point to the location where the particle would be had it not been accelerated. Somewhere between those two regimes the field lines are distorted and it is this distortion travelling away from the particle at the speed of light what we call electromagnetic radiation. The magnitude of these field distortions is proportional to the acceleration.

In a linear accelerator, for example, electrons are accelerated along the linac axis and therefore radiate. The degree of actual acceleration, however, is very low because electrons in a linear accelerator travel close to the velocity of light. The closer the particle velocity is to the velocity of light the smaller is the actual acceleration gained from a given force, and the radiation intensity is very small. In a circular accelerator like a synchrotron , on the other hand, particles are deflected transversely to their direction of motion by magnetic fields. Orthogonal acceleration or the rate of change in transverse velocity is very large because the transverse particle velocity can increase from zero to very large values in a very short time while passing through the magnetic field. Consequently, the emitted radiation intensity is very large. Synchrotron radiation sources come therefore generally in form of circular synchrotrons. Linear accelerators can be the source of intense synchrotron radiation in conjunction with a transversely deflecting magnet.

1.1.2 Spontaneous Synchrotron Radiation

Charged particles do not radiate while in uniform motion, but during acceleration a rearrangement of its electric fields is required and this field per-

turbation, traveling away from the charge at the velocity of light, is what we observe as electromagnetic radiation. Free accelerated electrons radiate similarly to those in a radio antenna, although now the source (antenna) is moving. Radiation from a fast moving particle source appears to the observer in the laboratory as being all emitted in the general direction of motion of the particle. This forward collimation is particularly effective for highly relativistic electrons where most of the radiation is concentrated into a small cone around the forward direction with an opening angle of $1/\gamma$, typically 0.1 to 1 mrad, where γ is the particle energy in units of its rest mass.

Radiation can be produced by magnetic deflection in a variety of ways. Whether it be a single kick-like deflection or a periodic right-left deflection, the radiation characteristics reflect the particular mode of deflection. Specific radiation characteristics can be gained through specific modes of deflections. Here, we will only shortly address the main processes of radiation generation and come back later for a much more detailled discussion of the physical dynamics.

In an *undulator* the electron beam is periodically deflected transversely to its direction of motion by weak sinusoidally varying magnetic fields, generating periodic perturbations of the electric field lines. A receiving electric field detector recognizes a periodic variation of the transverse electromagnetic field components and interprets this as quasi monochromatic radiation. In everyday life periodic acceleration of electrons occurs in radio and TV antennas and we may receive these periodic field perturbations with a radio or TV receiver tuned to the frequency of the periodic electron motion in the emitting antenna. The fact that we consider relativistic electrons is not fundamental, but we restrict ourselves in this text to high energy electrons only.

To the particle the wavelength of the emitted radiation is equal to the undulator period length (λ_p) divided by γ due to relativistic Lorentz contraction. In a stationary laboratory system, this wavelength appears to the observer further reduced by another factor 2γ due to the Doppler effect. The undulator period length of the order of centimeters is thus reduced by a factor γ^2 (10^6–10^8) to yield short wavelength radiation in the VUV and x-ray regime. The spectral resolution of the radiation is proportional to the number of undulator periods N_p and its wavelength can be shifted by varying the magnetic field. Most radiation is emitted within the small angle of $(\gamma\sqrt{N_\mathrm{p}})^{-1}$.

Increasing the magnetic field strength causes the pure sinusoidal transverse motion of electrons in an undulator to become distorted due to relativistic effects generating higher harmonic perturbations of the electron trajectory. Consequently, the monochromatic undulator spectrum exhibits higher harmonics and changes into a line spectrum. For very strong fields, many harmonics are generated which eventually merge into a continuous spectrum from IR to hard x-rays. In this extreme, we call the source magnet a *wig-*

gler magnet. The spectral intensity varies little over a broad wavelength range and drops off exponentially at photon energies higher than the critical photon energy, $\varepsilon_{\rm crit} \propto B\gamma^2$. Changing the magnetic field, one may vary the critical photon energy to suit experimental requirements. Compared to bending magnet radiation, wiggler radiation is enhanced by the number of magnet poles $N_{\rm p}$ and is well collimated within an angle of $1/\gamma$ to say $10/\gamma$, or a few mrad.

A *bending magnet* is technically the most simple radiation source**.** Radiation is emitted tangentially to the orbit similar to a search light while well collimated in the non-deflecting, or vertical plane. The observer at the experimental station sees radiation from only a small fraction of the circular path which can be described as a piece of a distorted sinusoidal motion. The radiation spectrum is therefore similar to that of a wiggler magnet while the intensity is due to only one pole. Because bending magnets define the geometry of the electron beam transport system or accelerator, it is not possible to freely choose the field strength and the critical photon energy is therefore fixed. Sometimes, specially in lower energy storage rings, it is desirable to extend the radiation spectrum to higher photon energies into the x-ray regime. This can be accomplished by replacing one or more conventional bending magnet with a superconducting magnet, or superbends, at much higher field strength. To preserve the ring geometry the length of these superbends must be chosen such that the deflection angle is the same as it was for the conventional magnet that has been replaced. Again, superbends are part of the ring geometry and therefore the field cannot be changed.

A more flexible version of a radiation hardening magnet is the wavelength shifter. This is a magnet which consists of a high field central pole and two weaker outside poles to compensate the deflection by the central pole. The total deflection angle is zero and therefore the field strength can be chosen freely to adjust the critical photon energy. It's design is mostly based on superconducting magnet technology, particularly in low energy accelerators, to extend (shift) the critical photon energy available from bending magnets to higher values.

A variety of more complicated magnetic field arrangements have been developed to primarily generate *circularly* or *elliptically polarized radiation.* In such magnets horizontal as well as vertical magnetic fields are sequentially employed to deflect electrons into some sort of helical motion giving raise to the desired polarization effect.

1.1.3 Stimulated Radiation

The well defined time structure and frequency of undulator radiation can be used to stimulate the emission of even more radiation. In an *optical klystron* [6] coherent radiation with a wavelength equal to the fundamental undulator wavelength enters an undulator together with the electron beam. Since the electron bunch length is much longer than the radiation wavelength, some electrons loose energy to the radiation field and some electrons gain energy

from the radiation field while interacting with the radiation field. This energy modulation can be transformed into a density modulation by passing the modulated electron beam through a dispersive section. This section consists of deflecting magnetic fields arranged in such a way that the total path length through the dispersive section depends on the electron energy. The periodic energy modulation of the electron bunch then converts into a periodic density modulation. Now we have microbunches at a distance of the undulator radiation wavelength. This microbunched beam travels through a second undulator where again particles can loose or gain energy from the radiation field. Due to the microbunching, however, all particles are concentrated at phases where there is only energy transfer from the particle to the radiation field, thus providing a high gain of radiation intensity.

In a more efficient variation of this principle, radiation emitted by electrons passing through an undulator is recycled by optical mirrors in such a way that it passes through the same undulator again together with another electron bunch. The external field stimulates more emission of radiation from the electrons, and is again is recycled to stimulate a subsequent electron bunch until there are no more bunches in the electron pulse. Generating from a linear accelerator a train of thousands of electron bunches one can generate a large number of interactions, leading to an exponential grows of electromagnetic radiation. Such a devise is called a *free electron laser, FEL.*

1.1.4 Electron Beam

In this text we consider radiation from relativistic electron beams. Such beams can be generated efficiently by acceleration in microwave fields. The oscillatory nature of microwaves makes it impossible to produce a uniform stream of particles, and the electron beam is modulated into bunches at the distance of the microwave wavelength. Typically the bunch length is a few percent of the wavelength. The circumference of the storage ring must be an integer multiple, the harmonic number, of the rf-wavelength. The rf-system actually provides potential wells, rf-buckets, which rotate around the ring. These buckets may or may not be filled with electrons and those electrons contained in a bucket are said to form an electron bunch. With special equipment in the injector it is possible to store any arbitrary pattern of electron bunches consistent with the equidistant distribution of the finite number of buckets equal to the harmonic number. Specifically, it is possible to operate the storage ring with all buckets filled or with just a single bunch or only a few bunches. The bunched nature of the electron beam and the fact that these bunches circulate in a storage ring determines the time structure and spectrum of the emitted radiation. Typically, the bunch length in storage rings is 30–100 ps at a distance of 2–3 ns depending on the rf-frequency.

During the storage time of the particle beam, the electrons radiate and it is this radiation that is extracted and used in experiments of basic and applied research. Considering, for example, only one bunch rotating in the

storage ring, the experimenter would observe a light flash at a frequency equal to the revolution frequency $f_{\rm rev}$. Because of the extremely short duration of the light flash many harmonics of the revolution frequency appear in the light spectrum. At the low frequency end of this spectrum, however, no radiation can be emitted for wavelength longer than about the dimensions of the metallic vacuum chamber surrounding the electron beam. For long wavelengths the metallic boundary conditions for electromagnetic fields cannot be met prohibiting the emission of radiation. Practically, useful radiation is observed from storage rings only for wavelengths below the microwave regime, or for $\lambda \lesssim 1$ mm.

1.2 Maxwell's Equations

Radiation theory deals largely with the description of charged particle dynamics in the presence of external electromagnetic fields or of fields generated by other charged particles. We use Maxwell's equations in a vacuum or material environment with uniform permittivity ϵ and permeability μ to describe these fields. Furthermore, the Lorentz force provides the tool to formulate particle dynamics under the influence of these electromagnetic fields[2].

$$\boldsymbol{\nabla} \boldsymbol{E} = \frac{4\pi}{[4\pi\epsilon_0]\ \epsilon_{\rm r}}\,\rho\,, \tag{1.1}$$

$$\boldsymbol{\nabla} \boldsymbol{B} = 0\,, \tag{1.2}$$

Faraday's law :

$$\boldsymbol{\nabla} \times \boldsymbol{E} = -\frac{[c]}{c}\frac{\partial \boldsymbol{B}}{\partial t}\,, \tag{1.3}$$

Ampère's law :

$$\boldsymbol{\nabla} \times \boldsymbol{B} = \frac{4\pi}{c}\left[\frac{c}{4\pi}\right][\mu_0]\mu_{\rm r}\,\rho\boldsymbol{v} + [c\epsilon_0\mu_0]\frac{\epsilon_{\rm r}\,\mu_{\rm r}}{c}\frac{\partial \boldsymbol{E}}{\partial t}\,. \tag{1.4}$$

Here, ρ is the charge density and $\boldsymbol{v}$ the velocity of the charged particle. In general, we are interested in particle dynamics in a material free environment and set therefore $\epsilon_{\rm r} = 1$ and $\mu_{\rm r} = 1$. For specific discussions we do, however, need to calculate fields in a material filled environment in which case we come back to this more general form of Maxwell's equations.

1.2.1 Conversion from cgs to MKS Units

In related literature we are faced with different choices of a system of units, mostly the cgs-or the MKS-system of units. While the cgs-system provides

[2] In this text we formulate equations both in the MKS-system (include factors in square brackets) and the cgs-system (ignore square brackets).

simple formulation of physical laws without the use of artificial factors, we cannot escape reality where we quantify and measure our results. In this text, we try to avoid differences in the formulation of physical laws between these systems whenever possible. Where this is not possible we include into the formulas factors in square brackets like $[4\pi\epsilon_0]$ which are to be used in case of MKS-units and to be ignored in case of cgs-units.

Generally, we use MKS-units to quote numerical results or expressing practical formulas. Sometimes, however, we find it necessary to perform numerical calculations with parameters given in different units or to compare with results given in another system of units. For such cases some helpful numerical conversions are compiled in Table 1.1.

Table 1.1. Numerical conversion factors

quantity	label	replace cgs units	by SI units
voltage	U	1 esu	300 V
electric field	E	1 esu	$3\ 10^4$ V/cm
current	I	1 esu	$10\ c = 2.9979\ 10^9$ A
charge	q	1 esu	$(10c)^{-1} = 3.3356\ 10^{-10}$ C
resistance	R	1 s/cm	$8.9876\ 10^{11}\ \Omega$
capacitance	C	1 cm	$\frac{1}{8.9876} 10^{-11}$ F
inductance	L	1 cm	$1\ 10^9$ Hy
magnetic induction	B	1 Gauss	$3\ 10^{-4}$ Tesla
magnetic field	H	1 Oersted	$\frac{1000}{4\pi} = 79.577$ A/m
force	f	1 dyn	10^{-5} N
energy	E	1 erg	10^{-7} J

Analogous conversion factors can be derived for electromagnetic quantities in formulas. Table 1.2 includes some of the most frequently used conversions from cgs to MKS-units which were used in this text to define the square bracket factors.

The dielectric constant or permittivity of free space is

$$\epsilon_0 = \frac{10^7}{4\pi c^2} \frac{\mathrm{C}}{\mathrm{V\ m}} = 8.854187817 \times 10^{-12} \frac{\mathrm{C}}{\mathrm{V\ m}}\,, \tag{1.5}$$

and the magnetic permeability

$$\mu_0 = 4\pi \times 10^{-7} \frac{\mathrm{V\ s}}{\mathrm{A\ m}} = 1.2566370614 \times 10^{-6} \frac{\mathrm{V\ s}}{\mathrm{A\ m}}\,. \tag{1.6}$$

Both constants are related to the speed of light v by

Table 1.2. Equation conversion factors

variable	replace cgs variable	by SI Variable
potential,voltage	$V_{\rm cgs}$	$\sqrt{4\pi\epsilon_0}\,V_{\rm MKS}$
electric field	$E_{\rm cgs}$	$\sqrt{4\pi\epsilon_0}\,E_{\rm MKS}$
current, current density	$I_{cgs}, j_{\rm cgs}$	$\frac{1}{\sqrt{4\pi\epsilon_0}}\ I_{\rm MKS}, j_{\rm MKS}$
charge, charge density	q, ρ	$\frac{1}{\sqrt{4\pi\epsilon_0}}\ q_{\rm MKS}, \rho_{\rm MKS}$
resistance	$R_{\rm cgs}$	$\sqrt{4\pi\epsilon_0}\,R_{\rm MKS}$
capacitance	$C_{\rm cgs}$	$\frac{1}{\sqrt{4\pi\epsilon_0}}\ C_{\rm MKS}$
inductance	$L_{\rm cgs}$	$\sqrt{4\pi\epsilon_0}\,L_{\rm MKS}$
magnetic induction	$B_{\rm cgs}$	$\sqrt{\frac{4\pi}{\mu_0}}\,B_{\rm MKS}$

$$\epsilon_0\epsilon_{\rm r}\mu_0\mu_{\rm r}\,v^2 = 1\,, \tag{1.7}$$

or in vacuum by

$$\epsilon_0\mu_0\,c^2 = 1\,, \tag{1.8}$$

1.2.2 Lorentz Force

Whatever the interaction of charged particles with electromagnetic fields and the reference system may be, in accelerator physics we depend on the invariance of the Lorentz force equations under coordinate transformations. All acceleration and beam guidance in accelerator physics will be derived from the Lorentz force which quantifies the force of an electric $\boldsymbol{E}$ and magnetic field $\boldsymbol{B}$ on a particle with charge q by

$$\boldsymbol{F} = q\,\boldsymbol{E} + q\,\frac{[c]}{c}\,(\boldsymbol{v}\,\times\boldsymbol{B})\,. \tag{1.9}$$

Throughout this text, we use particles with one unit of electrical charge e like electrons and protons unless otherwise noted. In case of multiply charged ions the single charge e must be replaced by eZ where Z is the charge multiplicity of the ion. Both components of the Lorentz force are used in accelerator physics where the force due to the electrical field is mostly used to actually increase the particle energy while magnetic fields are mostly used to guide particle beams along desired beam transport lines. This separation of functions, however, is not exclusive as the example of the betatron accelerator shows where particles are accelerated by generating a time dependent magnetic field. Similarly, electrical fields are used in specific cases to guide or separate particle beams.

Integrating the Lorentz force over the interaction time of a particle with the field we get the change in its momentum,

$$\Delta \boldsymbol{p} = \int \boldsymbol{F}\,\mathrm{d}t\,. \tag{1.10}$$

On the other hand, if the Lorentz force is integrated with respect to the path length we get the change in kinetic energy E_{kin} of the particle

$$\Delta E_{\mathrm{kin}} = \int \boldsymbol{F}\,\mathrm{d}\boldsymbol{s}\,. \tag{1.11}$$

Comparing the last two equations we find with $\mathrm{d}\boldsymbol{s} = \boldsymbol{v}\mathrm{d}t$ the relation between the momentum and kinetic energy differentials

$$c\boldsymbol{\beta}\,\mathrm{d}\boldsymbol{p} = \mathrm{d}E_{\mathrm{kin}}\,. \tag{1.12}$$

With the Lorentz force equation (1.9) and $\mathrm{d}\,\boldsymbol{s} = \boldsymbol{v}\mathrm{d}t$ in the second integral of (1.11) we get

$$\Delta E_{\mathrm{kin}} = e\int \boldsymbol{E}\,\mathrm{d}\boldsymbol{s} + e\frac{[c]}{c}\int (\boldsymbol{v}\times\boldsymbol{B})\,\boldsymbol{v}\,\mathrm{d}t\,. \tag{1.13}$$

The kinetic energy of a free particle increases whenever a finite electric field $\boldsymbol{E}$ component along the beam axis exists. This acceleration is independent of the particle velocity and acts even on a particle at rest $\boldsymbol{v} = 0$. Transverse field components do not affect the particle's kinetic energy, but do change its momentum vector (1.10). The second component of the Lorentz force, in contrast, depends on the particle velocity and is directed normal to the direction of propagation and normal to the magnetic field direction. The kinetic energy cannot be changed by the presence of magnetic fields since the scalar product $(\boldsymbol{v}\times\boldsymbol{B})\,\boldsymbol{v} = 0$ vanishes. The magnetic field causes only a change in the transverse momentum (1.10) or a deflection of the particle trajectory.

The Lorentz force is used to derive the equation of motion of charged particles in the presence of electromagnetic fields

$$\frac{\mathrm{d}}{\mathrm{d}t}\boldsymbol{p} = \frac{\mathrm{d}}{\mathrm{d}t}(\gamma m\,\boldsymbol{v}) = e\,Z\,\boldsymbol{E} + e\,Z\frac{[c]}{c}\,(\boldsymbol{v}\times\boldsymbol{B})\,, \tag{1.14}$$

noting that for ion accelerators the particle charge e must be replaced by eZ. The fields can be derived from electrical and magnetic potentials

$$\boldsymbol{E} = -\frac{[c]}{c}\frac{\partial \boldsymbol{A}}{\partial t} - \nabla\phi\,, \tag{1.15}$$

$$\boldsymbol{B} = \boldsymbol{\nabla}\times\boldsymbol{A}\,, \tag{1.16}$$

where ϕ is the scalar potential and $\boldsymbol{A}$ the vector potential. The particle momentum $\boldsymbol{p} = \gamma m\boldsymbol{v}$ and it's time derivative

$$\frac{\mathrm{d}\boldsymbol{p}}{\mathrm{d}t} = m\,\gamma\frac{\mathrm{d}\boldsymbol{v}}{\mathrm{d}t} + m\,\boldsymbol{v}\frac{\mathrm{d}\gamma}{\mathrm{d}t}\,. \tag{1.17}$$

With

$$\frac{\mathrm{d}\gamma}{\mathrm{d}t} = \frac{\mathrm{d}}{\mathrm{d}\beta}\frac{1}{\sqrt{1-\beta^2}}\frac{\mathrm{d}\beta}{\mathrm{d}t} = \gamma^3\frac{\beta}{c}\frac{\mathrm{d}v}{\mathrm{d}t}$$

we get the equation of motion

$$\boldsymbol{F} = \frac{\mathrm{d}\boldsymbol{p}}{\mathrm{d}t} = m\left(\gamma\frac{\mathrm{d}\boldsymbol{v}}{\mathrm{d}t} + \gamma^3\frac{\beta}{c}\frac{\mathrm{d}v}{\mathrm{d}t}\boldsymbol{v}\right). \tag{1.18}$$

For a force parallel to the particle propagation $\boldsymbol{v}$ we have $\dot{v}\boldsymbol{v} = \dot{\boldsymbol{v}}v$ and

$$\frac{\mathrm{d}\boldsymbol{p}_\parallel}{\mathrm{d}t} = m\gamma\left(1+\gamma^2\beta\frac{v}{c}\right)\frac{\mathrm{d}\boldsymbol{v}_\parallel}{\mathrm{d}t} = m\gamma^3\frac{\mathrm{d}\boldsymbol{v}_\parallel}{\mathrm{d}t}. \tag{1.19}$$

On the other hand, if the force is directed normal to the particle propagation we have $\dot{v} = 0$ and (1.18) reduces to

$$\frac{\mathrm{d}\boldsymbol{p}_\perp}{\mathrm{d}t} = m\gamma\frac{\mathrm{d}\boldsymbol{v}_\perp}{\mathrm{d}t}. \tag{1.20}$$

It is evident from these results how differently the dynamics of particle motion is affected by the direction of the Lorentz force. Specifically, the dynamics of highly relativistic particles under the influence of electromagnetic fields depends greatly on the direction of the force with respect to the direction of particle propagation. The difference between parallel and perpendicular acceleration has a great impact on the design of electron accelerators. The ultimate achievable electron energy depends greatly on the type of accelerator due to the emission of synchrotron radiation. This limitation is most severe for electrons in circular accelerators where the magnetic forces act perpendicular to the propagation compared to the acceleration in linear accelerators where the accelerating fields are parallel to the particle propagation. This argument is also true for protons or for that matter, any charged particle, although the much larger mass renders the amount of synchrotron radiation negligible except for extremely high energies.

1.3 The Lorentz Transformations

Beam dynamics is expressed in a fixed laboratory system of coordinates but some specific problems are better discussed in the moving coordinate system of a single particle or of the center of charge for a collection of particles. We use therefore frequently transformations of coordinates as well as fields between the laboratory frame of reference and the particle rest frame or some other suitable moving reference frame.

1.3.1 Lorentz Transformation of Coordinates

To define the transformation of coordinates we consider two reference systems of which one is fixed to the laboratory $\mathcal{L}$, and the other $\mathcal{L}^*$ is attached to the particle moving with respect to $\mathcal{L}$. For simplicity, we assume that the the particle and with it the system $\mathcal{L}^*$ is moving with velocity v_z along the positive z-axis of system $\mathcal{L}$. Transformation between the two reference systems is effected through a Lorentz transformation

$$\begin{aligned} x^* &= x\,, \\ y^* &= y\,, \\ z^* &= \frac{z-\beta_z\,ct}{\sqrt{1-\beta_z^2}} = \gamma\,(z-\beta_z\,ct)\;, \\ ct^* &= \frac{ct-\beta_z\,z}{\sqrt{1-\beta_z^2}} = \gamma\,(ct-\beta_z\,z)\;, \end{aligned} \tag{1.21}$$

where $\beta_z = v_z/c$, γ is the total particle energy E in units of the particle rest energy mc^2

$$\gamma = \frac{E}{m\,c^2} = \frac{1}{\sqrt{1-\beta_z^2}}\,, \tag{1.22}$$

and quantities designated with * are measured in the moving system $\mathcal{L}^*$. These Lorentz transformations can be expressed in matrix formulation by

$$\begin{pmatrix} x^* \\ y^* \\ z^* \\ ct^* \end{pmatrix} = \begin{pmatrix} 1\,0 & 0 & 0 \\ 0\,1 & 0 & 0 \\ 0\,0 & \gamma & -\beta\gamma \\ 0\,0 & -\beta\gamma & \gamma \end{pmatrix} \begin{pmatrix} x \\ y \\ z \\ ct \end{pmatrix}\,. \tag{1.23}$$

Characteristic for relativistic mechanics is the Lorentz contraction and time dilatation, both of which become significant in the description of particle dynamics. To describe the Lorentz contraction, we consider a rod at rest in $\mathcal{L}$ along the z-coordinate with the length $\Delta z = z_2 - z_1$. In the system $\mathcal{L}^*$ this rod appears to have the length $\Delta z^* = z_2^* - z_1^*$ related to the length in the $\mathcal{L}-$system by

$$\Delta z \;=\; \gamma\,(z_2^* + v_z t^*) - \gamma\,(z_1^* + v_z t^*) \;=\; \gamma\,\Delta z^*$$

or

$$\Delta z \;=\; \gamma\,\Delta z^*\,. \tag{1.24}$$

The rod appears shorter in the moving particle system by the factor γ and is longest in it's rest system.

Because of the Lorentz contraction, the volume of a body at rest in the system $\mathcal{L}$ appears also reduced in the moving system $\mathcal{L}^*$ and we have for the volume of a body in three dimensional space

$$V = \gamma V^* . \tag{1.25}$$

Only one dimension of this body is Lorentz contracted and therefore the volume scales only linearly with γ. As a consequence, the charge density ρ of a particle bunch with the volume V is lower in the laboratory system $\mathcal{L}$ compared to the density in the system $\mathcal{L}^*$ moving with this bunch and becomes

$$\rho = \frac{\rho^*}{\gamma} . \tag{1.26}$$

Similarly, we may derive the time dilatation or the elapsed time between two events occurring at the same point in both coordinate systems. From the Lorentz transformations we get with $z_2^* = z_1^*$

$$\Delta t = t_2 - t_1 = \gamma \left(t_2^* + \frac{\beta_z z_2^*}{c} \right) - \gamma \left(t_1^* + \frac{\beta_z z_1^*}{c} \right)$$

or

$$\Delta t = \gamma \Delta t^* . \tag{1.27}$$

For a particle at rest in the moving system $\mathcal{L}^*$ the time t^* varies slower than the time t in the laboratory system. This is the mathematical expression for the famous *twin paradox* where one of the twins moving in a space capsule at relativistic speed would age more slowly than the other twin who remains behind. This phenomenon becomes reality for unstable particles. For example, high-energy pion mesons, observed in the laboratory system, have a longer lifetime by the factor γ compared to low-energy pions with $\gamma = 1$. As a consequence we are able to transport high-energy pion beams a longer distance than low energy pions before they decay. This effect is of great importance, for example, where a pion beam is used for cancer therapy and must be transported from the high radiation environment of the source to a safe location behind shielding walls where the patient can be placed.

Lorentz transformation of fields. Electromagnetic fields and the interaction of charged particles with these fields play an important role in accelerator physics. We find it often useful to express the fields in either the laboratory system or the particle system. Transformation of the fields from one to the other system is determined by the Lorentz transformation of electromagnetic fields. We assume again the coordinate system $\mathcal{L}^*$ to move with the particle at a velocity v_z along the positive z-axis with respect to a right-handed (x, y, s) reference frame $\mathcal{L}$. The electromagnetic fields in this moving reference frame

can be expressed in terms of the fields in the laboratory frame of reference $\mathcal{L}$:

$$\begin{pmatrix} E_x^* \\ E_y^* \\ E_z^* \\ [c]B_x^* \\ [c]B_y^* \\ [c]B_z^* \end{pmatrix} = \begin{pmatrix} \gamma & 0 & 0 & 0 & -\beta_z\gamma & 0 \\ 0 & \gamma & 0 & \beta_z\gamma & 0 & 0 \\ 0 & 0 & 1 & 0 & 0 & 0 \\ 0 & \beta_z\gamma & 0 & \gamma & 0 & 0 \\ -\beta_z\gamma & 0 & 0 & 0 & \gamma & 0 \\ 0 & 0 & 0 & 0 & 0 & 1 \end{pmatrix} \begin{pmatrix} E_x \\ E_y \\ E_z \\ [c]B_x \\ [c]B_y \\ [c]B_z \end{pmatrix} . \tag{1.28}$$

These transformations exhibit interesting features for accelerator physics, where we often use magnetic or electrical fields, which are pure magnetic or pure electric fields when viewed in the laboratory system. For relativistic particles, however, these pure fields become a combination of electric and magnetic fields.

1.3.2 Energy and Momentum

The total energy of a particle is given by

$$E \;=\; \gamma\, E_0 \;=\; \gamma\, mc^2\,, \tag{1.29}$$

where $E_0 = mc^2$ is the rest energy of the particle. The kinetic energy is defined as the total energy minus the rest energy

$$E_{\rm kin} \;=\; E - E_0 \;=\; (\gamma - 1)\, mc^2\,. \tag{1.30}$$

In discussions of energy gain through acceleration we consider only energy differences and need therefore not to distinguish between total and kinetic energy. The particle momentum finally is defined by

$$c^2p^2 \;=\; E^2 - E_0^2 \tag{1.31}$$

or

$$cp = \sqrt{E^2 - E_0^2} = m\,c^2\,\sqrt{\gamma^2 - 1} = \beta\,\gamma\,m\,c^2 = \beta\,E\,, \tag{1.32}$$

where $\beta = v/c$. The simultaneous use of the terms energy and momentum might seem sometimes to be misleading. In this text, we use physically correct quantities in mathematical formulations even though we sometimes use the term "energy" for the quantity cp rather than calling it the particle momentum. In high energy electron accelerators, the numerical distinction between energy and momentum is insignificant and both "energy" and "momentum" are used synonymous. For proton accelerators and even more so for heavy ion accelerators the difference in both quantities is significant.

Often we need differential expressions or expressions for relative variations of a quantity in terms of variations of another quantity. Such relations can

be derived from the definitions in this section. From the variation of $cp = mc^2\sqrt{\gamma^2-1}$ we get, for example,

$$c\mathrm{d}p = \frac{mc^2}{\beta}\,\mathrm{d}\gamma = \frac{\mathrm{d}E}{\beta} = \frac{\mathrm{d}E_{\mathrm{kin}}}{\beta} \tag{1.33}$$

and

$$\frac{c\mathrm{d}p}{cp} = \frac{1}{\beta^2}\frac{\mathrm{d}\gamma}{\gamma}\,. \tag{1.34}$$

Varying $cp = \gamma\beta\, mc^2$ and eliminating $\mathrm{d}\gamma$ we get

$$c\mathrm{d}p = \gamma^3\, mc^2\,\mathrm{d}\beta \tag{1.35}$$

and

$$\frac{c\mathrm{d}p}{cp} = \gamma^2\,\frac{\mathrm{d}\beta}{\beta}\,. \tag{1.36}$$

In a similar way other relations can be derived.

Exercises *

Exercise 1.1 (S). Use the definition for β, the momentum, the total and kinetic energy and derive expressions $p(\beta, E_{\mathrm{kin}})$, $p(E_{\mathrm{kin}})$, and $E_{\mathrm{kin}}(\gamma)$.

Exercise 1.2 (S). Simplify the expressions obtained in exercise 1.1 for large energies, $\gamma \gg 1$. Derive from the relativistic expressions the classical nonrelativistic formulas.

Exercise 1.3 (S). Protons are accelerated to a kinetic energy of 200 MeV at the end of the Fermilab *Alvarez linear accelerator*. Calculate their total energy, their momentum and their velocity in units of the velocity of light.

Exercise 1.4 (S). Consider electrons to be accelerated in the 3 km long SLAC linear accelerator with a uniform gradient of 20 MeV/m. The electrons have a velocity $v = c/2$ at the beginning of the linac. What is the length of the linac in the rest frame of the electron? Assume the particles at the end of the 3 km long linac would enter another 3 km long tube and coast through it. How long would this tube appear to be to the electron?

Exercise 1.5 (S). An electron beam orbits in a circular accelerator with a circumference of 300 m at an average current of 250 mA and the beam consists of 500 equally spaced bunches each 1 cm long. How many particles are orbiting? How many electrons are there in each bunch? Assuming, the time structure of synchrotron radiation is the same as the electron beam time structure specify and plot the radiation time structure in a photon beam line.

* The argument (S) indicates an exercise for which a solution is given in Appendix A.

Exercise 1.6 (S). A $\pi^{\pm}$-meson is created at a kinetic energy of $E_{\rm kin} = 100$ MeV. Calculate it's velocity. What is the probability $P = \exp(-t/\tau_0)$ for the $\pi^{\pm}$-meson to travel 15 m before it decays. The pion half lifetime at rest is $\tau_0 = 26.0$ ns. This result is important for pion cancer therapy facilities. The pions are created in a highly radioactive environment where a high intensity proton beam strikes a target to produce pion-mesons. The beam line to carry the pions to the patient outside the thick radiation shielding wall is about 15 m long.

Exercise 1.7 (S). The half-life of muons μ at rest is $\tau_0 = 2.20$ μs. In 1941 the muon flux was measured on top of Mount Washington (2000 m above sea level) at 570 counts per hour. Another measurement at sea level detected 400 muons per hour. Estimate the kinetic energy of the cosmic ray muons $\left(m_\mu c^2 = 105.7 \text{ MeV}\right)$.

Exercise 1.8 (S). Consider a relativistic electron traveling along the z-axis. In its own system, the electrical field lines extend radially from the charge. Considering only the xz-plane, derive an expressions for the electrical field lines in the laboratory frame of reference. Sketch the field pattern in the electron rest frame and in the laboratory system of reference.

Exercise 1.9 (S). A circular accelerator with a circumference of 100 m contains a uniform distribution of singly charged particles orbiting with the speed of light. If the circulating current is 1 amp, how many particles are orbiting? We instantly turn on an ejection magnet so that all particles leave the accelerator during the time of one revolution. What is the peak current at the ejection point? How long is the current pulse duration? If the accelerator is a synchrotron accelerating particles at a rate of 100 acceleration cycles per second, what is the average ejected particle current?

Exercise 1.10. Verify the correctness of the unit conversion factors in Maxwell's equations (1.1) through (1.4).

Exercise 1.11. Show that $\frac{\mathrm{d}\gamma}{\mathrm{d}t} = \gamma^3 \beta \frac{\mathrm{d}\beta}{\mathrm{d}t}$.

Exercise 1.12. Determine the kinetic energy of an electron, a proton, and a Ar^+-ion which travel together at a speed of $0.95\,c$.

Exercise 1.13. How far will a 200 MeV pion travel before it has a 50% probability to decay?

Exercise 1.14. In a storage ring of 800 m circumference a total of 3×10^{12} relativistic electrons are circulating. They are distributed into 300 bunches. Show that the circulating beam current is 180 mA and the bunch current is 0.6 mA. Sketch the temporal structure of the photon beam.

Exercise 1.15. A total of 2.34×10^{12} electrons orbit in a circular accelerator with a revolution frequency of 1 MHz. Show that the circumference of the accelerator is 300 m and the total beam current 375 mA. The total beam be subdivided into 500 equally distant bunches. The instantaneous bunch current is 20.8 A. Show, that the bunch length is 1.2 cm and the distance between bunches 60 cm. Is the frequency of the rf-system 500 MHz? Why?

Exercise 1.16. Use the accelerator of exercise 1.15, but fill only every 5^{th} bunch. Keep the total circulating beam current. Show that the temporal distance between photon pulses is 180 ps. Now fill the ring only with one bunch for timing experiments. What is the temporal distance between photon pulses?

Exercise 1.17. Assume a beam of 1.46×10^{12} electrons circulating in a 243 m storage ring. Due to gas scattering, you loose a fraction 10^{-5} per second. Show that is takes 27.8 hours for the beam current to decay to 110 mA. What is the initial circulating beam current? How many electrons do you loose in the first turn? and how many per turn after 27.8 hours?

2. Fundamental Processes

The emission of electromagnetic radiation from free electrons is a classical phenomenon. We may therefore use a visual approach to gain some insight into conditions and mechanisms of radiation emission. First, we will discuss necessary conditions that must be met to allow an electron to emit or absorb a photon. Once such conditions are met, we derive from energy conservation a quantity, the Poynting vector, relating energy transport or radiation to electromagnetic fields. This will give us the basis for further theoretical definitions and discussions of radiation phenomena.

2.1 Conservation Laws and Radiation

The emission of electromagnetic radiation involves two components, the electron and the radiation field. For the combined system energy-momentum conservation must be fulfilled. These conservation laws impose very specific selection rules on the kind of emission processes possible. To demonstrate this, we plot the energy versus momentum for both electron and photon. In relativistic terms, we have the relation $\gamma = \sqrt{1 + (\beta\gamma)^2}$ between energy γ and momentum $\beta\gamma$. For consistency in quantities used we normalize the photon energy to the electron rest energy, $\gamma_\mathrm{p} = \varepsilon_\mathrm{p}/mc^2$, where ε_p is the photon energy and mc^2 the electron rest mass. Similarly, we express the speed of light by $\beta_\mathrm{p} = c_\mathrm{p}/c = 1/n$ where $n > 1$ is the refractive index of the medium surrounding the photon. With these definitions and assuming, for now, vacuum as the medium ($n = 1$) the location of a particle or photon in energy-momentum space is shown in Fig. 2.1a.

Energy and momentum of a particle are related such that it must be located on the "particle"-line in Fig. 2.1a. Similarly, a photon is always located on the "photon"-line. Transfer of energy between particle and photon must obey energy-momentum conservation. In Fig. 2.1b we apply this principle to a free electron in vacuum emitting (absorbing) a photon. To create a photon the electron would have to loose (gain) an amount of momentum which is numerically equal to the energy gained (lost) by the photon. Clearly, in this case the electron would end up at a location off the "particle"-line, thus violating momentum conservation. That cannot be, and such a process is

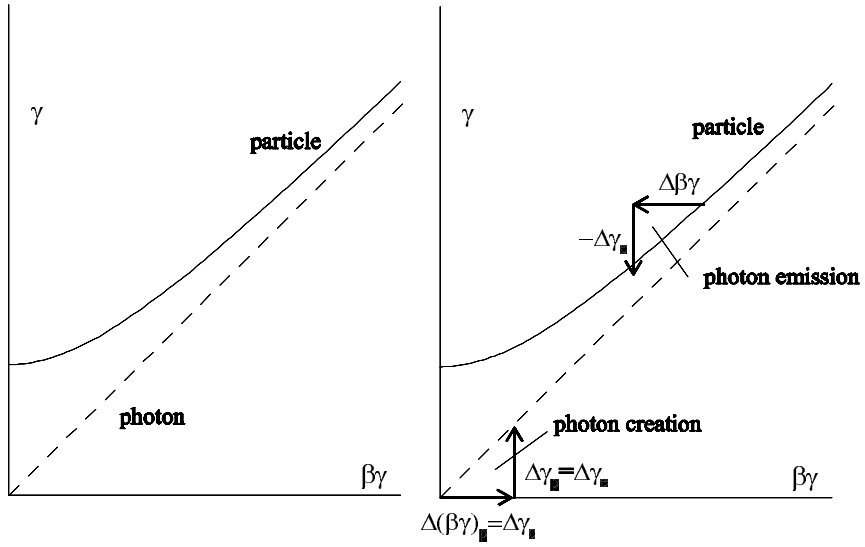

Fig. 2.1. Energy-momentum relationship for particles and photons (*left*). Violation of energy or momentum conservation during emission and absorption of electromagnetic radiation by a free electron travelling in perfect vacuum ($\beta_\mathrm{p} = 1$) (*right*).

therefore not permitted. A free electron in vacuum cannot emit or absorb a photon without violating energy-momentum conservation.

2.1.1 Cherenkov Radiation

We have been careful to assume an electron in perfect vacuum. What happens in a material environment is shown in Fig. 2.2. Because the refractive index $n > 1$, the phase velocity of radiation is less than the velocity of light in vacuum and with $\beta = 1/n$, the "photon"-line is tilted towards the momentum axis.

Formally, we obtain this for a photon from the derivative $\mathrm{d}\gamma/\mathrm{d}(\beta\gamma)$,which we expand to $\frac{\mathrm{d}\gamma}{\mathrm{d}(\beta\gamma)} = \frac{\mathrm{d}\gamma}{\mathrm{d}\omega}\frac{\mathrm{d}\omega}{\mathrm{d}k}\frac{\mathrm{d}k}{\mathrm{d}(\beta\gamma)}$ and get with $\gamma = \hbar\omega/mc^2, k = n\frac{\omega}{c}$, and the momentum $\beta\gamma = \frac{\hbar}{mc}k$, the derivative

$$\frac{\mathrm{d}\gamma_\mathrm{p}}{\mathrm{d}\,(\beta\gamma)_\mathrm{p}} = \frac{1}{n} < 1\,, \tag{2.1}$$

where we have added the subscript $_\mathrm{p}$ to differentiate between photon and electron parameters.

The dispersion function for a photon in a material environment has a slope less than unity as shown in Fig. 2.2. In this case, the numerical value of the photon momentum is less than the photon energy, analogous to the

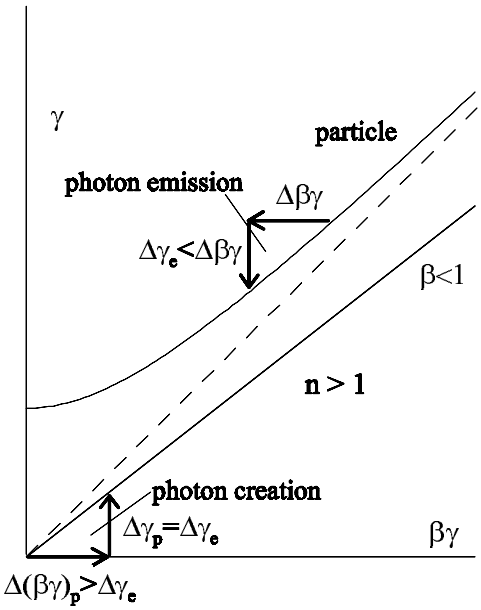

Fig. 2.2. Energy and momentum conservation in a refractive environment with $n > 1$

particle case. To create a photon of energy $\gamma_{\rm p}$ we set $\gamma_{\rm p} = -\Delta\gamma = -\beta\Delta\beta\gamma$ from (1.30), where from (2.1) the photon energy $\gamma_{\rm p} = \frac{1}{n}(\beta\gamma)_{\rm p}$ and get from both relations $(\beta\gamma)_{\rm p} = -n\beta\Delta\beta\gamma$. Because of symmetry, no momentum transverse to the particle trajectory can be exchanged, which means radiation is emitted uniformly in azimuth. The change in longitudinal momentum along the trajectory is $-\Delta\beta\gamma = (\beta\gamma)_{\rm p}\Big|_{\parallel} = (\beta\gamma)_{\rm p}\cos\theta$. In a dielectric environment, free electrons can indeed emit or absorb a photon although, only in a direction given by the angle θ with respect to the electron trajectory. This radiation is called Cherenkov radiation, and the Cherenkov angle θ is given by the Cherenkov condition

$$n\beta\cos\theta = 1\,. \tag{2.2}$$

Note , that this condition is not the same as saying whenever an electron passes though a refractive medium with $n > 1$ there is Cherenkov radiation. The Cherenkov condition requires that $n\beta > 1$ which is, for example, not the case for an electron beam of less than 20 MeV traveling through air.

2.1.2 Compton Radiation

To generate electromagnetic radiation from free electrons in vacuum without violating energy-momentum conservation, we may employ the Compton ef-

fect which is the scattering of an incoming photon by the electron. In energy-momentum space this process is shown in Fig. 2.3. The electron, colliding head-on with an incoming photon absorbs this photon and emits again a photon of different energy. In this process it gains energy but looses momentum bringing the electron in the energy-momentum space to an intermediate point, P_I , from where it can reach its final state on the "particle"-line by emitting a photon as shown in Fig. 2.3. This is the process involved in the generation of synchrotron radiation. Static magnetic fields in the laboratory system appear as electromagnetic fields like an incoming (virtual) photon in the electron system with which the electron can collide. Energy-momentum conservation give us the fundamental and necessary conditions under which a free charged particle can emit or absorb a photon. We turn our attention now to the actual interaction of charged particles with an electromagnetic field.

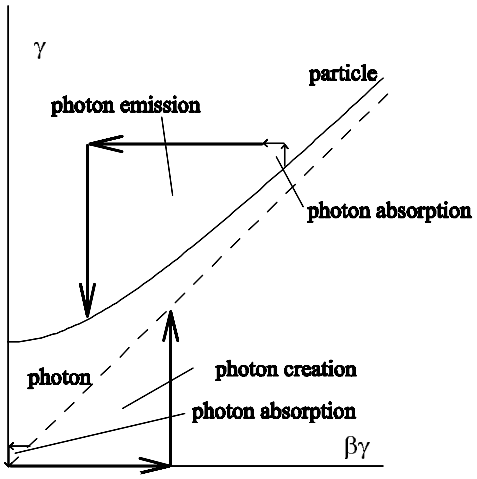

Fig. 2.3. Energy and momentum conservation for Compton scattering process

2.2 The Poynting Vector

The rate of work done in a charged particle-field environment is defined by the Lorentz force and the particle velocity

$$\boldsymbol{F}_{\mathrm{L}}\boldsymbol{v} = \left(e\boldsymbol{E} + e\frac{[c]}{c}\left[\boldsymbol{v}\times\boldsymbol{B}\right]\right)\boldsymbol{v}\,. \tag{2.3}$$

Noting that $[\boldsymbol{v}\times\boldsymbol{B}]\,\boldsymbol{v}=0$ we set $e\boldsymbol{E}\boldsymbol{v} = \boldsymbol{j}\boldsymbol{E}$ and the total rate of work done by all particles and fields is the integral over all particles and fields

$$\int \boldsymbol{j}\boldsymbol{E}\mathrm{d}V = \frac{c}{4\pi}\left[4\pi\epsilon_0\right]\int\left(\left[c\right]\boldsymbol{\nabla}\times\boldsymbol{B} - \frac{1}{c}\dot{\boldsymbol{E}}\right)\boldsymbol{E}\,\mathrm{d}V\,. \tag{2.4}$$

With the vector relation ($B.17$) we get

$$\begin{aligned}\int \boldsymbol{j}\boldsymbol{E}\,\mathrm{d}V &= \frac{c}{4\pi}\left[4\pi\epsilon_0\right]\int\left[\left[c\right]\boldsymbol{B}\underbrace{\boldsymbol{\nabla}\times\boldsymbol{E}}_{=-\frac{1}{c}\dot{\boldsymbol{B}}} - \left[c\right]\boldsymbol{\nabla}\left(\boldsymbol{E}\times\boldsymbol{B}\right) - \tfrac{1}{c}\dot{\boldsymbol{E}}\boldsymbol{E}\right]\mathrm{d}V \\ &= \int\left[\frac{\mathrm{d}\,u}{\mathrm{d}\,t} + \frac{c}{4\pi}\left[4\pi c\epsilon_0\right]\boldsymbol{\nabla}\left(\boldsymbol{E}\times\boldsymbol{B}\right)\right]\mathrm{d}V\,,\end{aligned} \tag{2.5}$$

where $u = \frac{\left[4\pi\epsilon_0\right]}{8\pi}\left(E^2 + \left[c^2\right]B^2\right)$ is the field energy density. Applying Gauss's theorem (B.28) to the vector product we get an expression for the energy conservation of the complete particle-field system

$$\underbrace{\frac{\mathrm{d}}{\mathrm{d}t}\int u\,\mathrm{d}V}_{\substack{\text{change of}\\ \text{field energy}}} + \underbrace{\int \boldsymbol{j}\boldsymbol{E}\,\mathrm{d}V}_{\substack{\text{particle energy}\\ \text{loss or gain}}} + \underbrace{\oint \boldsymbol{S}\boldsymbol{n}\,\mathrm{d}s}_{\substack{\text{radiation loss through}\\ \text{closed surface } s}} = 0\,, \tag{2.6}$$

where the Poynting vector is defined by

$$\boldsymbol{S} = \frac{c}{4\pi}\left[4\pi c\epsilon_0\right]\left(\boldsymbol{E}\times\boldsymbol{B}\right)\,. \tag{2.7}$$

Equation (2.7) exhibits characteristic features of electromagnetic radiation. Both electric and magnetic fields are orthogonal to each other ($\boldsymbol{E}\perp\boldsymbol{B}$), orthogonal to the direction of propagation ($\boldsymbol{E}\perp\boldsymbol{n}$, $\boldsymbol{B}\perp\boldsymbol{n}$), and the vectors $\boldsymbol{E}, \boldsymbol{B}, \boldsymbol{S}$ form a right handed orthogonal system. For plane waves,

$$\boldsymbol{n}\times\boldsymbol{E} = \left[c\right]\boldsymbol{B}\,, \tag{2.8}$$

(Exercise 2.7) and (2.7) reduces to

$$\boldsymbol{S} = \frac{c}{4\pi}\left[4\pi\epsilon_0\right]\boldsymbol{E}^2\,\boldsymbol{n}\,. \tag{2.9}$$

The Poynting vector is defined as the radiation energy flow through a unit surface area in the direction $\boldsymbol{n}$ and scales proportionally to the square of the electric radiation field.

2.3 Electromagnetic Radiation

Phenomenologically, synchrotron radiation is the consequence of a finite value for the velocity of light. Electric fields extend infinitely into space from

charged particles in uniform motion. When charged particles become accelerated, however, parts of these fields cannot catch up with the particle anymore and give rise to synchrotron radiation. This happens more so as the particle velocity approaches the velocity of light.

The emission of light can be described by applying Maxwell's equations to moving charged particles. The mathematical derivation of the theory of radiation from Maxwell's equations is straightforward although mathematically somewhat elaborate and we will postpone this to Chap. 10 and 11 of this text. Here we follow a more intuitive discussion [7] which displays visually the physics of synchrotron radiation from basic physical principles.

Electromagnetic radiation occurs wherever electric and magnetic fields exist with components orthogonal to each other such that the Poynting vector

$$\boldsymbol{S} = \frac{c}{4\pi} \left[4\pi c \epsilon_0\right] \left[\boldsymbol{E} \times \boldsymbol{B}\right] \neq 0\,. \tag{2.10}$$

It is interesting to ask what happens if we have a static electric and magnetic field such that $[\boldsymbol{E} \times \boldsymbol{B}] \neq 0$. We know there is no radiation but the Poynting vector is nonzero. Applying (2.6), we find the first two terms to be zero which renders the third term zero as well. For a static electric and magnetic field the integral defining the radiation loss or absorption is equal to zero and therefore no radiation or energy transport occurs.

Similarly, in case of a stationary electrostatic charge, we note that the electrostatic fields extend radially from the charge to infinity which violates the requirement that the field be orthogonal to the direction of observation or energy flow. Furthermore, the charge is stationary and therefore there is no magnetic field.

2.3.1 Coulomb Regime

Next we consider a charge in uniform motion. In the rest frame of the moving charge we have no radiation since the charge is at rest as just discussed. In the laboratory system, however, the field components are different. Since the charge is moving, it constitutes an electric current which generates a magnetic field. Formulating the Poynting vector in the laboratory system we express the fields by the pure electric field in the particle rest frame $\mathcal{L}^*$. That we accomplish by an inverse Lorentz transformations to (1.28), where the laboratory system $\mathcal{L}$ now moves with the velocity $-\beta_z$ with respect to $\mathcal{L}^*$ and β_z in (1.28) must be replaced by -β_z for

$$\begin{pmatrix} E_x \\ E_y \\ E_z \\ [c]B_x \\ [c]B_y \\ [c]B_z \end{pmatrix} = \begin{pmatrix} \gamma & 0 & 0 & 0 & \beta_z\gamma & 0 \\ 0 & \gamma & 0 & -\beta_z\gamma & 0 & 0 \\ 0 & 0 & 1 & 0 & 0 & 0 \\ 0 & -\beta_z\gamma & 0 & \gamma & 0 & 0 \\ \beta_z\gamma & 0 & 0 & 0 & \gamma & 0 \\ 0 & 0 & 0 & 0 & 0 & 1 \end{pmatrix} \begin{pmatrix} E_x^* \\ E_y^* \\ E_z^* \\ [c]B_x^* \\ [c]B_y^* \\ [c]B_z^* \end{pmatrix}\,. \tag{2.11}$$

In the laboratory system $\mathcal{L}$, the components of the Poynting vector (2.10) become then

$$\begin{aligned}
\frac{4\pi}{c}S_x &= [4\pi\epsilon_0]\gamma\beta_z E_x^* E_z^* \,, \\
\frac{4\pi}{c}S_y &= [4\pi\epsilon_0]\gamma\beta_z E_y^* E_z^* \,, \\
\frac{4\pi}{c}S_z &= -[4\pi\epsilon_0]\gamma^2\beta_z \left(E_x^{*2} + E_y^{*2}\right) \,,
\end{aligned} \tag{2.12}$$

where * indicates quantities in the moving system $\mathcal{L}^*$, and $\beta_z = v_z/c$. The Poynting vector is nonzero and describes the flow of field energy in the environment of a moving charged particle. The fields drop off rapidly with distance from the particle and the "radiation" is therefore confined close to the location of the particle. Specifically, the fields are attached to the charge and travel in the vicinity and with the charge. This part of electromagnetic radiation is called the Coulomb regime in contrast to the radiation regime and is, for example, responsible for the transport of electric energy along electrical wires and transmission lines.

We will ignore this regime in our further discussion of synchrotron radiation because we are interested only in free radiation which is not anymore connected to electric charges. It should be noted, however, that measurements of radiation parameters close to radiating charges may be affected by the presence of the Coulomb radiation regime. Such situations occur, for example, when radiation is observed close to the source point. Related theories deal with this mixing by specifying a formation length defining the minimum distance from the source required to sufficiently separate the Coulomb regime from the radiation regime.

2.3.2 Radiation Regime

In this text we are only interested in the radiation regime and therefore ignore from now on the Coulomb regime. To describe the physics of emission of radiation, we consider a coordinate system moving with a constant velocity equal to that of the charged particle and associated electric fields. The charge is at rest in the moving reference system, the electric field lines extend radially out to infinity, and there is no radiation as discussed before. Acceleration of the charge causes it to move with respect to this reference system generating a distortion of the purely radial electric fields of a uniformly moving charge (Fig. 2.4). This distortion, resulting in a rearrangement of field lines to the new charge position, travels outward at the velocity of light giving rise to what we call radiation.

To be more specific, we consider a positive charge in uniform motion for $t \leqslant 0$, apply an accelerating force at time $t = 0$ for a time ΔT and observe the charged particle and its fields in the uniformly moving frame of reference. Due to acceleration the charge moves in this reference system during the time ΔT

from point A to point B and as a consequence the field lines become distorted within a radius $c\Delta T$ from the original location A of the particle. It is this distortion, travelling away from the source at the speed of light, that we call radiation.

The effects on the fields are shown schematically in Fig. 2.4 for an acceleration of a positive charge along its direction of motion. At time $t = 0$ all electric field lines extend radially from the charge located at point A to infinity. During acceleration fieldlines emerge from the charge now at locations between A and B. The new field lines must join the old field lines which, due to the finite velocity of light, are still unperturbed at distances larger than $c\Delta T$. As long as the acceleration lasts, a nonradial field component, parallel and opposite to the acceleration, is created. Furthermore, the moving charge creates an azimuthal magnetic field $H^*_\varphi(t)$ and the Poynting vector becomes nonzero causing the emission of radiation from an accelerated electrical charge.

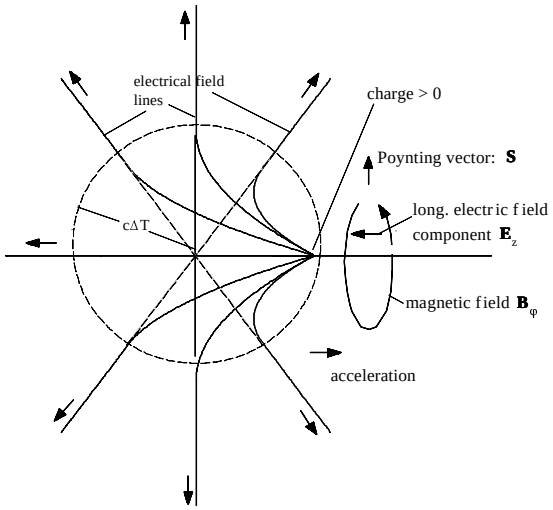

Fig. 2.4. Distortion of fields due to longitudinal acceleration

Obviously, acceleration would not result in any radiation if the velocity of propagation for electromagnetic fields were infinite, $c \to \infty$. In this case the radial fields at all distances from the charge would instantly move in synchrony with the movement of the charge. Only the Coulomb regime would exist.

The electrical field perturbation is proportional to the electrical charge q and the acceleration a^*. Acceleration along the z-axis generates an electric field $\boldsymbol{E}^*_z \neq 0$ and its component normal to the direction of observation scales

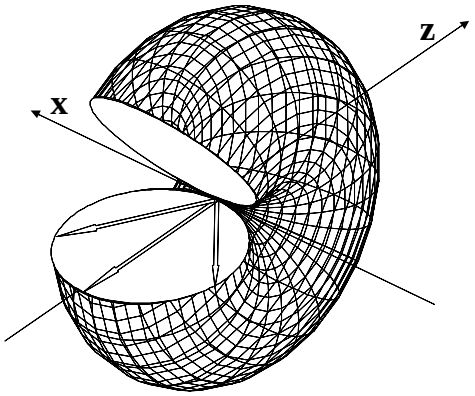

Fig. 2.5. Spatial radiation distribution in the rest frame of the radiating charge

like $\sin\Theta^*$, where Θ^* is the angle between the line of observation and the direction of particle acceleration. During the acceleration a fixed amount of field energy is created which propagates radially outward from the source. Since the total radiation energy must stay constant and the volume of the expanding spherical sheath of field perturbation increases like R^2, the field strength decays linear with distance R. With this, we make the ansatz

$$\boldsymbol{E}_{\parallel}^{*} = -\left[\frac{1}{4\pi\epsilon_0}\right]\frac{e\boldsymbol{a}^{*}}{c^2 R}\sin\Theta^{*} \tag{2.13}$$

for the electric field, where we have added a factor c^2 in the denominator to be dimensionally correct. For an electron, $e < 0$, and the field perturbation points in the direction of the acceleration. As expected from the definition of the Poynting vector, the radiation is emitted predominantly orthogonal to the direction of acceleration and is highly polarized in the direction of acceleration. From (2.9)

$$\boldsymbol{S}=\frac{c}{4\pi}[4\pi\epsilon_0]\,E_{\parallel}^{*2}\boldsymbol{n}^{*}\,, \tag{2.14}$$

where $\mathbf{n}^*$ is the unit vector in the direction of observation from the observer toward the radiation source. The result is consistent with our earlier finding that no free radiation is emitted from a charge at rest or uniform motion ($\boldsymbol{a}^* \to 0$). The spatial radiation distribution is from (2.13) and (2.14) characterized by a $\sin^2\Theta^*$-distribution resembling the shape of a doughnut as shown in Fig. 2.5, where the acceleration occurs along the x-axis.

Acceleration may not only occur in the longitudinal direction but also in the direction transverse to the velocity of the particle as shown in Fig. 2.6.The distortion of field lines in this case creates primarily transverse or radial field components. The radiation field component transverse to the direction of observation is

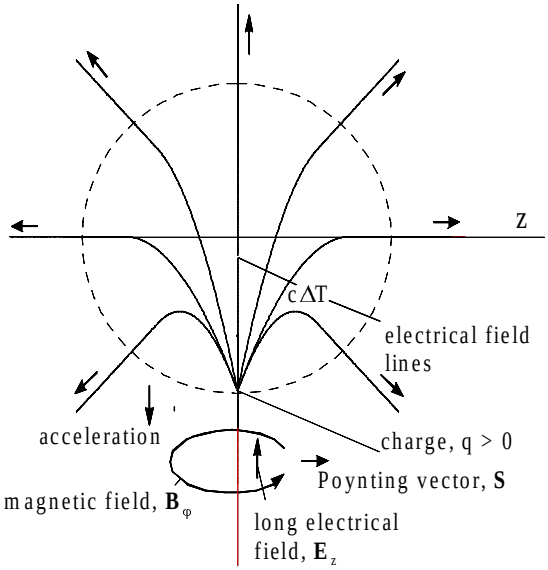

Fig. 2.6. Distortion of field lines due to transverse acceleration

$$\boldsymbol{E}_{\perp}^{*} = -\left[\frac{1}{4\pi\epsilon_0}\right]\frac{e\,\boldsymbol{a}^{*}}{c^2 R}\cos\Theta^{*}\,. \tag{2.15}$$

This case of transverse acceleration describes the appearance of synchrotron radiation created by charged particles being deflected in magnetic fields. Similar to (2.14) the Poynting vector for transverse acceleration is

$$\boldsymbol{S}=\frac{c}{4\pi}[4\pi\epsilon_0]\,E_{\perp}^{*2}\boldsymbol{n}^{*}\,. \tag{2.16}$$

2.4 Spatial and Spectral Properties of Radiation

Although the acceleration and the creation of radiation fields is not periodic, we may Fourier-decompose the radiation pulse and obtain a spectrum of plane waves

$$E^{*} = E_0^{*}\mathrm{e}^{\mathrm{i}\,\Phi^{*}}\,, \tag{2.17}$$

where the phase is defined by

$$\Phi^{*} = \omega^{*}\left[t^{*} - \tfrac{1}{c}\left(n_x^{*}x^{*} + n_y^{*}y^{*} + n_z^{*}z^{*}\right)\right]\,. \tag{2.18}$$

The phase of an electromagnetic wave is proportional to the product of the momentum-energy and space-time 4-vectors. Like any other product of

two 4-vectors this product is invariant under Lorentz transformations. We have therefore the equality $\Phi^* = \Phi$ or

$$\omega^* \left[ct^* - n_x^* x^* - n_y^* y^* - n_z^* z^*\right] = \omega \left[ct - n_x x - n_y y - n_z z\right] \tag{2.19}$$

between the phases as measured in both the laboratory $\mathcal{L}$ and the particle frame of reference $\mathcal{L}^*$. To derive the relationships between similar quantities in both systems, we use the Lorentz transformations noting that the particle reference frame is the frame, where the particle or radiation source is at rest. We use the Lorentz transformations (1.23) to replace the coordinates (x^*, y^*, z^*, ct^*) in (2.19) by those in the laboratory system. Since the space-time coordinates are independent we may equate their coefficients on either side of the equation separately. In so doing, we get from the ct-coefficients for the oscillation frequency

$$\omega^* \gamma \left(1 + \beta_z \, n_z^*\right) = \omega \,, \tag{2.20}$$

which expresses the relativistic Doppler effect. Looking parallel to the direction of particle motion $n_z^* = 1$ the observed oscillation frequency is increased by the factor $(1 + \beta_z)\,\gamma \approx 2$ for highly relativistic particles. The Doppler effect is reduced if the radiation is viewed at some finite angle or even normal to the direction of motion when $n_z^* = 0$. For viewing angles in between these two extremes we set $n_z^* = \cos\Theta^*$.

Similarly, we obtain from (2.19) also the transformation of spatial directions

$$n_x = \frac{n_x^*}{\gamma\left(1 + \beta_z \, n_z^*\right)} \,, \tag{2.21}$$

$$n_y = \frac{n_y^*}{\gamma\left(1 + \beta_z \, n_z^*\right)} \,, \tag{2.22}$$

$$n_z = \frac{\beta_z + n_z^*}{\left(1 + \beta_z \, n_z^*\right)} \,. \tag{2.23}$$

These transformations define the spatial distribution of radiation in the laboratory system. In case of transverse acceleration the radiation in the particle rest frame is distributed like $\cos^2\Theta^*$ about the direction of motion. This distribution becomes greatly collimated into the forward direction in the laboratory system. With $n_x^{*2} + n_y^{*2} = \sin^2\,\Theta^*$ and $n_x^2 + n_y^2 = \sin^2\,\Theta \approx \Theta^2$ and $n_z^* = \cos\Theta^*$ we find

$$\Theta \approx \frac{\sin\Theta^*}{\gamma(1 + \beta\cos\Theta^*)} \,. \tag{2.24}$$

In other words, radiation from relativistic particles, emitted in the particle system into an angle $-\pi/2 < \Theta^* < \pi/2$ appears in the laboratory system highly collimated in the forward direction within an angle of

$$\Theta \approx \frac{1}{\gamma}. \tag{2.25}$$

This angle is very small for highly relativistic electrons like those in a storage ring, where γ is of the order of $10^3 - 10^4$.

Exercises *

Exercise 2.1 (S). Use a 10 MeV electron beam passing through atmospheric air. Can you observe Cherenkov radiation and if so at what angle? Answer the same questions also for a 50 MeV electron beam. Describe and explain with Fig. 2.2 the fundamental difference of your results ($n_{\mathrm{air}} = 1.0002769$ for $\lambda = 5600$ Å).

Exercise 2.2 (S). A 10 MeV electron beam passes with normal incidence through a plate of translucent plastic ($n = 1.7$). Is there any Cherenkov radiation and if so at what angle? Where does this radiation escape the plate?

Exercise 2.3 (S). Show that the product of two 4-vectors is Lorentz invariant.

Exercise 2.4 (S). Show that the product of the 4-momentum and 4-spacetime of a photon is proportional to the phase of the electromagnetic wave.

Exercise 2.5 (S). Derive from (2.20) the formula for the classical Doppler effect valid for sound waves emitted at a frequency f_{s} from a source moving with velocity v and received at an angle ϑ.

Exercise 2.6 (S). From Heisenberg's uncertainty relation construct a "characteristic volume" of a photon with energy $\varepsilon_{\mathrm{ph}} = \hbar\omega$. What is the average electric field in this volume for a 1 eV photon and an x-ray photon of 10 keV?

Exercise 2.7 (S). Prove that $\boldsymbol{n} \times \boldsymbol{E} = [c]\,\boldsymbol{B}$ for plane waves.

Exercise 2.8 (S). Show that equations (2.7) and (2.9) are the same for electromagnetic waves.

Exercise 2.9. Resketch Fig. 2.4 to show the electric field lines from the charge to infinity at a time $t \gtrsim \Delta t$ after the acceleration has stopped.

Exercise 2.10. Derive the equations of transformation for the frequency (2.20), and the direction of observations (2.21–2.23), from (2.19).

* The argument (S) indicates an exercise for which a solution is given in Appendix A.

Exercise 2.11. Verify the equality of $(C.25)$ and $(C.26)$.

Exercise 2.12. Consider a beam of 123.8 meV and 10 keV photons, both at a power density of 100 Watt/mm^2. How many photons occupy their respective "characteristic volumes"? . Show that the photon flux density is 1.875×10^{10} photons(100 meV)/mm^3 and 1.875×10^5 photons(10 keV)/mm^3. Verify that, 61.07 photons(123.8 meV) and 1.44×10^{-18} photons (10 keV) occupy, on average, each characteristic volume in a 100 W/mm^2 beam. The x-ray photon distribution is indeed sparse among it's characteristic volume. What are the respective characteristic volumes?

Exercise 2.13. Verify that for a 10 MeV electron colliding head-on with a Ti-Saphire laser ($\lambda = 0.8\ \mu$m) the wavelength in it's own system is $\lambda^* = 40.88$ nm. Also show that the wavelength of the backscattered photon in the laboratory system is $\lambda_\gamma = 10.4$ Å. What electron beam energy do you need to produce 1 Å radiation? What is the maximum acceptance angle allowable to still get a photon beam with a band width of 10% or less? Show that the acceptance angle is ± 18.15 mrad.

3. Overview of Synchrotron Radiation

After Schott's [3] unsuccessful attempt to explain atomic radiation with his electromagnetic theory no further progress was made for some 40 years mainly because of lack of interest. Only in the mid forties did the theory of electromagnetic radiation from free electrons became interesting again with the successful development of circular high-energy electron accelerators. At this time powerful betatrons [8] have been put into operation and it was Ivanenko and Pomeranchouk [9], who first in 1944 pointed out a possible limit to the betatron principle and maximum energy due to energy loss from emission of electromagnetic radiation. This prediction was used by Blewett [10] to calculate the radiation energy loss per turn in a newly constructed 100 MeV betatron at General Electric. In 1946 he measured the shrinkage of the orbit due to radiation losses and the results agreed with predictions. On April 24, 1947 visible radiation was observed for the first time at the 70 MeV synchrotron built at General Electric [11, 12, 13]. Since then, this radiation is called synchrotron radiation.

The energy loss of particles to synchrotron radiation causes technical and economic limits for circular electron or positron accelerators. As the particle energy is driven higher and higher, more and more rf-power must be supplied to the beam not only to accelerate particles but also to overcome energy losses due to synchrotron radiation. The limit is reached when the radiation power grows to high enough levels exceeding technical cooling capabilities or exceeding the funds available to pay for the high cost of electrical power. To somewhat ameliorate this limit, high-energy electron accelerators have been constructed with ever increasing circumference to allow a more gentle bending of the particle beam. Since the synchrotron radiation power scales like the square of the particle energy (assuming constant magnetic fields) the circumference must scale similar for a constant amount of rf-power. Usually, a compromise is reached by increasing the circumference less and adding more rf-power in spaces along the ring lattice made available by the increased circumference. In general the maximum energy in large circular electron accelerators is limited by the available rf-power while the maximum energy of proton or ion accelerators and low energy electron accelerators is more likely limited by the maximum achievable magnetic fields in bending magnets.

What is a nuisance for researchers in one field can provide tremendous opportunities for others. Synchrotron radiation is emitted tangentially from the particle orbit and within a highly collimated angle of $\pm 1/\gamma$. The spectrum reaches from the far infrared up to hard x-rays, the radiation is polarized and the intensities greatly exceed other sources specifically in the vacuum ultra violet to x-ray region. With these properties synchrotron radiation was soon recognized to be a powerful research tool for material sciences, crystallography, surface physics, chemistry, biophysics, and medicine to name only a few areas of research. While in the past most of this research was done parasitically on accelerators built and optimized for high-energy physics the usefulness of synchrotron radiation for research has become important in its own right to justify the construction and operation of dedicated synchrotron radiation sources all over the world.

3.1 Radiation Power

Integrating the Poynting vector (2.14) over a closed surface enclosing the radiating charge we get with (2.13) and $\mathbf{n}^* \mathrm{d}\mathbf{A}^* = R^2 \sin\Theta^* \mathrm{d}\Theta^* \mathrm{d}\Phi^*$ the radiation power

$$P^* = \int \boldsymbol{S}^* \, \mathrm{d}\boldsymbol{A}^* = \tfrac{2}{3} r_\mathrm{c} \frac{mc^2}{c^3} \, a^{*2} \,, \tag{3.1}$$

where we have set $q^2 = [4\pi\epsilon_0] \; r_\mathrm{c} mc^2$. From the discussion of 4-vectors in Chapter C, we know that the square of the 4-acceleration is invariant to Lorentz transformations and get from $(C.26)$ finally for the radiation power in the laboratory system

$$P = \tfrac{2}{3} r_\mathrm{c} mc \, \gamma^6 \left[\dot{\boldsymbol{\beta}}^2 - \left(\boldsymbol{\beta} \times \dot{\boldsymbol{\beta}} \right)^2 \right] . \tag{3.2}$$

Equation (3.2) expresses the radiation power in a simple way and allows us to calculate other radiation characteristics based on beam parameters in the laboratory system. The radiation power is greatly determined by the geometric path of the particle trajectory through the quantities $\boldsymbol{\beta}$ and $\dot{\boldsymbol{\beta}}$. Specifically, if this path has strong oscillatory components we expect that motion to be reflected in the synchrotron radiation power spectrum. This aspect will be discussed later in more detail. Here we distinguish only between acceleration parallel $\dot{\boldsymbol{\beta}}_\parallel$ or perpendicular $\dot{\boldsymbol{\beta}}_\perp$ to the propagation $\boldsymbol{\beta}$ of the charge and set therefore

$$\dot{\boldsymbol{\beta}} = \dot{\boldsymbol{\beta}}_\parallel + \dot{\boldsymbol{\beta}}_\perp \,. \tag{3.3}$$

Insertion into (3.2) shows the total radiation power to be composed of separate contributions from parallel and orthogonal acceleration. Separating

both contributions we get the synchrotron radiation power for both parallel and transverse acceleration respectively

$$P_{\parallel} = \tfrac{2}{3} r_{\mathrm{c}} mc\, \gamma^6\, \dot{\boldsymbol{\beta}}_{\parallel}^2 \,, \tag{3.4}$$

$$P_{\perp} = \tfrac{2}{3} r_{\mathrm{c}} mc\, \gamma^4 \dot{\boldsymbol{\beta}}_{\perp}^2 \,. \tag{3.5}$$

Expressions have been derived that define the radiation power for parallel acceleration like in a linear accelerator or orthogonal acceleration found in circular accelerators or deflecting systems. We note a similarity for both contributions except for the energy dependence. At highly relativistic energies the same acceleration force leads to much less radiation if the acceleration is parallel to the motion of the particle compared to orthogonal acceleration. Parallel acceleration is related to the accelerating force by $m\dot{\boldsymbol{v}}_{\parallel} = \frac{1}{\gamma^3}\mathrm{d}\boldsymbol{p}_{\parallel}/\mathrm{d}t$ and after insertion into (3.4) the radiation power due to parallel acceleration becomes

$$P_{\parallel} = \frac{2}{3}\frac{r_{\mathrm{c}}}{mc}\left(\frac{\mathrm{d}\boldsymbol{p}_{\parallel}}{\mathrm{d}\,t}\right)^2 . \tag{3.6}$$

The radiation power for acceleration along the propagation of the charged particle is therefore independent of the energy of the particle and depends only on the accelerating force or with $\mathrm{d}\boldsymbol{p}_{\parallel}/\mathrm{d}t = \mathrm{d}\boldsymbol{E}/\mathrm{d}z$ on the energy increase per unit length of accelerator. Different from circular electron accelerators we encounter therefore no practical energy limit in a linear accelerator at very high energies. In contrast very different radiation characteristics exist for transverse acceleration as it happens, for example, during the transverse deflection of a charged particle in a magnetic field. The transverse acceleration $\dot{\boldsymbol{v}}_{\perp}$ is expressed by the Lorentz force

$$\frac{\mathrm{d}\boldsymbol{p}_{\perp}}{\mathrm{d}\,t} = \gamma m \dot{\boldsymbol{v}}_{\perp} = e\frac{[c]}{c}\,[\boldsymbol{v} \times \boldsymbol{B}] \tag{3.7}$$

and after insertion into (3.5) the radiation power from transversely accelerated particles becomes

$$P_{\perp} = \tfrac{2}{3}\frac{r_{\mathrm{c}}}{mc}\,\gamma^2\left(\frac{\mathrm{d}\boldsymbol{p}_{\perp}}{\mathrm{d}\,t}\right)^2 . \tag{3.8}$$

From (3.6, 3.8) we find that the same accelerating force leads to a much higher radiation power by a factor γ^2 for transverse acceleration compared to longitudinal acceleration. For all practical purposes, technical limitations prevent the occurrence of sufficient longitudinal acceleration to generate noticeable radiation. From here on we will stop considering longitudinal acceleration unless specifically mentioned and eliminate, therefore, the index $\perp$ setting for the radiation power $P_{\perp} = P_{\gamma}$. We also restrict from now on the discussion to singly charged particles and set $q = e$ ignoring extremely high

energies, where multiple charged ions may start to radiate. Replacing the force in (3.8) by the Lorentz force (3.7) we get

$$P_\gamma = \left[\frac{4\pi}{\mu_0}\right] \frac{2\, r_c^2\, c}{3\,(mc^2)^2}\, B^2\, E^2 = C_B B^2\, E^2\,, \tag{3.9}$$

where

$$C_B = \left[\frac{4\pi}{\mu_0}\right] \frac{2\, r_c^2\, c}{3\,(mc^2)^2} = 6.077\,9 \times 10^{-8}\, \frac{\mathrm{W}}{\mathrm{T^2 GeV^2}} = 379.35\, \frac{1}{\mathrm{T^2 GeV\,s}}\,. \tag{3.10}$$

The synchrotron radiation power scales like the square of the magnetic field and the square of the particle energy. Replacing the deflecting magnetic field $\boldsymbol{B}$ by the bending radius ρ (6.7) the instantaneous synchrotron radiation power becomes

$$P_\gamma = \tfrac{2}{3}\, r_c mc^3 \frac{\beta^4 \gamma^4}{\rho^2} \tag{3.11}$$

or in more practical units,

$$P_\gamma = \frac{c\, C_\gamma}{2\pi} \frac{E^4}{\rho^2}\,. \tag{3.12}$$

Here we use the definition of Sand's radiation constant for electrons [14]

$$C_\gamma = \frac{4\pi}{3} \frac{r_c}{(mc^2)^3} = 1.41733\, \times 10^{-14}\, \frac{\mathrm{msW}}{\mathrm{GeV^4}} = 8.8460 \times 10^{-5}\, \frac{\mathrm{m}}{\mathrm{GeV^3}}\,. \tag{3.13}$$

The electromagnetic radiation of charged particles in transverse magnetic fields is proportional to the fourth power of the particle momentum $\beta\gamma$ and inversely proportional to the square of the bending radius ρ. The synchrotron radiation power increases very fast for high-energy particles and provides the most severe limitation to the maximum energy achievable in circular accelerators. We note, however, also a strong dependence on the kind of particles involved in the process of radiation. Because of the much heavier mass of protons compared to the lighter electrons we find appreciable synchrotron radiation only in electron accelerators.

In storage rings with different magnets and including insertion devices it is important to formulate the average radiation power of an electron during the course of one turn. In this case we calculate the average

$$\langle P_\gamma \rangle = \frac{c}{2\pi} C_\gamma E^4 \left\langle \frac{1}{\rho^2} \right\rangle = C_\gamma E^4 \frac{f_{\mathrm{rev}}}{2\pi} \oint \frac{\mathrm{d}s}{\rho^2}\,. \tag{3.14}$$

The radiation power of protons actually is smaller compared to that for electrons by the fourth power of the mass ratio or by the factor

$$\frac{P_\mathrm{e}}{P_\mathrm{p}} = 1836^4 = 1.1367 \times 10^{13} \,. \tag{3.15}$$

In spite of this enormous difference measurable synchrotron radiation has been predicted by Coisson [15] and was indeed detected at the 400 GeV proton synchrotron, SPS (Super Proton Synchrotron), at CERN in Geneva [16, 17]. Substantial synchrotron radiation is expected in multi-TeV proton colliders like the LHC (Large Hadron Collider) at CERN [18].

Knowledge of the synchrotron radiation power allows us now to calculate the energy loss per turn of a particle in a circular accelerator by integrating the radiation power along the circumference of the circular accelerator

$$U_0 = \oint P_\gamma \mathrm{d}t = \tfrac{2}{3} r_\mathrm{c} mc^2 \beta^3 \gamma^4 \oint \frac{\mathrm{d}s}{\rho^2} \,. \tag{3.16}$$

In an isomagnetic lattice, where the bending radius is the same for all bending magnets ρ =const., the integration around a circular accelerator can be performed and the energy loss per turn due to synchrotron radiation is

$$U_0 = P_\gamma \frac{2\pi\rho}{\beta c} = \tfrac{4\pi}{3} r_\mathrm{c} mc^2 \beta^3 \frac{\gamma^4}{\rho} \,. \tag{3.17}$$

The integration obviously is to be performed only along those parts of the circular accelerator, where synchrotron radiation occurs, or along bending magnets only. In more practical units, the energy loss of relativistic electrons per revolution in a circular accelerator with an isomagnetic lattice and a bending radius ρ is given by

$$U_{0,\mathrm{iso}}\,(\mathrm{GeV}) = C_\gamma \frac{E^4(\mathrm{GeV}^4)}{\rho(m)} \,. \tag{3.18}$$

For a beam of N_e particles or a circulating beam current $I = e f_\mathrm{rev} N_\mathrm{e}$ the total average radiation power is

$$\langle P_\mathrm{s} \rangle = U_0 \frac{I}{e} \,, \tag{3.19}$$

or in more practical units

$$\langle P_\mathrm{s}\,(\mathrm{MW}) \rangle_\mathrm{iso} = 0.088463 \, \frac{E^4\,(\mathrm{GeV})}{\rho\,(\mathrm{m})} \, I\,(\mathrm{A}) \,. \tag{3.20}$$

The total synchrotron radiation power scales like the fourth power of the particle energy and is inversely proportional to the bending radius. The strong dependence of the radiation on the particle energy causes severe practical limitations on the maximum achievable energy in a circular accelerator.

3.2 Spectrum

Synchrotron radiation from relativistic charged particles is emitted over a wide spectrum of photon energies. The basic characteristics of this spectrum can be derived from simple principles as suggested in [19]. For an observer synchrotron light has the appearance similar to the light coming from a lighthouse. Although the light is emitted continuously an observer sees only a periodic flash of light as the aperture mechanism rotates in the lighthouse. Similarly, synchrotron light emitted from relativistic particles will appear to an observer as a single flash if it comes from a bending magnet in a transport line passed through by a particle only once or as a series of equidistant light flashes as bunches of particles orbit in a circular accelerator.

Since the duration of the light flashes is very short the observer notes a broad spectrum of frequencies as his eyes or instruments Fourier analyze the pulse of electromagnetic energy. The spectrum of synchrotron light from a circular accelerator is composed of a large number of harmonics with fundamental frequency equal to the revolution frequency of the particle in the circular accelerator. These harmonics reach a cutoff, where the period of the radiation becomes comparable to the duration of the light pulse. Even though the aperture of the observers eyes or instruments are assumed to be infinitely narrow we still note a finite duration of the light flash. This is a consequence

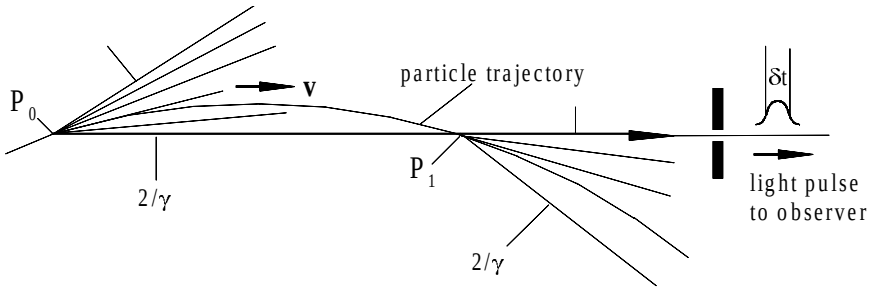

Fig. 3.1. Temporal pulse formation of synchrotron radiation

of the finite opening angle of the radiation as illustrated in Fig. 3.1. Synchrotron light emitted by a particle travelling along the orbit cannot reach the observer before it has reached the point P_0 when those photons emitted on one edge of the radiation cone at an angle $-1/\gamma$ aim directly toward the observer. Similarly, the last photons to reach the observer are emitted from point P_1 at an angle of $+1/\gamma$. Between point P_0 and point P_1 we have therefore a deflection angle of $2/\gamma$. The duration of the light flash for the observer is not the time it takes the particle to travel from point P_0 to point P_1 but must be corrected for the finite time of flight for the photon emitted at P_0 . If particle and photon would travel toward the observer with exactly the same

velocity the light pulse would be infinitely short. However, particles move slower following a slight detour and therefore the duration of the light pulse equals the time difference between the first photons from point P_0 arriving at the observer and the last photons being emitted by the particles at point P_1. Although the particle reaches point P_0 at time $t = 0$ the first photon can be observed at point P_1 only after a time

$$t_\gamma = \frac{2\rho \sin \frac{1}{\gamma}}{c} . \tag{3.21}$$

The last photon to reach the observer is emitted when the particle arrives at point P_1 at the time

$$t_\mathrm{e} = \frac{2\rho}{\beta c \gamma} . \tag{3.22}$$

The duration of the light pulse δt is therefore given by the difference of both travel times (3.21, 3.22)

$$\delta t = t_\mathrm{e} - t_\gamma = \frac{2\rho}{\beta c \gamma} - \frac{2\rho \sin \frac{1}{\gamma}}{c} . \tag{3.23}$$

The sine-function can be expanded for small angles keeping linear and third order terms only and the duration of the light pulse at the location of the observer is after some manipulation

$$\delta t = \frac{4\rho}{3c\gamma^3} . \tag{3.24}$$

The total duration of the electromagnetic pulse is very short scaling inversely proportional to the third power of γ. This short pulse translates into a broad spectrum. Using only half the pulse length for the effective pulse duration the spectrum reaches up to a maximum frequency of about

$$\omega_\mathrm{c} \approx \frac{1}{\frac{1}{2}\delta t} \approx \tfrac{3}{2}\, c \frac{\gamma^3}{\rho} , \tag{3.25}$$

which is called the critical photon frequency of synchrotron radiation. The critical photon energy $\varepsilon_\mathrm{c} = \hbar\omega_\mathrm{c}$ is then given by

$$\varepsilon_\mathrm{c} = C_\mathrm{c} \frac{E^3}{\rho} , \tag{3.26}$$

with

$$C_\mathrm{c} = \frac{3\,\hbar c}{2\,(mc^2)^3} . \tag{3.27}$$

For electrons, numerical expressions are

$$\varepsilon_{\mathrm{c}}\,(\mathrm{keV}) = 2.2183\frac{E^3\left(\mathrm{GeV}^3\right)}{\rho\,(\mathrm{m})} = 0.66503\,E^2\left(\mathrm{GeV}^2\right)B\,(\mathrm{T})\ . \tag{3.28}$$

The synchrotron radiation spectrum from relativistic particles in a circular accelerator is made up of harmonics of the particle revolution frequency ω_0 with values up to and beyond the critical frequency (3.28). Generally, a real synchrotron radiation beam from say a storage ring will not display this harmonic structure. The distance between harmonics is extremely small compared to the extracted photon frequencies in the VUV and x-ray regime while the line width is finite due to the energy spread and beam emittance.

For a single pass of particles through a bending magnet in a beam transport line we observe the same spectrum. Specifically, the maximum frequency is the same assuming similar parameters. Synchrotron radiation is emitted in a particular spatial and spectral distribution, both of which will be derived in Chapter 9, and we will use here only some of these results. A useful parameter to characterize the photon intensity is the photon flux per unit solid angle into a frequency bin $\Delta\omega/\omega$ and from a circulating beam current I defined by

$$\frac{\mathrm{d}^2\dot{N}_{\mathrm{ph}}}{\mathrm{d}\theta\mathrm{d}\psi} = C_\Omega E^2 I\,\frac{\Delta\omega}{\omega}\left(\frac{\omega}{\omega_{\mathrm{c}}}\right)^2 K^2_{2/3}\,(\xi)\ F\,(\xi,\theta)\ , \tag{3.29}$$

where ψ is the angle in the deflecting plane and θ the angle normal to the deflecting plane,

$$C_\Omega = \frac{3\alpha}{4\pi^2 e\,(mc^2)^2} = 1.3255\times 10^{16}\ \frac{\text{photons}}{\text{s mrad}^2\ \text{GeV}^2\ \text{A}\ 100\%\text{BW}}\ , \tag{3.30}$$

α the fine structure constant and

$$F\,(\xi,\theta) = \left(1+\gamma^2\theta^2\right)^2\left(1+\frac{\gamma^2\theta^2}{1+\gamma^2\theta^2}\frac{K^2_{1/3}\,(\xi)}{K^2_{2/3}\,(\xi)}\right)\ . \tag{3.31}$$

The functions $K_{1/3}\,(\xi)$ and $K_{2/3}\,(\xi)$, displayed in Fig. 3.2, are modified Bessel's functions with the argument

$$\xi = \tfrac{1}{2}\frac{\omega}{\omega_{\mathrm{c}}}\left(1+\gamma^2\theta^2\right)^{3/2}\ . \tag{3.32}$$

Synchrotron radiation is highly polarized in the plane normal (σ-mode), and parallel (π-mode), to the deflecting magnetic field. The relative flux in both polarization directions is given by the two components in the second bracket of function $F\,(\xi,\theta)$ in (3.31). The first component is equal to unity and determines the photon flux for the polarization normal to the magnetic field or σ-mode, while the second term relates to the polarization parallel to the magnetic field which is also called the π-mode. Equation (3.29) expresses both the spectral and spatial photon flux for both the σ-mode radiation in

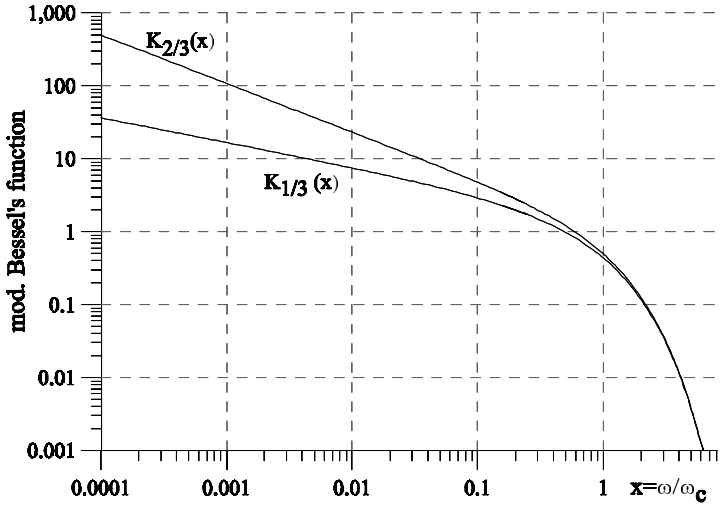

Fig. 3.2. Modified Bessel's functions $K_{1/3}(\xi)$ and $K_{2/3}(\xi)$

the forward direction within an angle of about $\pm 1/\gamma$ and for the π-mode off axis.

For highly relativistic particles the synchrotron radiation is collimated very much in the forward direction and we may assume that all radiation in the nondeflecting plane is accepted by the experimental beam line. In this case we are interested in the photon flux integrated over all angles θ. This integration will be performed in Chapter 9 with the result (9.158)

$$\frac{\mathrm{d}\dot{N}_{\mathrm{ph}}}{\mathrm{d}\psi} = \frac{4\alpha}{9}\,\gamma\,\frac{I}{e}\,\frac{\Delta\omega}{\omega}\,S\left(\frac{\omega}{\omega_{\mathrm{c}}}\right)\ , \tag{3.33}$$

where ψ is the deflection angle in the bending magnet, α the fine structure constant and the function $S(x)$ is defined by

$$S\left(\frac{\omega}{\omega_{\mathrm{c}}}\right) = \frac{9\sqrt{3}}{8\pi}\,\frac{\omega}{\omega_{\mathrm{c}}}\int\limits_{\omega/\omega_{\mathrm{c}}}^{\infty} K_{5/3}(\bar{x})\,\mathrm{d}\bar{x} \tag{3.34}$$

with $K_{5/3}(x)$ a modified Bessel's function. The function $S(\omega/\omega_{\mathrm{c}})$ is known as the universal function of synchrotron radiation and is shown in Fig. 3.3. In practical units, the angle integrated photon flux is

$$\frac{\mathrm{d}\dot{N}_{\mathrm{ph}}}{\mathrm{d}\psi} = C_{\psi}\,E\,I\,\frac{\Delta\omega}{\omega}\,S\left(\frac{\omega}{\omega_{\mathrm{c}}}\right) \tag{3.35}$$

with C_{ψ} defined by

$$C_\psi = \frac{4\alpha}{9e\,mc^2} = 3.9614 \times 10^{19}\ \frac{\text{photons}}{\text{s rad A GeV}}\,. \tag{3.36}$$

The spectral distribution depends only on the particle energy, the critical frequency ω_c and a purely mathematical function. This result has been derived originally by Ivanenko and Sokolov [20] and independently by Schwinger [21]. Specifically it should be noted that the spectral distribution, if normalized to the critical frequency, does not depend on the particle energy and can therefore be represented by a universal distribution shown in Fig. 3.3.

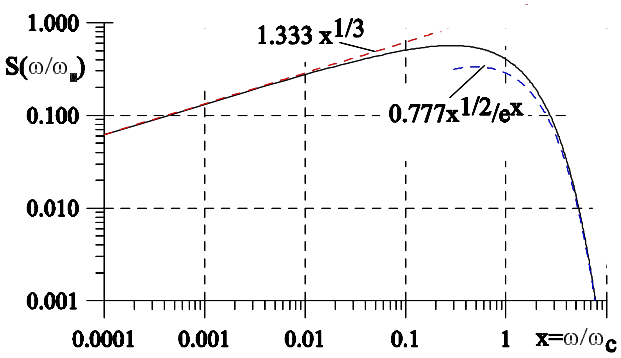

Fig. 3.3. Universal function of the synchrotron radiation spectrum, $S(\omega/\omega_c)$

The energy dependence is contained in the cubic dependence of the critical frequency acting as a scaling factor for the actual spectral distribution. The synchrotron radiation spectrum in Fig. 3.3 is rather uniform up to the critical frequency beyond which the intensity falls off rapidly. This synchrotron radiation spectrum has been verified experimentally soon after such radiation sources became available [22, 23].

Equation (3.33) is not well suited for quick calculation of the radiation intensity at a particular frequency. We may, however, express (3.33) in much simpler form for very low and very large frequencies making use of limiting expressions of Bessel's functions for large and small arguments. For small arguments $x = \frac{\omega}{\omega_c} \ll 1$ an asymptotic approximation [24] for the modified Bessel's function may be used to give instead of (3.35)

$$\frac{\mathrm{d}\dot{N}_{\mathrm{ph}}}{\mathrm{d}\psi} \approx C_\psi\, E\, I\, \frac{\Delta\omega}{\omega}\, 1.333 \left(\frac{\omega}{\omega_c}\right)^{1/3}\,. \tag{3.37}$$

Similarly, for high photon frequencies $x = \frac{\omega}{\omega_c} \gg 1$ we get

$$\frac{\mathrm{d}\dot{N}_{\mathrm{ph}}}{\mathrm{d}\psi} \approx C_\psi\, E\, I\, \frac{\Delta\omega}{\omega}\, 0.77736 \frac{\sqrt{x}}{e^x}\,, \tag{3.38}$$

where $x = \frac{\omega}{\omega_c}$. Both approximations are included in Fig. 3.3 and display actually a rather good representation of the real spectral radiation distribution over all but the central portion of the spectrum. Specifically, we note the slow increase in the radiation intensity at low frequencies and the exponential drop off above the critical frequency.

3.3 Spatial Photon Distribution

The expressions for the photon fluxes (3.29, 3.33) provide the opportunity to calculate the spectral distribution of the photon beam divergence. Photons are emitted into a narrow angle and we may represent this narrow angular distribution by a Gaussian distribution. The effective width of a Gaussian distribution is $\sqrt{2\pi\sigma_\theta}$ and we set

$$\frac{\mathrm{d}\dot{N}_{\mathrm{ph}}}{\mathrm{d}\psi} \approx \frac{\mathrm{d}^2\dot{N}_{\mathrm{ph}}}{\mathrm{d}\theta\,\mathrm{d}\psi}\sqrt{2\pi\sigma_\theta}\,. \tag{3.39}$$

With (3.29, 3.35) the angular divergence of the forward lobe of the photon beam or for a beam polarized in the σ-mode is

$$\sigma_\theta\,(\mathrm{mrad}) = \frac{C_\psi}{\sqrt{2\pi}C_\Omega}\frac{1}{E}\frac{S\,(x)}{x^2K^2_{2/3}\left(\frac{1}{2}x\right)} = \frac{f\,(x)}{E\,(\mathrm{GeV})}\,, \tag{3.40}$$

where $x = \omega/\omega_{\mathrm{c}}$. For the forward direction $\theta \approx 0$ the function $f(x) = \sigma_\theta\,(\mathrm{mrad})\;E\,(\mathrm{GeV})$ is shown in Fig. 3.4 for easy numerical calculations.

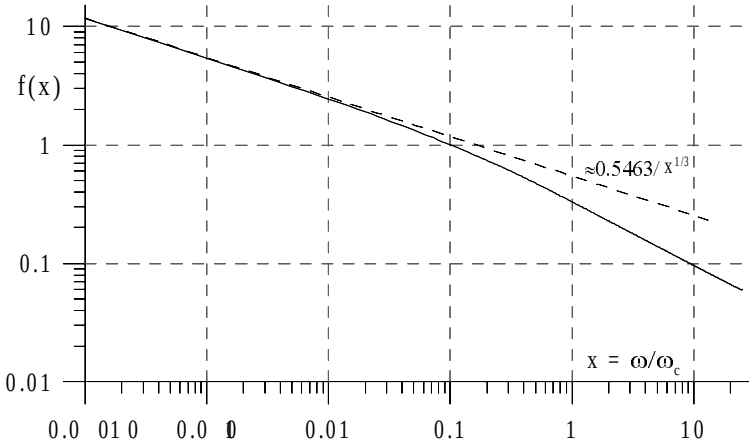

Fig. 3.4. Scaling function $f(x) = \sigma_\theta(\mathrm{mrad})\,E(\mathrm{GeV})$ for the photon beam divergence in (3.40)

For wavelengths $\omega \ll \omega_c$, (3.40) can be greatly simplified to become in more practical units

$$\sigma_\theta\,(\mathrm{mrad}) \approx \frac{0.54626}{E\,(\mathrm{GeV})}\left(\frac{\omega}{\omega_c}\right)^{1/3} = \frac{7.124}{[\rho\,(\mathrm{m})\;\epsilon_{\mathrm{ph}}\;(\mathrm{eV})]^{1/3}}\,, \tag{3.41}$$

where ρ is the bending radius and ϵ_{ph} the photon energy. The photon beam divergence for low photon energies compared to the critical photon energy is independent of the particle energy and scales inversely proportional to the third root of the bending radius and photon energy.

3.4 Fraunhofer Diffraction

Synchrotron radiation is emitted from a rather small area equal to the cross section of the electron beam. In the extreme and depending on the photon wavelength the radiation may be spatially coherent because the beam cross section in phase space is smaller than the wavelength. This possibility to create spatially coherent radiation is important for many experiments specifically for holography and we will discuss in more detail the conditions for the particle beam to emit such radiation.

Reducing the particle beam cross section in phase space by diminishing the particle beam emittance reduces also the source size of the photon beam. This process of reducing the beam emittance is, however, effective only to some point. Further reduction of the particle beam emittance would have no effect on the photon beam emittance because of diffraction effects. A point like photon source appears in an optical instrument as a disk with concentric illuminated rings. For synchrotron radiation sources it is of great interest to maximize the photon beam brightness which is the photon density in phase space. On the other hand designing a lattice for a very small beam emittance can causes beam stability problems. It is therefore prudent not to push the particle beam emittance to values much less than the diffraction limited photon beam emittance. In the following we will therefore define diffraction limited photon beam emittance as a guide for low emittance lattice design.

For highly collimated synchrotron radiation it is appropriate to assume Fraunhofer diffraction . Radiation from an extended light source appears diffracted in the image plane with a radiation pattern which is characteristic for the particular source size and radiation distribution as well as for the geometry of the apertures involved. For simplicity, we will use the case of a round aperture being the boundaries of the beam itself although in most cases the beam cross section is more elliptical. In spite of this simplification, however, we will obtain all basic physical properties of diffraction which are of interest to us. We consider a circular light source with diameter $2a$. The

radiation field at point P in the image plane is then determined by the Fraunhofer diffraction integral [25]

$$U(P) = C \int_0^a \int_0^{2\pi} \mathrm{e}^{-\mathrm{i}k\rho w \cos(\Theta - \psi)} \mathrm{d}\Theta \, \rho \mathrm{d}\rho. \tag{3.42}$$

Here k is the wave number of the radiation and w is the sine of the angle between the light ray and the optical axis as shown in Fig. 3.5.

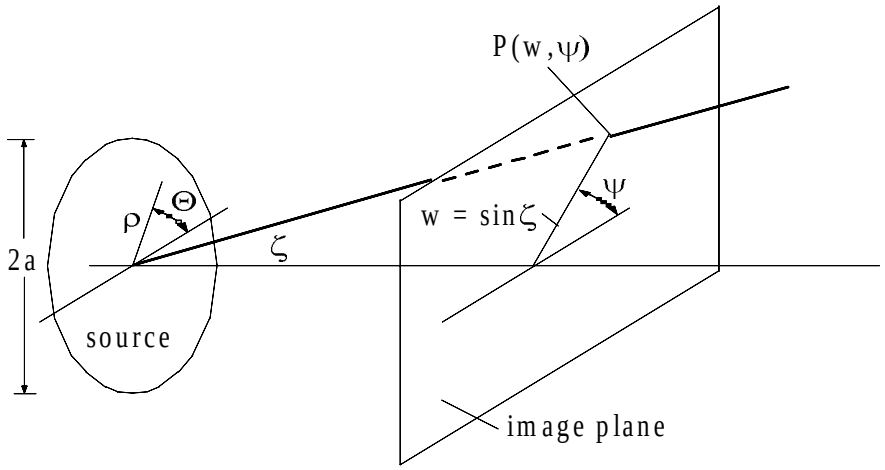

Fig. 3.5. Diffraction geometry

With $\alpha = \Theta - \psi$ and the definition of the lowest order Bessel's function $J_0(x) = \frac{1}{2\pi} \int_0^{2\pi} \mathrm{e}^{-\mathrm{i}x\cos\alpha} \mathrm{d}\alpha$, (3.42) can be expressed by the integral

$$U(P) = 2\pi C \int_0^a J_0(k\rho w) \, \rho \mathrm{d}\rho. \tag{3.43}$$

This integral can be solved analytically as well with the identity $\int_0^x J_0(y) \, y \, \mathrm{d}y = x J_1(x)$. The radiation intensity is proportional to the square of the radiation field and we get finally for the radiation intensity in the image plane at the point P

$$I(P) = I_0 \frac{4 J_1^2(kaw)}{(kaw)^2}, \tag{3.44}$$

where $I(P) = |U(P)|^2$ and $I_0 = I(w \to 0)$ is the radiation intensity at the image center. This result has been derived first by Airy [26]. The radiation intensity from a light source of small circular cross section is distributed in

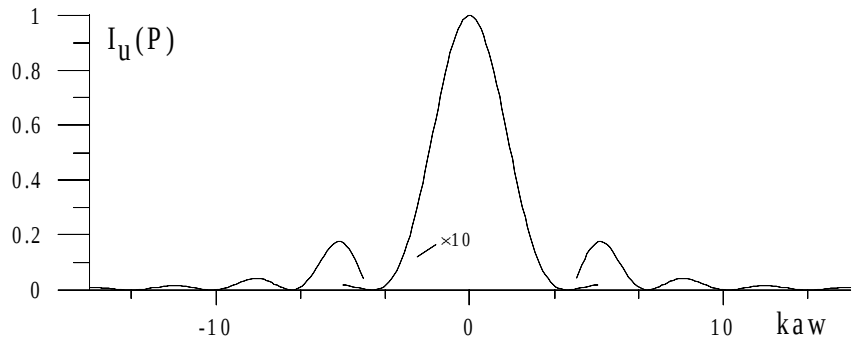

Fig. 3.6. Fraunhofer diffraction for a cicular uniform light source

the image plane due to diffraction into a central circle and concentric rings illuminated as shown in Fig. 3.6.

Tacitly, we have assumed that the distribution of emission at the source is uniform which is generally not correct for a particle beam. A Gaussian distribution is more realistic resembling the distribution of independently radiating particles. We must be careful in the choice of the scaling parameter. The relevant quantity for the Fraunhofer integral is not the actual particle beam size at the source point but rather the apparent beam size and distribution. By folding the particle density distribution with the argument of the Fraunhofer diffraction integral we get the radiation field from a round, Gaussian particle beam,

$$U_{\mathrm{G}}(P) = \text{const.} \int_0^\infty \exp\left(-\frac{\rho^2}{2\sigma_r^2}\right) J_0(k\rho w)\ \rho \mathrm{d}\rho\,, \tag{3.45}$$

where σ_r is the apparent standard source radius. Introducing the variable $x = \rho/\sqrt{2}\sigma_r$ and replacing $k\rho w = \sqrt{2}xk\,\sigma_r w = 2x\sqrt{z}$ we get from (3.45)

$$U_{\mathrm{G}}(P) = \text{const.} \int_0^\infty \mathrm{e}^{-x^2}\, x\, J_0\left(2x\sqrt{z}\right)\, \mathrm{d}x \tag{3.46}$$

and after integration

$$U_{\mathrm{G}}(P) = \text{const.}\ \exp\left[-\tfrac{1}{2}\ (k\sigma_r w)^2\right]\,. \tag{3.47}$$

The diffraction pattern from a Gaussian light source (Fig. 3.7) does not exhibit the ring structure of a uniform source. The radiation field assumes rather the form of a Gaussian distribution in the emission angles w with a standard width of $\sigma_{r'}^2 = \langle w^2 \rangle$ or

$$\sigma_{r'} = \frac{1}{k\,\sigma_r}\,. \tag{3.48}$$

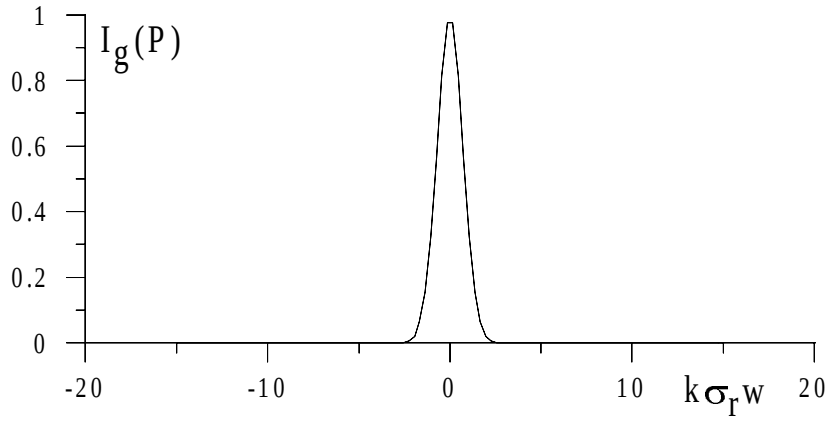

Fig. 3.7. Fraunhofer diffraction for a Gaussian luminescence at the light source

3.5 Spatial Coherence

Synchrotron radiation is emitted into a broad spectrum with the lowest frequency equal to the revolution frequency and the highest frequency not far above the critical photon energy. Detailed observation of the whole radiation spectrum, however, may reveal significant differences to these theoretical spectra at the low frequency end. At low photon frequencies we may observe an enhancement of the synchrotron radiation beyond intensities predicted by the theory of synchrotron radiation as discussed so far. We note from the definition of the Poynting vector that the radiation power is a quadratic effect with respect to the electric charge. For photon wavelengths equal and longer than the bunch length, we expect therefore all particles within a bunch to radiate coherently and the intensity to be proportional to the square of the number N_e of particles rather than linearly proportional as is the case for high frequencies. This quadratic effect can greatly enhance the radiation since the bunch population can be from $10^8 - 10^{11}$ electrons.

Generally such radiation is not emitted from a storage ring beam because radiation with wavelengths longer than the vacuum chamber dimensions are greatly damped and will not propagate along a metallic beam pipe [27] . This radiation shielding is fortunate for storage ring operation since it eliminates an otherwise significant energy loss mechanism. Actually, since this shielding affects all radiation of sufficient wavelength both the ordinary synchrotron radiation and the coherent radiation is suppressed. New developments in storage ring physics, however, may make it possible to reduce the bunch length by as much as an order of magnitude below presently achieved short bunches of the order of 10 mm. Such bunches would then be much shorter than vacuum chamber dimensions and the emission of coherent radiation in some limited

frequency range would be possible. Much shorter electron bunches of the order of 1 - 2 mm and associated coherent radiation can be produced in linear accelerators [28] [29], and specifically with bunch compression [30] a significant fraction of synchrotron radiation is emitted spontaneously as coherent radiation [31].

In this section we will discuss the physics of spontaneous coherent synchrotron radiation while distinguishing two kinds of coherence in synchrotron radiation, the temporal coherence and the spatial coherence. Temporal coherence occurs when all radiating electrons are located within a short bunch of the order of the wavelength of the radiation. In this case the radiation from all electrons is emitted with about the same phase. For spatial coherence the electrons may be contained in a long bunch but the transverse beam emittance must be smaller than the radiation wavelength. In either case there is a smooth transition from incoherent radiation to coherent radiation as determined by a formfactor which depends on the bunch length or transverse emittance.

Similar to the particle beam characterization through its emittance we may do the same for the photon beam and doing so for the horizontal or vertical plane we have with $\sigma_{x,y} = \sigma_r/\sqrt{2}$ and $\sigma_{x',y'} = \sigma_{r'}/\sqrt{2}$ the photon beam emittance

$$\epsilon_{\mathrm{ph},x,y} = \tfrac{1}{2}\sigma_r\sigma_{r'} = \frac{\lambda}{4\pi}\,. \tag{3.49}$$

This is the diffraction limited photon emittance and reducing the electron beam emittance below this value would not lead to an additional reduction in the photon beam emittance. To produce a spatially coherent or diffraction limited radiation source the particle beam emittance must be less than the diffraction limited photon emittance

$$\epsilon_{x,y} \leq \frac{\lambda}{4\pi}\,. \tag{3.50}$$

Obviously, this condition is easier to achieve for long wavelengths. For visible light, for example, the electron beam emittance must be smaller than about 5×10^{-8} rad-m to be a spatially coherent radiation source. After having determined the diffraction limited photon emittance we may also determine the apparent photon beam size and divergence. The photon source extends over some finite length L along the particle path which could be either the path length required for a deflection angle of $2/\gamma$ or a much longer length in the case of an undulator radiation source to be discussed in the next section. With $\sigma_{r'}$ the diffraction limited beam divergence the photons seem to come from a disc with diameter (Fig. 3.8)

$$D = \sigma_{r'}L\,. \tag{3.51}$$

On the other hand, we know from diffraction theory the correlation

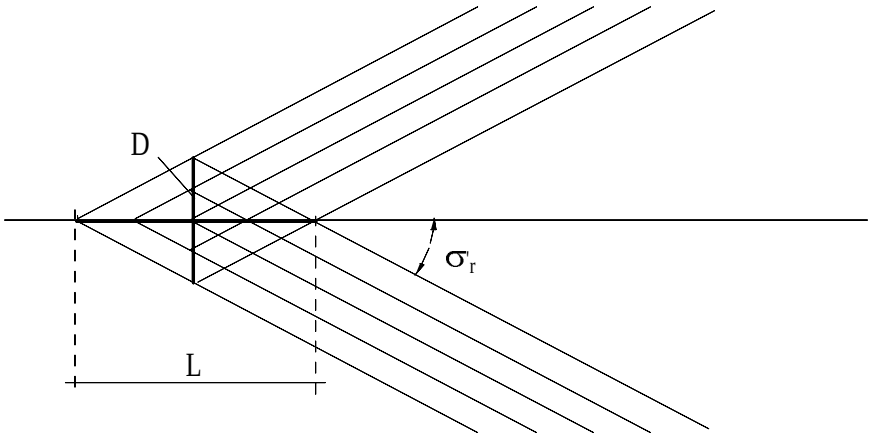

Fig. 3.8. Apparent photon source size

$$D \sin \sigma_{r'} \approx D \, \sigma_{r'} = \lambda \tag{3.52}$$

and eliminating D from both equations gives the diffraction limited photon beam divergence

$$\sigma_{r'} = \sqrt{\frac{\lambda}{L}} . \tag{3.53}$$

With this we get finally from (3.48) also the diffraction limited source size

$$\sigma_r = \frac{1}{2\pi} \sqrt{\lambda L} . \tag{3.54}$$

The apparent diffraction limited, radial photon beam size and divergence depend both on the photon wavelength of interest and the length of the source.

3.6 Temporal Coherence

To discuss the appearance of temporal coherent synchrotron radiation, we consider the radiation emitted from each particle within a bunch. The radiation field at a frequency ω from a single electron is

$$\mathcal{E}_j \propto \mathrm{e}^{\mathrm{i}\left(\omega t + \varphi_j\right)} , \tag{3.55}$$

where φ_j describes the position of the j-th electron with respect to the bunch center. With z_j the distance from the bunch center, the phase is

$$\varphi_j = \frac{2\pi}{\lambda} z_j \,. \tag{3.56}$$

Here we assume that the cross section of the particle beam is small compared to the distance to the observer such that the path length differences from any point of the beam cross section to observer are small compared to the shortest wavelength involved. The radiation power is proportional to the square of the radiation field and summing over all electrons we get

$$\begin{aligned} P(\omega) &\propto \sum_{j,l}^{N_\mathrm{e}} \mathcal{E}_j \mathcal{E}_l^* \propto \sum_{j,l}^{N_\mathrm{e}} \mathrm{e}^{\mathrm{i}\left(\omega t+\varphi_j\right)} \mathrm{e}^{-\mathrm{i}(\omega t+\varphi_l)} \\ &= \sum_{j,l}^{N_\mathrm{e}} \exp \mathrm{i}(\varphi_j - \varphi_l) = N_\mathrm{e} + \sum_{j\neq l}^{N_\mathrm{e}} \exp \mathrm{i}\left(\varphi_j - \varphi_l\right) \,. \end{aligned} \tag{3.57}$$

The first term N_e on the r.h.s. of (3.57) represents the ordinary incoherent synchrotron radiation with a power proportional to the number of radiating particles. The second term averages to zero for all but long wavelengths. The actual coherent radiation power spectrum depends on the particular particle distribution in the bunch. For a storage ring bunch it is safe to assume a Gaussian particle distribution and we use therefore the density distribution

$$\Psi_\mathrm{G}(z) = \frac{N_\mathrm{e}}{\sqrt{2\pi}\sigma} \exp\left(-\frac{z^2}{2\sigma^2}\right) \,, \tag{3.58}$$

where σ is the standard value of the Gaussian bunch length. Instead of summing over all electrons we integrate over all phases and folding the density distribution (3.58) with the radiation power (3.57) we get with (3.56)

$$P(\omega) \propto N_\mathrm{e} + N_\mathrm{e} \frac{N_\mathrm{e}-1}{2\pi\sigma^2} I_1 I_2 \,, \tag{3.59}$$

where the integrals I_1 and I_2 are defined by

$$I_1 = \int_{-\infty}^{+\infty} \exp\left(-\frac{z^2}{2\sigma^2} + \mathrm{i}\, 2\pi \frac{z}{\lambda}\right) \mathrm{d}\, z \,, \tag{3.60a}$$

$$I_2 = \int_{-\infty}^{+\infty} \exp\left(-\frac{w^2}{2\sigma^2} + \mathrm{i}\, 2\pi \frac{w}{\lambda}\right) \mathrm{d}w \,, \tag{3.60b}$$

and $z = \frac{1}{2}\pi\lambda\varphi_j$ and $w = \frac{1}{2}\pi\lambda\varphi_l$. The factor $N_\mathrm{e} - 1$ reflects the fact that we integrate only over different particles. Both integrals are equal to the Fourier transform for a Gaussian particle distribution. With

$$\int_{-\infty}^{+\infty} \exp\left(-\frac{z^2}{2\sigma^2} + \mathrm{i}\, 2\pi \frac{z}{\lambda}\right) \mathrm{d}\, z = \sqrt{2\pi}\sigma \exp\left[-2\pi^2 \left(\frac{\sigma}{\lambda}\right)^2\right] \tag{3.61}$$

we get from (3.59) for the total radiation power at the frequency $\omega = 2\pi c/\lambda$

$$P(\omega) = p(\omega)\ N_{\mathrm{e}}\left[1 + (N_{\mathrm{e}} - 1)\ g^2(\sigma,\lambda)\right] , \tag{3.62}$$

where $p(\omega)$ is the radiation power from one electron and the Fourier transform

$$g^2(\sigma,\lambda) = \exp\left[-2\pi^2\left(\frac{\sigma}{\lambda}\right)^2\right] \tag{3.63}$$

is called the formfactor. With the effective bunch length

$$\ell = \sqrt{2\pi}\sigma \tag{3.64}$$

this formfactor becomes finally

$$g^2(\ell,\lambda) = \exp\left[-\pi\frac{\ell^2}{\lambda^2}\right] . \tag{3.65}$$

The coherent radiation power falls off rapidly for wavelengths as short or even shorter than the effective bunch length ℓ. In Fig. 3.9 the relative coherent radiation power is shown as a function of the effective bunch length in units of the radiation wavelength. The fast drop off is evident and for an effective bunch length of about $\ell \approx 0.6\,\lambda$ the radiation power is reduced to only about 10% of the maximum power for very short bunches, when $\ell \ll \lambda$. Particle beams from a linear accelerator have often a more compressed particle distribution of a form between a Gaussian and a rectangular distribution. If we take the extreme of a rectangular distribution

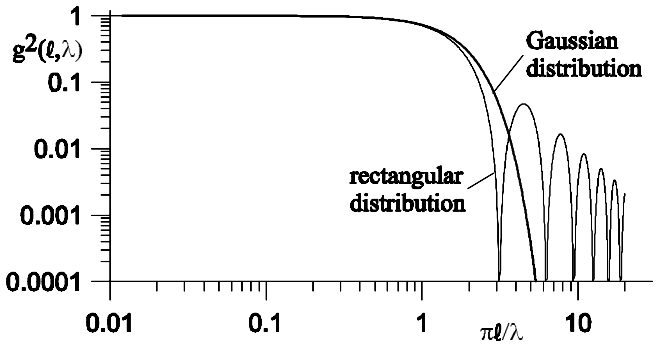

Fig. 3.9. Formfactor $g^2(\ell,\lambda)$ for a Gaussian and rectangular particle distribution

$$\Psi_{\mathrm{r}}(z) = \begin{cases} 1 & \text{for } -\frac{1}{2}\ell < z < \frac{1}{2}\ell \\ 0 & \text{otherwise} \end{cases} , \tag{3.66}$$

we expect to extend the radiation spectrum since the corners and sharp changes of the particle density require a broader spectrum in the Fourier

transform. Following the procedure for the Gaussian beam we get for a rectangular particle distribution the Fourier transform

$$g(\ell) = \frac{\sin x}{x}\,, \tag{3.67}$$

where $x = \pi\ell/\lambda$. Fig. 3.9 also shows the relative coherent radiation power for this distribution and we note a significant but scalloping extension to higher radiation frequencies. Experiments have been performed with picosecond electron bunches from linear accelerators both at Tohoku University [28] and at Cornell University [29] which confirm the appearance of this coherent part of synchrotron radiation.

3.7 Spectral Brightness

The optical quality of a photon beam is characterized by the spectral brightness defined as the six-dimensional volume occupied by the photon beam in phase space

$$\mathcal{B} = \frac{\dot{N}_{\rm ph}}{4\pi^2 \sigma_x\, \sigma_{x'}\, \sigma_y\, \sigma_{y'}\, \frac{{\rm d}\omega}{\omega}}\,, \tag{3.68}$$

where $\dot{N}_{\rm ph}$ is the photon flux defined in (3.35). For bending magnet radiation there is a uniform angular distribution in the deflecting plane and we must therefore replace the Gaussian divergence $\sigma_{x'}$ by the total acceptance angle $\Delta\psi$ of the photon beam line or experiment. The particle beam emittance must be minimized to achieve maximum spectral photon beam brightness. However, unlimited reduction of the particle beam emittance will, at some point, seize to further increase the brightness. Because of diffraction effects the photon beam emittance need not be reduced significantly below the limit (3.49) discussed in the previous section.

For a negligible particle beam emittance and deflection angle $\Delta\psi$ the maximum spectral brightness is therefore from (3.49, 3.68)

$$\mathcal{B}_{\rm max} = \frac{4}{\lambda^2 \frac{{\rm d}\omega}{\omega}} \dot{N}_{\rm ph}\,. \tag{3.69}$$

For a realistic synchrotron light source the finite beam emittance of the particle beam must be taken into account as well which is often even the dominant emittance being larger than the diffraction limited photon beam emittance. We may add both contributions in quadrature and have for the total source parameters

$$\begin{aligned}
\sigma_{\mathrm{tot},x} &= \sqrt{\sigma_{\mathrm{b},x}^2 + \tfrac{1}{2}\,\sigma_r^2}\,, \\
\sigma_{\mathrm{tot},y} &= \sqrt{\sigma_{\mathrm{b},y}^2 + \tfrac{1}{2}\,\sigma_r^2}\,, \\
\sigma_{\mathrm{tot},x'} &= \sqrt{\sigma_{\mathrm{b},x'}^2 + \tfrac{1}{2}\,\sigma_{r'}^2}\,, \\
\sigma_{\mathrm{tot},y'} &= \sqrt{\sigma_{\mathrm{b},y'}^2 + \tfrac{1}{2}\,\sigma_{r'}^2}\,,
\end{aligned} \tag{3.70}$$

where σ_{b} refers to the respective particle beam parameters.

3.7.1 Matching

A finite particle beam emittance does reduce the photon beam brightness from it's ideal maximum. The amount of reduction, however, depends on the *matching to the photon beam*. The photon beam size and divergence are the result of folding the diffraction limited source emittance with the electron beam size and divergence. In cases where the electron beam emittance becomes comparable to the diffraction limited emittance the effective photon beam brightness can be greatly affected by the mutual orientation of both emittances. Matching both orientations will maximize the photon beam brightness.

This matching process is demonstrated in Fig. 3.10. The left side shows a situation of poor matching in 2-dimensional $x - x'$-phase space. In this case the electron beam width is very large compared to the diffraction limited source size and while its divergence is small compared to the diffraction limit. The effective photon beam distribution in phase space is the folding of both electron beam parameters and diffraction limit and is much larger than either one of its components. The photon beam width is dominated by the electron beam width and the photon beam divergence is dominated by the diffraction limit. Consequently, the effective photon density in phase space and photon beam brightness is reduced.

To improve the situation one would focus the electron beam to a smaller beam size at the source point at the expense of beam divergence. The reduction of the electron beam width increases directly the photon beam brightness while the related increase of the electron beam divergence is ineffective because the diffraction limit is the dominant term. Applying more focusing may give a situation shown on the right side of Fig. 3.10 where the folded photon phase space distribution is reduced and the brightness correspondingly increased. Of course, if the electron beam is focused too much we have the opposite situation as discussed. There is an optimum focusing for optimum matching.

To find this optimum we use the particle beam parameters

$$\sigma_{\mathrm{b},x,y}^2 \;=\; \epsilon_{x,y}\beta_{x,y} \qquad \text{and} \qquad \sigma_{\mathrm{b},x',y'}^2 \;=\; \frac{\epsilon_{x,y}}{\beta_{x,y}}\,, \tag{3.71}$$

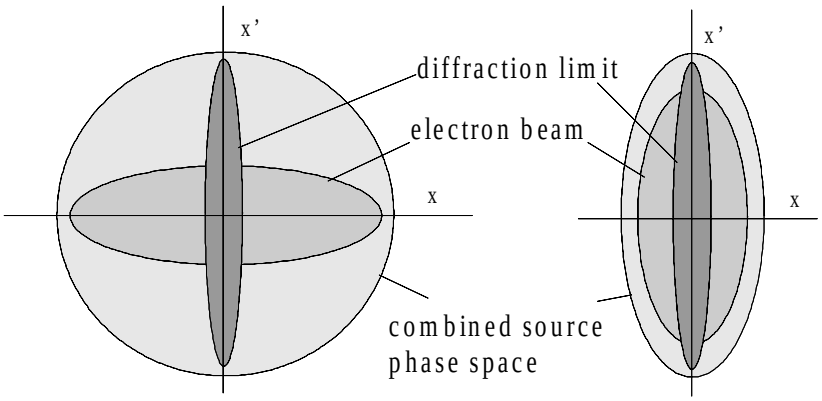

Fig. 3.10. Matching of the electron beam emittance to the diffraction limited emittance to gain maximum photon beam brightness

where $\beta_{x,y}$ are the betatron functions at the photon source location and $\epsilon_{x,y}$ the beam emittances, in the horizontal and vertical plane respectively. Including diffraction limits, the product

$$\sigma_{\mathrm{tot},x}\sigma_{\mathrm{tot},x'} = \sqrt{\epsilon_x\beta_x + \tfrac{1}{2}\,\sigma_r^2}\,\sqrt{\frac{\epsilon_x}{\beta_x} + \tfrac{1}{2}\,\sigma_{r'}^2} \tag{3.72}$$

has a minimum ($\frac{\mathrm{d}}{\mathrm{d}\beta_x}\sigma_{\mathrm{tot},x}\sigma_{\mathrm{tot},x'} = 0$) for

$$\beta_x = \frac{\sigma_r}{\sigma_{r'}} = \frac{L}{2\pi}\,. \tag{3.73}$$

A similar optimum occurs for the vertical betatron function at the source point. The optimum value of the betatron functions at the source point depends only on the length of the undulator.

The values of the horizontal and vertical betatron functions should be adjusted according to (3.73) for optimum photon beam brightness. In case the particle beam emittance is much larger than the diffraction limited photon beam emittance, this minimum is very shallow and almost nonexistent in which case the importance of matching becomes irrelevant. As useful as matching may appear to be, it is not always possible to reach perfect matching because of limitations in the storage ring focusing system. Furthermore it is practically impossible to get a perfect matching for bending magnet radiation since the effective source length L is very small, $L = 2\rho/\gamma$.

Exercises *

Exercise 3.1 (S). Consider an electron storage ring at an energy of 800 MeV, a circulating current of 1 amp and a bending radius of $\rho = 1.784$ m. Calculate the energy loss per turn, and the total synchrotron radiation power from all bending magnets. What would the radiation power be if the particles were 800 MeV muons.

Exercise 3.2 (S). For the electron beam of exercise 3.1 calculate the critical energy and plot the radiation spectrum. What is the useful frequency range for experimentation assuming that the spectral intensity should be within 1 % of the maximum value? Express the maximum useful photon energy in terms of the critical photon energy (only one significant digit!).

Exercise 3.3 (S). What beam energy would be required to produce x-rays from the storage ring of Exercise 3.1 at a critical photon energy of 10 keV? Is that energy feasible from a conventional magnet point of view or would the ring have to be larger? What would the new bending radius have to be?

Exercise 3.4 (S). The design of the European Large Hadron Collider [18], calls for a circular proton accelerator for energies up to 10 TeV. The circumference is 26.7 km and the bending radius $\rho = 2887$ m. Calculate the energy loss per turn due to synchrotron radiation and the critical photon energy. What is the synchrotron radiation power for a circulating beam of 164 ma?

Exercise 3.5 (S). Consider a 7 GeV electron ring with a circulating beam of 200 mA and a bending radius of $\rho = 20$ m. Your experiment requires a photon flux of 10^6 photons/sec at a photon energy of 8 keV, within a band width of 10^{-4} onto a sample with a cross section of 10×10 μm^2 and your experiment is 15 m away from the source point. Can you do your experiment on a bending magnet beam line of this ring?

Exercise 3.6 (S). Bending magnet radiation ($\rho = 2$ m) from a 800 MeV, 500 mA storage ring includes a high intensity component of infrared radiation. Calculate the photon beam brightness for $\lambda = 10$ μm radiation at the experimental station which is 5 m away from the source. The electron beam cross section is $\sigma_{\mathrm{b},x} \times \sigma_{\mathrm{b},y} = 1.1 \times 0.11$ mm and its divergence $\sigma_{\mathrm{b},x'} \times \sigma_{\mathrm{b},y'} = 0.11 \times 0.011$ mrad. What is the corresponding brightness for infrared radiation from a black body radiator at 2000 ^{o}K with a source size of $x \times y = 10 \times 2$ mm? (Hint: the source length $L = \rho 2\theta_{\mathrm{rad}}$, where $\pm\theta_{\mathrm{rad}}$ is the vertical opening angle of the radiation.)

Exercise 3.7 (S). How well are the electron beam parameters of Exercise 3.6 at the source matched to the photon beam? Show the phase space ellipses of both the electron and the photon beam in phase space and in x and y.

* The argument (S) indicates an exercise for which a solution is given in Appendix A.

Exercise 3.8. With the definition of the world time $\tau = \sqrt{-\bar{\mathbf{s}}^2}$ show that $\gamma \mathrm{d}\tau = \mathrm{d}t$ and express the 4-velocity and 4-acceleration in terms of laboratory coordinates.

Exercise 3.9. Verify the equality of (3.1) and (3.2)

Exercise 3.10. Verify the numerical validity of Eqs. (3.20, 3.28, D.5, D.6) and (3.40).

4. Radiation Sources

Deflection of a relativistic particle beam causes the emission of electromagnetic radiation which can be observed in the laboratory system as broadband radiation, highly collimated in the forward direction. The emission is related to the deflection of a charged particle beam and therefore sweeps like a search light across the detection apparatus of the observer. It is this shortness of the observable radiation pulse which implies that the radiation is detected as synchrotron radiation with a broad spectrum as shown in Fig. 3.3. The width of the spectrum is characterized by the critical photon energy (3.26) and depends only on the particle energy and the bending radius of the magnet. Generally, the radiation is produced in bending magnets of a storage ring, where an electron beam is circulating for hours.

In order to adjust the radiation characteristics to special experimental needs, other magnetic devices are being used as synchrotron radiation sources. Such magnets are known as insertion devices since they do not contribute to the overall deflection of the particle beam in the circular accelerator. Their effect is localized and the total deflection in an insertion device is zero. In this chapter, we give a short overview of all radiation sources and their characteristics and postpone more detailed discussions of insertion device radiation to Chap. 10.

4.1 Bending Magnet Radiation

The radiation from bending magnets is emitted tangentially from any point along the curved path like that of a searchlight and appears therefore as a swath of radiation around the storage ring as shown in Fig. 4.1. In the vertical, nondeflecting plane, however, the radiation is very much collimated with a typical opening angle of $\pm 1/\gamma$.

The temporal structure of synchrotron radiation reflects that of the electron beam. Electrons circulating in the storage ring are concentrated into equidistant bunches. The distance between bunches is equal to an integer multiple (usually equal to unity) of the rf-wavelength (60 cm for 500 MHz) while the bunch length itself is of the order of 1 to 3 cm or 30 to 100 ps depending on beam energy and rf-voltage. As a consequence, the photon beam

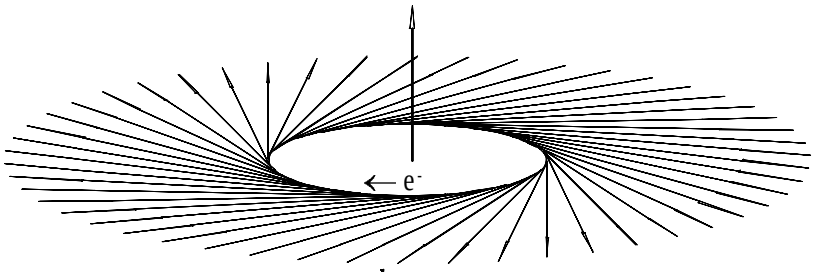

Fig. 4.1. Radiation swath from bending magnets in an electron storage ring

consists of a series of short 30–100 ps flashes every 2 ns (500 MHz) or integer multiples thereof.

Radiation is emitted in a broad spectrum (see Fig. 3.3) reaching, in principal, from mircowaves up to the critically photon energy (3.26) and beyond with fast declining intensities. The long wavelength limit of the radiation spectrum is actually limited by the vacuum chamber, which causes the suppression of radiation at wavelength longer than its dimensions. The strength of bending magnets, being a part of the geometry of the storage ring cannot be freely varied to optimize for desired photon beam characteristics. This is specifically limiting in the choice of the critical photon energy. While the lower photon energy spectrum is well covered even for rather low energy storage rings, the x-ray region requires high beam energies and/or high magnetic fields. Often, the requirements for x-rays cannot be met with existing bending magnet and storage ring parameters.

4.2 Superbends

The critical photon energy from bending magnet radiation (3.28) is determined by the magnet field and the particle energy. The combination of both quantities may not be sufficient to extend the synchrotron radiation spectrum into the hard x-ray regime, especially in low energy storage rings. In this case, it is possible to replace some or all original bending magnets by much stronger but shorter magnets, called superbends. To be more specific, conventional bending magnets are replaced by high field, shorter superconducting magnets deflecting the electron beam by the same angle to preserve the storage ring geometry. Since conventional bending magnet fields rarely exceed 1.5 Tesla, but superconducting magnets can be operated at 5 to 6 Tesla or higher, one can gain a factor of 3 to 4 in the critical photon energy and extend the photon spectrum towards or even into the hard x-ray regime.

4.3 Wavelength Shifter

The installation of superbends is not always feasible or desirable. To still meet the need for harder x-ray radiation in a low energy storage ring, it is customary to use a wavelength shifter. Such a device may consist of three or five superconducting dipole magnets with alternating magnetic field directions. For this latter reason, a wavelength shifter is a true insertion device. The limitation to three or five poles is purely technical and may be eased as superconducting magnet and cryo-technology progresses. Figure 4.2 shows schematically a three-pole wavelength shifter.

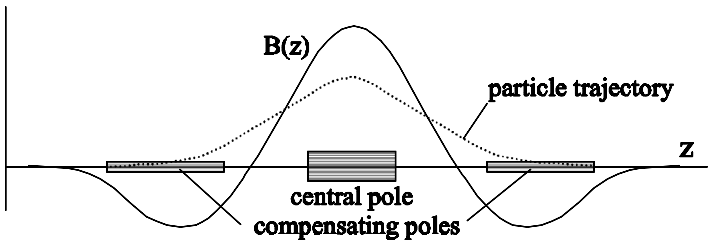

Fig. 4.2. Magnetic field distribution along the beam path for a wave length shifter

The particle beam passing through this wavelength shifter is deflected up and down or left and right in such a way that no net deflection remains. To meet this condition, the longitudinal field distribution of a horizontally deflecting wavelength shifter must obey the condition

$$\int_{-\infty}^{\infty} B_y\,(y=0,z)\;\mathrm{d}\,z = 0\,. \tag{4.1}$$

A wavelength shifter with such field properties is neutral on the geometry of the particle beam path through a storage ring and therefore can be made in principle as strong as necessary or technically feasible.

Only the central high field pole is used as the radiation source, while the two side poles compensate the beam deflection from the central pole. In a five-pole wavelength shifter the three central poles would be used as radiators, while both end poles again act as compensators. Mostly, the end poles are longer than the central poles and operate at a lower field. As their name implies, the primary objective in wavelength shifters is to extend the photon spectrum while the enhancement of intensity through radiation accumulation from many poles, while desirable, is of secondary importance. To maximize the desired effect, wavelength shifters are often constructed as high field superconducting magnets to maximize the critical photon energy for the given particle beam energy. Some limitations apply for such devices as well as for

any other insertion device. The end fields of magnets can introduce particle focusing and nonlinear field components may introduce aberrations and cause beam instability. Both effects must either be kept below a critical level or be compensated.

4.4 Wiggler Magnet Radiation

The principle of a wavelength shifter is extended in the case of a wiggler-magnet. Such a magnet consists of a series of equal dipole magnets with alternating magnetic field direction. Again, the end poles must be configured to make the total device neutral to the geometry of the particle beam path such that the condition (4.1) is met.

The main advantage of using many magnet poles is to increase the photon flux. Like a single bending magnet, each of the N_{m} magnet poles produces a fan of radiation in the forward direction and the total photon flux is N_{m}-times larger than that from a single pole. Wiggler-magnets may be constructed as electromagnets with fields up to $2T$ to function both as a flux enhancer and as a more modest wavelength shifter compared to the superconducting type. An example of an 8-pole, 1.8 T electromagnetic wiggler-magnet [32] is shown in Fig. 4.3.

In this picture, the magnet gap is wide open, to display the flat vacuum chamber running through the magnet between the poles. The pole pieces in the lower row are visible surrounded by water cooled excitation coils. During operation, both rows of wiggler poles are closed to almost touch the flat vacuum chamber. When the magnet is closed, a maximum magnetic field of 1.8 T can be obtained. Strong fields can be obtained from electromagnets, but the space requirement for the excitation coils limits the number of poles that can be installed within a given length.

Progress in the manufacturing of high field permanent magnet material permits the installation of many more poles into the same space compared to an electromagnet. An example of a modern 26 pole, 2.0 T permanent magnet wiggler magnet is shown in Fig. 4.4 [33].

Figure 4.4 shows the wiggler magnet during magnetic measurement with the rail in front of the magnet holding and guiding the Hall probe. The increased number of poles and simplified design compared to the electromagnetic wiggler in Fig. 4.3 are clearly visible.

For short wiggler poles, we express the magnetic field by

$$B_y\,(x, y = 0, z) = B_0 \sin \frac{2\pi z}{\lambda_{\mathrm{p}}} \tag{4.2}$$

and the maximum beam deflection from the axis is equal to the deflection angle per half pole (6.11)

Fig. 4.3. Electromagnetic wiggler magnet with eight 1.8 T poles

$$\vartheta = \frac{B_0}{B\rho}\int_0^{\lambda_\mathrm{p}/4} \sin\frac{2\pi z}{\lambda_\mathrm{p}}\,\mathrm{d}\,z = \frac{B_0}{B\rho}\frac{\lambda_\mathrm{p}}{2\pi}\,, \tag{4.3}$$

where $B\rho$ is the beam rigidity defined in (6.7). Multiplying this with the beam energy γ, we define the wiggler strength parameter

$$K = \gamma\vartheta = \frac{[c]\,eB_0}{mc^2}\frac{\lambda_\mathrm{p}}{2\pi} = 0.934\,B_0\,(\mathrm{T})\;\lambda_\mathrm{p}\,(\mathrm{cm})\;. \tag{4.4}$$

This wiggler strength parameter is generally much larger than unity. Conversely, a series of alternating magnet poles is called a wiggler magnet if the strength parameter $K \gg 1$ and condition (4.1) is met. As we will see later, a weak wiggler magnet with $K \ll 1$ is called an undulator and produces radiation with significant different characteristics. The magnetic field strength can be varied in both electromagnetic wigglers as well as in permanent magnet wigglers . While this is obvious for electromagnets, the magnetic field strength in permanent magnets depends on the distance between magnet poles or on the gap height g. By varying mechanically the gap height of a permanent magnet wiggler, the magnetic field strength can be varied as well. The field strength also depends on the period length and on the design and magnet materials used. For a wiggler magnet constructed as a hybrid magnet with Vanadium Permendur poles, the field strength along the midplane axis scales

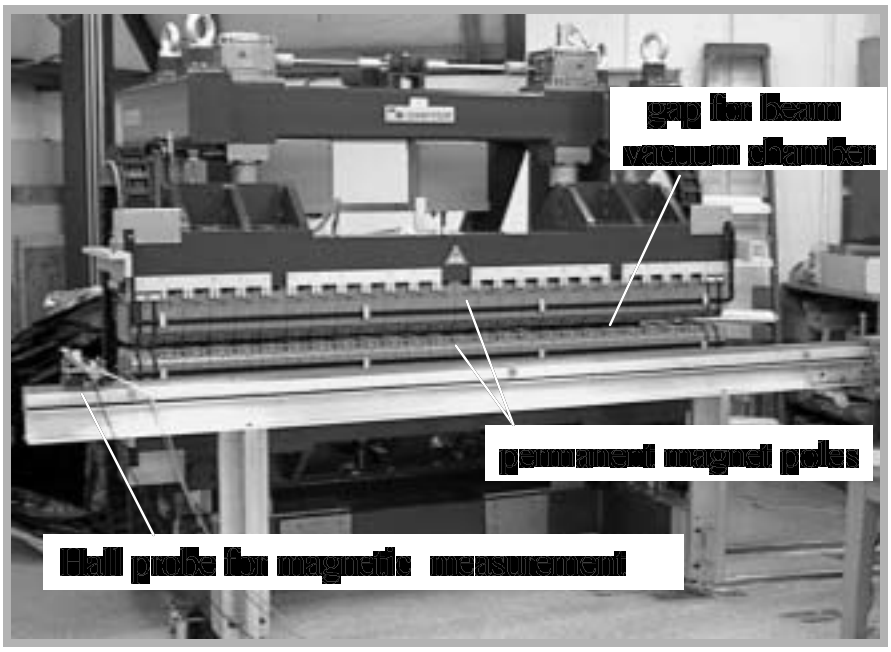

Fig. 4.4. Permanent magnet wiggler magnet with 26 poles, a 175 mm period length and a maximum field of 2.0 T

approximately like [34]

$$B_y\,(\mathrm{T}) \approx 3.33 \exp\left[-\frac{g}{\lambda_\mathrm{p}}\left(5.47 - 1.8\frac{g}{\lambda_\mathrm{p}}\right)\right] , \quad \text{for} \;\; 0.1\,\lambda_\mathrm{p} \lessapprox g \lessapprox 10\,\lambda_\mathrm{p} , \;\; (4.5)$$

where g is the gap aperture between magnet poles. This dependency is also shown in Fig. 4.5 and we note immediately that the field strength drops off dramatically for magnet gaps of the order of a period length or greater.

On the other hand, significant field strengths can be obtained for small gap apertures and it is therefore important to install the insertion device at a location, where the beam dimension normal to the deflection plane is small.

The total radiation power can be derived by integrating (3.9) through the wiggler magnet. The result of this integration is

$$\langle P_\gamma \rangle = \tfrac{1}{3}\, r_\mathrm{c} mc^2\, c\, \gamma^2 K^2 \frac{4\pi^2}{\lambda_\mathrm{p}^2} , \qquad (4.6)$$

or in practical units

$$\langle P_\gamma\,(\mathrm{W}) \rangle = 632.7\, E^2\, B_0^2\, I\, L_\mathrm{u} , \qquad (4.7)$$

where I is the ciculating beam current, and $L_\mathrm{u} = N_\mathrm{p}\lambda_\mathrm{p}$ the length of the wiggler magnet.

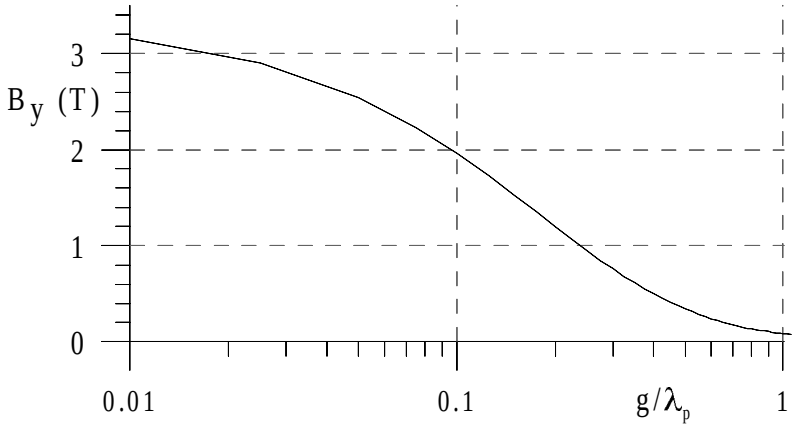

Fig. 4.5. On-axis field strength in a vanadium Permendur hybrid wiggler magnet as a function of gap aperture (4.5)

For a sinusoidal field distribution $B_0 \sin \frac{2\pi}{\lambda_p} z$, the desired wavelength shifting property of a strong wiggler magnet can be obtained only in the forward direction. Radiation emitted at a finite angle with respect to the wiggler axis is softer because it is generated at a source point where the field is lower. The hardest radiation is emitted in the forward direction from the crest of the magnetic field. For a distance Δz away from the crest, the emission angle in the deflection plane is $\psi = \frac{1}{\rho_0} \frac{\lambda_p}{2\pi} \sin \frac{2\pi}{\lambda_p} \Delta z$ and the curvature at the source point is $\frac{1}{\rho} = \frac{1}{\rho_0} \sqrt{1 - \left(\frac{\gamma\psi}{K}\right)^2}$, where we have made use of (4.4). Consequently, the critical photon energy for radiation in the direction ψ with respect to the wiggler axis varies with the emission angle ψ like

$$\varepsilon_c = \varepsilon_{c0} \sqrt{1 - \left(\frac{\gamma\psi}{K}\right)^2} . \tag{4.8}$$

At the maximum deflection angle $\psi_{max} = \theta = K/\gamma$ the critical photon energy has dropped to zero, reflecting a zero magnetic field at the source point.

This property is undesirable if more than one experimental station is supposed to receive hard radiation from the same wiggler magnet. The strength of the wiggler magnet sweeps the electron beam over a considerable angle, a feature which can be exploited to direct radiation not only to one experimental station along the axis but also to two or more side-stations on either side of the wiggler axis. However, these side beam lines at an angle $\psi \neq 0$ receive softer radiation than the main beam line. This can be avoided if the poles of the wiggler magnet are lengthened thus flattening the sinusoidal field crest.

As the flat part of the field crest is increased, hard radiation is emitted into an increasing angular cone.

4.5 Undulator Radiation

So far, we discussed insertion devices designed specifically to harden the radiation spectrum or to increase the radiation intensity. Equally common is the implementation of insertion devices to optimize photon beam quality by maximizing its brightness or to provide specific characteristics like elliptically polarized radiation. This is done with the use of undulator magnets, which are constructed similar to wiggler magnets, but are operated at a much reduced field strength.

Fundamentally, an undulator magnet causes particles to be only very weakly deflected with an angle of less than $\pm 1/\gamma$ and consequently the transverse motion of particles is nonrelativistic. In this picture, the electron motion viewed from far away along the beam axis appears as a purely sinusoidal transverse oscillation similar to the electron motion in a linear radio antenna driven by a transmitter and oscillating at the station's carrier frequency. The radiation emitted is therefore monochromatic with a period equal to the oscillation period.

To be more precise, viewed from far away the particle appears to be at rest or uniform motion as long as the electron has not yet reached the undulator magnet. Upon entering the magnet the electron performs sinusoidal transverse oscillations and returns to its original motion again after it exits the undulator. As a consequence of this motion and in light of earlier discussions, we observe emission of radiation at the frequency of the transverse oscillating beam motion. If N_p is the number of undulator periods, the electric field lines have been perturbed periodically N_p-times and the radiation pulse is composed of N_p oscillations. In the particle rest frame $\mathcal{L}^*$ the undulator periodlength is Lorentz contracted to $\lambda_\gamma^* = \lambda_\mathrm{p}/\gamma$ which is the wavelength of the emitted radiation. Because the radiation includes only a finite number of N_p oscillations, the radiation is not quite monochromatic but rather quasi monochromatic with a band width of $1/N_\mathrm{p}$. This situation is illustrated in Fig. 4.6**a**.

In Fig. 4.6**b** the radiation lobe and spectrum is shown the laboratory system. The monochromatic nature of the radiation is somewhat lost because radiation emitted at different angles experiences different Doppler shifts. Of course, the radiation is again quasi monochromatic even in the laboratory system when observed through a narrow pin hole along the axis. This monochromatic radiation is called the fundamental undulator radiation and has for $K \ll 1$ a wavelength of

$$\lambda_\gamma \approx \frac{\lambda_\mathrm{p}}{2\gamma^2}. \tag{4.9}$$

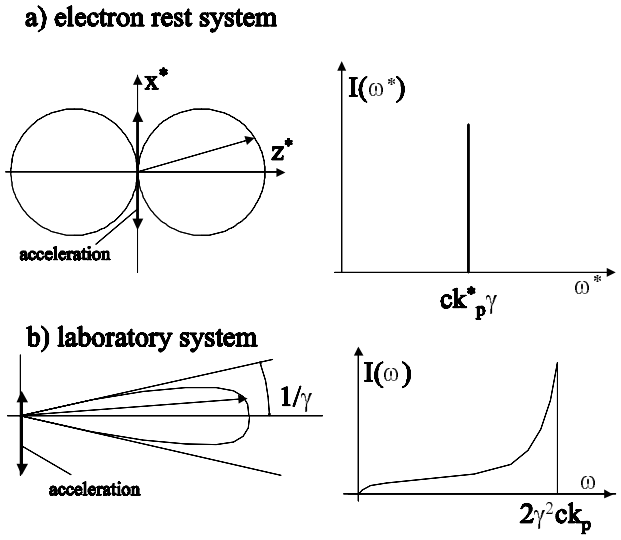

Fig. 4.6. Beam dynamics and radiation lobes in the particle rest system (a) and the laboratory system (b) for a weak undulator ($K \ll 1$).

The situation becomes more complicated as the undulator strength is increased. Two new phenomena appear, an oscillatory forward motion and a transverse relativistic effect. The first phenomenon that we need to discuss is the fact that the transverse motion becomes relativistic. As a consequence of this, the pure sinusoidal transverse motion becomes distorted. There is a periodic Lorentz contraction of the longitudinal coordinate, which is larger when the particle travels almost parallel to the axis in the vicinity of the oscillation crests and is smaller when in between crests. The cusps and valleys of the sinusoidal motion become Lorentz-contracted in the particle system thus perturbing the sinusoidal motion as shown in Fig. 4.7.

This perturbation is symmetric about the cusps and valleys causing the appearance of odd and only odd (3^{rd}, 5^{th}, 7^{th} ...) harmonics of the fundamental oscillation period. From an undulator of medium strength ($K \gtrsim 1$) we observe therefore along the axis a line spectrum of odd harmonics in addition to the fundamental undulator radiation.

The second phenomenon to be discussed is the periodic modulation of the longitudinal motion. The longitudinal component of the particle velocity is maximum when the particle travels close to the crest of the oscillations and at a minimum when it is close to the axis crossings. In a reference system which moves uniformly with the average longitudinal particle velocity along the axis, the particle performs periodic longitudinal oscillations in addition to the transverse oscillations. For each transverse period, the particle performs two longitudinal oscillations and its path looks therefore like a figure of "8". This situation is shown in Fig. 4.8.

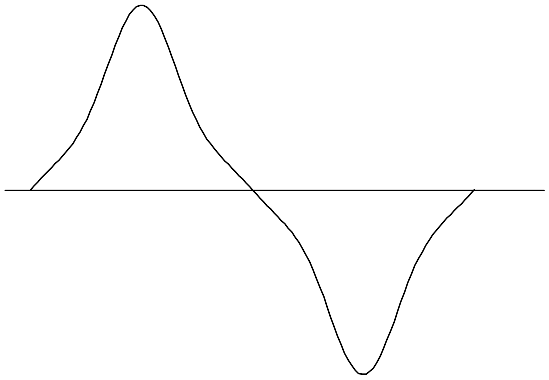

Fig. 4.7. Distortion of sinusoidal motion due to relativistic perturbation of transverse motion

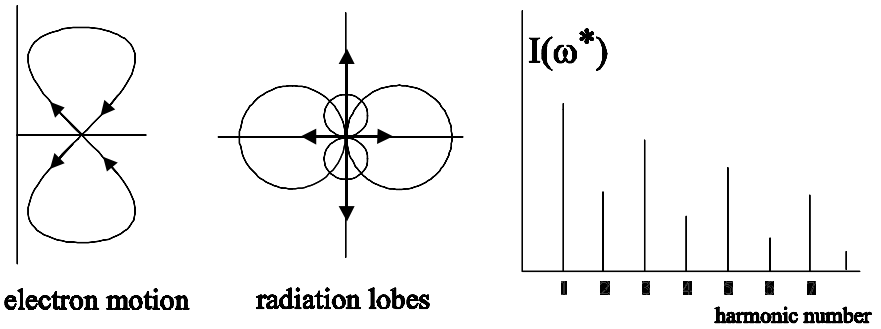

Fig. 4.8. Beam dynamics and radiation lobes in the particle rest system (**a**) and the laboratory system (**b**) for a stronger undulator ($K \gtrsim 1$).

We have now two orthogonal accelerations, one transverse and one longitudinal, and two radiation lobes as indicated in Fig. 4.8. Since the longitudinal motion occurs at twice the frequency of the transverse motion, we observe now radiation also at twice the fundamental frequency. Of course, the relativistic perturbation applies here too and we have therefore a line spectrum which includes two series, one with all odd harmonics and one with only even harmonics. Even and odd harmonic radiation is emitted in the particle system in orthogonal directions and therefore we find both radiation lobes in the laboratory system spatially separated as well. The odd harmonics all have their highest intensities along the undulator axis, while the even harmonic radiation is emitted preferentially into an angle $1/\gamma$ with respect to the axis and has zero intensity along the axis.

In another equally valid view of undulator radiation, the static and periodic magnetic undulator field appears in the rest frame of the electron as a Lorentz contracted electromagnetic field or as monochromatic photon of

wavelength $\lambda^* = \lambda_p/\gamma$. The emission of photons can therefore be described as Thomson scattering of virtual photons by free electrons [35] resulting in monochromatic radiation in the direction of the particle path. Viewed from the laboratory system, the radiation is Doppler shifted and applying (2.20) the wavelength of the backscattered photons is

$$\lambda_{ph} = \frac{\lambda_p}{\gamma^2 (1 + \beta n_z^*)} . \tag{4.10}$$

Viewing the radiation parallel to the forward direction ($\vartheta \approx 0$), (2.23) becomes with $n_z = \cos\vartheta^* \approx 1 - \frac{1}{2}\vartheta^{*2}$, and $\beta \approx 1$

$$1 + \beta n_z^* = \frac{\beta + n_z^*}{n_z} \approx 2 - \tfrac{1}{2}\frac{\vartheta^{*2}}{n_z} . \tag{4.11}$$

Setting $n_z \approx 1$, the fundamental wavelength of the emitted radiation is

$$\lambda_1 = \frac{\lambda_p}{\gamma^2} \frac{1}{2 - \frac{1}{2}\frac{\vartheta^{*2}}{n_z}} \approx \frac{\lambda_p}{2\gamma^2}\left(1 + \tfrac{1}{4}\,\vartheta^{*2}\right) . \tag{4.12}$$

With (2.24) the angle ϑ^* of the particle trajectory with respect to the direction of observation is transformed into the laboratory system for $\vartheta^* = 2\gamma\vartheta$. We distinguish two configurations. One where $\vartheta = K/\gamma$ =const. describing the particle motion in a helical undulator, where the magnetic field being normal to the undulator axis rotates about this axis. The other more common case is that of a flat undulator , where the particle motion follows a sinusoidal path in which case $\vartheta = \vartheta_{und} + \vartheta_{obs}$. Here $\vartheta_{und} = \frac{K}{\gamma}\sin k_p z$ is the observation angle due to the periodic motion of the electrons in the undulator and ϑ_{obs} is the actual observation angle. With these definitions and taking the average $\langle \vartheta_{und}^2 \rangle$ we get $\gamma^2\vartheta^2 = \frac{1}{2}K^2 + \gamma^2\vartheta_{obs}^2$. Depending on the type of undulator, the wavelength of radiation from an undulator with a strength parameter K is

$$\lambda_1 = \begin{cases} \dfrac{\lambda_p}{2\gamma^2}\left(1 + K^2 + \gamma^2\vartheta_{obs}^2\right) & \text{for a helical undulator} \\ \dfrac{\lambda_p}{2\gamma^2}\left(1 + \frac{1}{2}K^2 + \gamma^2\vartheta_{obs}^2\right) & \text{for a flat undulator.} \end{cases} \tag{4.13}$$

From now on only flat undulators will be considered in this text and readers interested in more detail of helical undulators are referred to [36]. No special assumptions have been made here which would prevent us to apply this derivation also to higher harmonic radiation and we get the general expression for the wavelength of the k-th harmonic

$$\lambda_k = \frac{\lambda_p}{2\gamma^2 k}\left(1 + \tfrac{1}{2}K^2 + \gamma^2\vartheta_{obs}^2\right) . \tag{4.14}$$

The additional terms $\frac{1}{2}K^2 + \gamma^2\vartheta_{obs}^2$ compared to (4.9) comes from the correct application of the Doppler effect. Since the particles are deflected periodically

in the undulator, we view even the on-axis radiation at a periodically varying angle which accounts for the $\frac{1}{2}K^2$-term. Of course, observation of the radiation at a finite angle $\vartheta_{\rm obs}$ generates an additional red-shift expressed by the term $\gamma^2\vartheta^2_{\rm obs}$.

In more practical units, the undulator wavelengths for the k-th harmonic are expressed from (4.14) by

$$\lambda_k\,(\text{Å}) = 13.056\,\frac{\lambda_{\rm p}\,(\text{cm})}{k\,E^2\,(\text{GeV}^2)}\left(1+\tfrac{1}{2}\,K^2+\gamma^2\vartheta^2_{\rm obs}\right) \tag{4.15}$$

and the corresponding photon energies are

$$\epsilon_k\,(\text{eV}) = 950\,\frac{k\,E^2\,(\text{GeV}^2)}{\lambda_{\rm p}\,(\text{cm})\left(1+\frac{1}{2}\,K^2+\gamma^2\vartheta^2_{\rm obs}\right)}\,. \tag{4.16}$$

Recollecting the discussion of undulator radiation, we found that the first harmonic or fundamental radiation is the only radiation emitted for $K \ll 1$. As the undulator parameter increases, however, the oscillatory motion of the particle in the undulator deviates from a pure sinusoidal oscillation. For $K > 1$ the transverse motion becomes relativistic, causing a deformation of the sinusoidal motion and the creation of higher harmonics. These harmonics appear at integral multiples of the fundamental radiation energy. Only odd harmonics are emitted along the axis ($\vartheta \approx 0$) while even harmonics are emitted into a small angle from the axis. As the undulator strength is further increased more and more harmonics appear, each of them having a finite width due to the finite number of undulator periods, and finally merging into the well-known broad spectrum of bending or wiggler magnet radiation (Fig. 4.9).

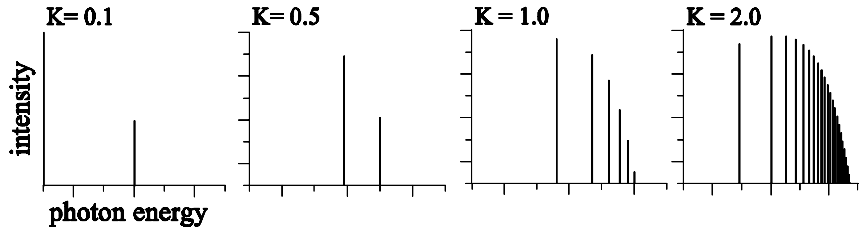

Fig. 4.9. Transition from quasi-monochromatic undulator radiation to broad band wiggler radiation

We find no fundamental difference between undulator and wiggler magnets, one being just a stronger version of the other. From a practical point of view, the radiation characteristics are very different and users of synchrotron

radiation make use of this difference to optimize their experimental capabilities. In Chapter 10 we will discuss the features of undulator radiation in much more detail.

The electron motion through an undulator with N_p periods includes that many oscillations and so does the radiation field. Applying a Fourier transformation to the field, we find the spectral width of the radiation to be

$$\frac{\Delta\lambda}{\lambda} = \frac{1}{N_\mathrm{p}} . \tag{4.17}$$

In reality, this line width is increased due to the finite aperture of the radiation detection elements, and due to a finite energy spread and finite divergence of the electron beam. Typical experimental undulator spectra are shown in Fig. 4.10 for increasing undulator strength K [37].

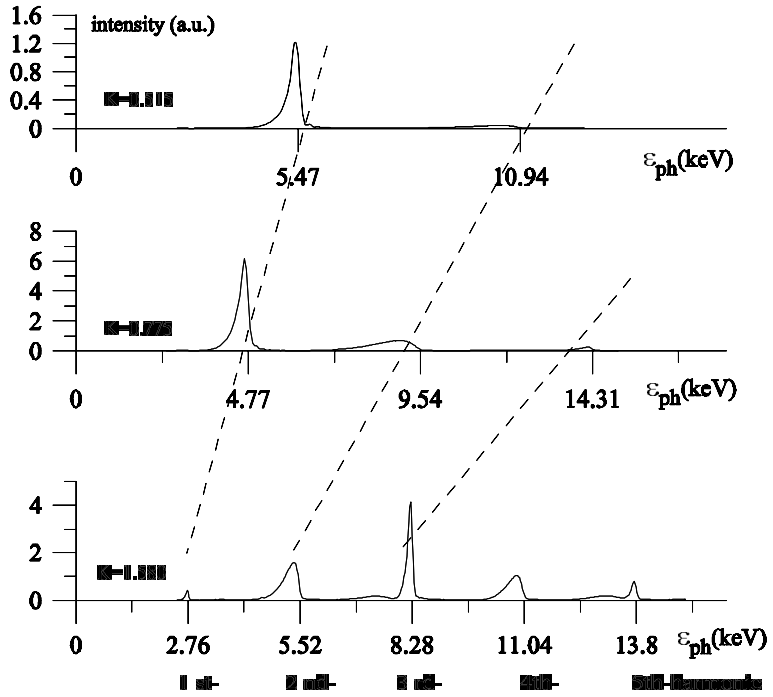

Fig. 4.10. Measured radiation spectrum from an undulator for different strength parameters K . The intensity at low photon energies are reduced by absorption in a Be-window

Although this radiation was measured through a pin hole and on-axis, we still recognize even harmonic radiation since the pin hole covers a finite solid angle and lets some even harmonic radiation through. Furthermore,

the measured intensities of the line spectrum does not reflect the theoretical expectation for the lowest harmonics at higher values of K. This is an artifact of the experimental circumstances, where the x-rays have been extracted from the storage ring vacuum chamber through a Be-window. Such a window works very well for hard x-rays but absorbs heavily at photon energies below some 3 keV.

The concentration of all radiation into one or few spectral lines is very desirable for many experiments utilizing monochromatic photon beams since radiation is produced only in the vicinity of the desired wavelength at high brightness. Radiation at other wavelengths creating undesired heating effects on optical elements and samples is greatly eliminated.

4.6 Back Scattered Photons

The principle of Thomson backscattering or Compton scattering of the static undulator fields can be expanded to that of photon beams colliding head on with the particle beam. In the electron system of reference the electromagnetic field of this photon beam looks fundamentally no different than the electromagnetic field from the undulator magnet. We may therefore apply similar arguments to determine the wavelength of back scattered photons. The basic difference of both effects is that in the case of back scattered photons the photon beam moves with the velocity of light towards the electron beam and therefore the electron *sees* twice the Lorentz contracted photon frequency and we expect therefore a back scattered photon beam at twice Doppler shifted frequency. That extra factor of two does not apply for undulator radiation since the undulator field is static and the relative velocity with respect to the electron beam is c. If λ_{L} is the wavelength of the incident radiation or incident laser, the wavelength of the backscattered photons is

$$\lambda_\gamma = \frac{\lambda_{\mathrm{L}}}{4\gamma^2}\left(1+\gamma^2\vartheta_{\mathrm{obs}}^2\right) , \tag{4.18}$$

where ϑ_{obs} is the angle between the direction of observation and the particle beam axis. Scattering, for example, a high intensity laser beam from high-energy electrons produces a monochromatic beam of hard x-rays which is highly collimated within an angle of $\pm 1/\gamma$. If the laser wavelength is, for example, λ_{L}=10 μm and the particle energy is 100 MeV the wavelength of the backscattered x-rays would be 1.3 Å or the photon energy would be 9.5 keV which is well within the hard x-ray regime.

4.6.1 Photon Flux

The intensity of the backscattered photons can be calculated in a simple way utilizing the Thomson scattering cross section [35]

$$\sigma_{\mathrm{Th}} = \tfrac{8\pi}{3} r_{\mathrm{c}}^2 = 6.65 \times 10^{-25}\ \mathrm{cm}^2. \tag{4.19}$$

The total scattering event rate or the number of back scattered photons per unit time is then

$$N_{\mathrm{sc}} = \sigma_{\mathrm{Th}}\, \mathcal{L}\,, \tag{4.20}$$

where $\mathcal{L}$ is called the luminosity. The value of the luminosity is independent of the nature of the physical reaction and depends only on the intensities and geometrical dimensions of the colliding beams. The definition of the luminosity is the product of the target density of one beam by the "particle"-flux of the other beam onto this target. Therefore the luminosity can be determined by folding the particle density in one beam with the incident "particles" per unit time of the other beam. Obviously, only those parts of the beam cross sections count which overlap with the cross section of the other beam. For simplicity, we assume a Gaussian distribution in both beams and assume that both beam cross sections are the same. In a real setup one would focus the electron beam and the photon beam to the same optimum cross section given by the Rayleigh length (11.58). We further consider the particle beam as the target for the photon beam.

With N_{e} electrons in each bunch of the particle beam within a cross section of $2\pi\sigma_x\sigma_y$ the particle density is $N_{\mathrm{e}}/\,2\pi\sigma_x\sigma_y$.We consider now a photon beam with the same time structure as the electron beam. If this is not the case only that part of the photon beam which actually collides with the particle beam within the collision zone may be considered. For an effective photon flux $\dot{N}_{\mathrm{ph}}$ the luminosity is

$$\mathcal{L} = \frac{N_{\mathrm{e}} \dot{N}_{\mathrm{ph}}}{2\pi\sigma_x\sigma_y}\,. \tag{4.21}$$

Although the Thomson cross-section and therefore the photon yield is very small, this technique can be used to produce photon beams with very specific characteristics. By analyzing the scattering distribution this procedure can also be used to determine the degree of polarization of an electron beam in a storage ring.

So far, it was assumed that the incident and scattered photon energies are much smaller than the particle energy in which case it was appropriate to use the classical case of Thomson scattering. However, we note from (4.18) that the backscattered photonenergy increases quadratically with the particle energy and therefore at some energy the photon energy becomes larger than the particle energy which is nonphysical. In case of large photon energies comparable with the particle energy, Compton corrections [38] [39] [40] must be included. The Compton cross-section for head-on collision is given by [41]

$$\sigma_{\mathrm{C}} = \frac{3\,\sigma_{\mathrm{Th}}}{4x}\left[\left(1 - \frac{4}{x} - \frac{8}{x^2}\right)\ln\left(1+x\right) + \tfrac{1}{2} + \frac{8}{x^2} - \frac{1}{2\left(1+x\right)^2}\right], \tag{4.22}$$

where $x = \frac{4\gamma\hbar\omega_0}{mc^2}$, and $\hbar\omega_0$ the incident photon energy. The energy spectrum of the scattered photons is then [41]

$$\frac{\mathrm{d}\,\sigma_{\mathrm{C}}}{\mathrm{d}\,y} = \frac{3\,\sigma_{\mathrm{Th}}}{4x}\left[1 - y + \frac{1}{1-y} - \frac{4y}{x\,(1+y)} + \frac{4y^2}{x^2\,(1-y)^2}\right], \tag{4.23}$$

where $y = \hbar\omega/E$ is the scattered photon energy in units of the particle energy.

Exercises *

Exercise 4.1 (S). Assume a proton storage ring in space surrounding the earth at an average radius of 150 km. Further, assume a circulating current of 10 mA and 50 W of rf-power available to compensate for synchrotron radiation. What is the maximum proton energy that can be reached with permanent magnets producing a maximum field of 2 Tesla? Is the energy limited by the maximum magnetic field or synchrotron radiation losses? Calculate the energy loss per turn, critical photon energy, and the total radiation power.

Exercise 4.2 (S). Specify main parameters for a synchrotron radiation source for digital subtractive angiography. In this medical procedure, two hard x-ray beams are selected from monochromators, one just below and the other just above the K-edge of iodine. With each beam an x-ray picture of, for example, the human heart with peripheral arteries is taken, while the blood stream contains some iodine. Both pictures differ only where there is iodine because of the very different absorption coefficient for both x-ray beams. Displaying the difference of both pictures shows the blood vessels alone. Select parameters for beam energy, wiggler magnet field, number of poles and beam current to produce an x-ray beam at 33 keV of 2×10^{14} photons/sec/0.1%BW into an opening angle of 25 mrad, while keeping the 66 keV and 99 keV contamination to less than 1% of the 33 keV radiation.

Exercise 4.3 (S). Consider a 30-pole wiggler magnet with 10 cm wide poles, a field distribution $B_y(\mathrm{T}) = 2.0 \sin\frac{2\pi}{\lambda_{\mathrm{p}}} z$ and a period length of $\lambda_{\mathrm{p}} = 7.0$ cm. Determine the magnetic force between the upper and lower row of poles. Is this force attractive or repulsive? why?

Exercise 4.4 (S). Derive an expression for the total synchrotron radiation power from a wiggler magnet.

Exercise 4.5 (S). In Chapter 2 we described undulator radiation as a result of Compton scattering of the undulator field by the electrons. Derive the fundamental undulator wavelength from the process of Compton scattering.

* The argument (S) indicates an exercise for which a solution is given in Appendix A.

Exercise 4.6 (S). An undulator is constructed from hybrid permanent magnet material with a period length of $\lambda_p = 5.0$ cm. What is the fundamental wavelength range in a 800 MeV storage ring and in a 7 GeV storage ring if the undulator gap is to be at least 10 mm?

Exercise 4.7 (S). Determine the tuning range for a hybrid magnet undulator in a 2.5 GeV storage ring with an adjustable gap $g \geqq 10$ mm. Plot the fundamental wavelength as a function of magnet gap for two different period lengths, $\lambda_p = 15$ mm and $\lambda_p = 75$ mm. Why are the tuning ranges so different?

Exercise 4.8. Consider an electron storage ring at an energy of 1 GeV, a circulating current of 200 mA and a bending radius of $\rho = 2.22$ m. Calculate the energy loss per turn, the critical energy and the total synchrotron radiation power. At what frequency in units of the critical frequency has the intensity dropped to 1% of the maximum? Plot the radiation spectrum and determine the frequency range available for experimentation.

Exercise 4.9. What beam energy would be required to produce x-rays from the storage ring of exercise 4.8 at a critical photon energy of 10 keV? Is that energy feasible from a conventional magnet point of view or would the ring have to be larger? What would the new beam energy and bending radius have to be?

Exercise 4.10. Consider a storage ring with an energy of 1 GeV and a bending radius of $\rho = 2.5$ m. Calculate the angular photon flux density $\mathrm{d}\dot{N}/\mathrm{d}\psi$ for a high photon energy $\hat{\varepsilon}$ where the intensity is still 1% of the maximum spectral intensity. What is this maximum photon energy? Installing a wavelength shifter with a field of $B = 6$ T allows the spectrum to be greatly extended. By how much does the spectral intensity increase at the photon energy $\hat{\varepsilon}$ and what is the new photon energy limit for the wavelength shifter?

Exercise 4.11. Derive an expression for the average velocity component $\bar{\beta}_z = \bar{v}_z/c$ of a particle traveling through an undulator magnet of strength K.

Exercise 4.12. Consider an electromagnetic wavelength shifter in a 1 GeV storage ring with a central pole length of 30 cm and a maximum field of 6 T. The side poles are 60 cm long and for simplicity, assume that the field in all poles has a sinusoidal distribution along the axis. Determine the focal length due to edge focusing for the total wavelength shifter. To be negligible, the focal length should typically be longer than about 30 m. Is this the case for this wavelength shifter?

Exercise 4.13. Use the tuning graphs of the two undulators of problem 4.7 and add the tuning ranges for the 3^{rd} and 5^{th} harmonic to it. Is it possible in both cases to produce radiation over the whole spectral range between 1^{st} and 5^{th} harmonic?

Exercise 4.14. Consider a 26-pole wiggler magnet with a field $B_y(\mathrm{T}) = 2.0 \sin \frac{2\pi}{\lambda_\mathrm{p}} z$ and a period length of $\lambda_\mathrm{p} = 15.0$ cm as the radiation source for a straight through photon beam line and two side stations at an angle $\vartheta = \pm 4$ mr in a storage ring with a beam energy of 2.0 GeV. What is the critical photon energy for the photon beam in the straight ahead beam line and in the two side stations?

Exercise 4.15. Collide a 25 MeV electron beam with a 1 kW CO_2 laser beam ($\lambda = 10.0$ μm). What is the energy of the backscattered photons? Assume a diffraction limited interaction length of twice the Rayleigh length and an electron beam cross section matching the photon beam. Calculate the x-ray photon flux for an electron beam from a 3 GHz linear accelerator with a pulse length of 1 μm and a pulse current of 100 mA.

5. Accelerator Physics

A beam of charged particles can emit synchrotron radiation whenever it is deflected by a magnetic or electric field. The intensity and spectrum of the radiation depends greatly on the relativistic factor γ of the charged particle. For this reason, only electron or positron beams are considered as potential synchrotron radiation sources and we concentrate on accelerator systems which can produce highly relativistic electron or positron beams. In the future we will not distinguish anymore between electrons and positrons. Some synchrotron radiation facilities operate with a positron beam to avoid sometimes detrimental effects of positive ion-clouds surrounding an electron beam.

The energy of an electron is measured in units of an "electron Volt". This is equal to the kinetic energy gained by an electron while being accelerated in the field between two electrodes with a potential difference of 1 Volt. Electrons become relativistic if their kinetic energy exceeds that of the restmass or about 511000 eV. Most synchrotron radiation sources are based on electron beams with kinetic energies of several hundred million electron volts and higher. We use for such high energies the units MeV (10^6 eV) or GeV(10^9 eV). The photon energy of synchrotron radiation is also measured in eV. Photon energies of general interest reach up to about 20 keV, where 1 keV=1000 eV. For scaling it is useful to remember that a photon wavelength of 1Å is equivalent to an energy of 12398 eV or 12.4 keV.

In this brief overview on accelerator physics, we consider only magnetic fields for relativistic electron beam guidance since technically feasible magnetic fields are much more effective than equally feasible electric fields (1 Tesla of magnetic field corresponds to 3.0 MV/cm of electric field!). For application and research one would like to have a continuous emission of photons which can be accomplished in an electron storage ring.

A storage ring is a circular accelerator which is widely used as a synchrotron radiation source. After injection, electrons circulate in this ring for many hours at constant energy serving as the source of continuous synchrotron radiation. A storage ring is therefore not a true accelerator although a beam can be accelerated very slowly if required (e.g. if the injection energy is lower than the operating energy). While the electrons circulate in the storage ring they emit electromagnetic radiation whenever they pass through a magnetic field. This radiation can be extracted from the ring through long

pipes, called photon beam lines leading to experimental stations and be used for basic and applied science.

The intensity of synchrotron radiation is proportional to the number of electrons circulating in the storage ring. We define a circulating beam current by

$$I_{\mathrm{b}} = eN_{\mathrm{e}}f_{\mathrm{rev}} ,$$

where N_{e} is the total number of electrons circulating in the storage ring, e the unit of electric charge, and f_{rev} is the revolution frequency.

The storage ring operating at energies above several hundred MeV is enclosed in a concrete tunnel or behind a concrete shielding wall to shield people from ionizing radiation. The photon beam escapes this radiation environment through small holes in the shielding wall to the experimental stations. To establish and sustain an electron beam in a storage ring, many technical components are required. The nature and functioning of the major ones will be discussed in more detail.

Every circular accelerator is composed of technical components, like magnets, ultra-high vacuum system, rf-system, injector system, beam monitoring, control system etc. Basically, all main components are installed along a closed loop defining the orbit along which the electrons travel. In the schematic Fig. 5.1 the principle layout of the main components is displayed.

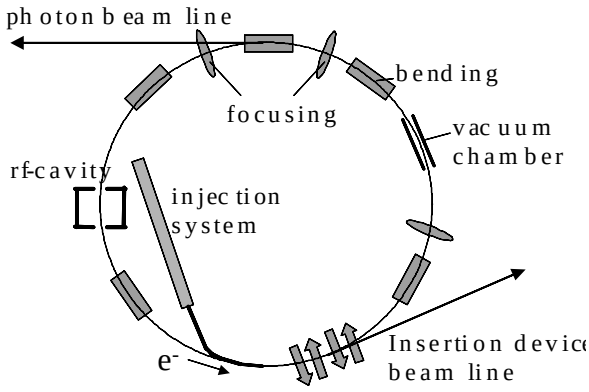

Fig. 5.1. Main storage ring components

- **Bending magnets** are used to deflect the electron beam. Placing bending magnets in a well ordered arrangement such as to form a closed ring forces the beam to follow a closed path along the circular accelerator. The location and deflection angle of bending magnets defines the geometry of the storage

ring. Although we call this a circular accelerator, the shape is actually not circular. A series of arc sections (bending magnets) is interrupted by straight sections to make space for other components. Bending magnets also serve as sources of synchrotron radiation.

- **Quadrupole magnets** are placed in straight sections between bending magnets. Quadrupoles act much like glass lenses in light optics by providing a restoring or focusing force to particles which deviate too much from the orbital path or ideal orbit, thus assuring the survival of the particle beam for many revolutions. We will borrow many terms and techniques from light optics since the functions are very similar.
- **Sextupole magnets** are used to correct for chromatic aberrations caused by focusing errors on particles with different energies.
- **Vacuum system:** The electron beam must be enclosed in a vacuum chamber where the air pressure is reduced to some 10^{-9} Torr or lower to prevent particle losses due to scattering on residual gas atoms. Electrons, once injected into a storage ring, are expected to circulate and produce synchrotron radiation for many hours with a minimum rate of loss. This low pressure is achieved by placing many vacuum pumps along the circular path. Due to gas desorption caused by radiation hitting the vacuum chamber surface continuous pumping is required.
- **Rf-system:** Electrons are expected to circulate for many hours at constant energy in a storage ring to produce synchrotron radiation. Although the particle energy is kept constant, energy loss into synchrotron radiation occurs and must be compensated by equivalent acceleration. Special accelerating cavities are installed along the orbit generating an accelerating electric field in synchronism with the arrival of electrons. The acceleration exactly compensates for the energy loss to radiation. The electric fields oscillate at frequencies of the order of 500 MHz and proper acceleration occurs only when electrons pass through the cavity at a specific time which is the reason for the bunched character of the circulating electron beam. The circulating beam is composed of one or more electron clusters, called bunches, where the distance between bunches is an integer multiple of the rf-wavelength. For the same reason, the circumference also must be an integer multiple of the rf-wavelength.
- **Beam controls:** A number of beam controls are included in the design of a storage ring. Beam monitors are used to measure the circulating beam current, beam lifetime and transverse beam position. Due to field and alignment errors of main magnets, the particle beam follows a distorted closed loop. These distortions must be corrected as much as possible by steering magnet. Generally, a storage ring is controlled by a computer, setting and recording component parameters as well as monitoring beam current and safety equipment.
- **Injection system:** Electrons are generated in an injector system consisting of an electron source, a low energy accelerator (mostly a linear accel-

erator) and a booster synchrotron to accelerate the electrons from the low linac energy to the operating energy of the storage ring. After acceleration in the booster, the electrons are transferred to the storage ring. To reach high beam intensities in the storage ring many booster pulses are injected.

Insertion devices. Synchrotron radiation emitted from bending magnets do not always meet all requirements of the users. In order to provide the desired radiation characteristics (photon energy, broad band, narrow band etc.) insertion devices are placed in magnetfree sections along the orbit. Such magnets are composed of more than one pole with opposing polarities such that the total beam deflection in the insertion device is zero.

- **Wiggler** magnets are used to produce high intensity broad band radiation, up to photon energies which can greatly exceeding those available from bending magnets. In addition, a wiggler is composed of many poles thus increasing the total photon flux by a factor equal to the number of wiggler poles.
- **Wavelength shifters** are generally 3-pole wiggler magnets with a super-high field in the central pole to reach hard x-rays in low energy storage rings. The lateral poles are of opposite and much lower field strength to compensate the deflection of the central pole.
- **Undulator magnets** are essentially weak field wiggler magnets and produce high brightness, quasi monochromatic radiation.
- **Other,** specially designed magnets, may produce circularly polarized radiation.

Exercise *

Exercise 5.1 (S). An electron bunch of $\tau = 30$ ps duration and an instantaneous current of current of $I_b = 100$ mA is injected into a storage ring with a circumference of 300 m. Calculate the circulating beam current per bunch. How many electrons are injected into the storage ring during each pulse containing only one bunch. How many such pulses must be injected to reach a circulating beam current of 200 mA? What is the storage ring filling time, if the injection system can operate at 10 Hz? How many bunches must be injected per pulse to keep the injection time at 5 min or less?

* The argument (S) indicates an exercise for which a solution is given in Appendix A.

6. Particle Beam Optics

Bending and focusing of high energy, relativistic particles are effected by the Lorentz force

$$\boldsymbol{F} = e\boldsymbol{E} + e\frac{[c]}{c}[\boldsymbol{v} \times \boldsymbol{B}]\,. \tag{6.1}$$

A magnetic field of 1 Tesla exerts the same force on a relativistic electron as does an electric field of 3.0 MV/cm. A magnetic field of 1 Tesla is rather easy to produce while the corresponding electric field is beyond technical feasibility. For the manipulation of relativistic particles we use therefore magnetic fields.

6.1 Deflection in Bending Magnets

Charged particle beams are deflected in the uniform field of bending magnets. A transverse magnetic field being constant and homogeneous in space at least in the vicinity of the particle beam, is the lowest order field in beam guidance or beam transport systems. Such a field is called a dipole field and can be generated, for example, between the poles of an electromagnetic bending magnet with a cross section as shown schematically in Fig. 6.1.

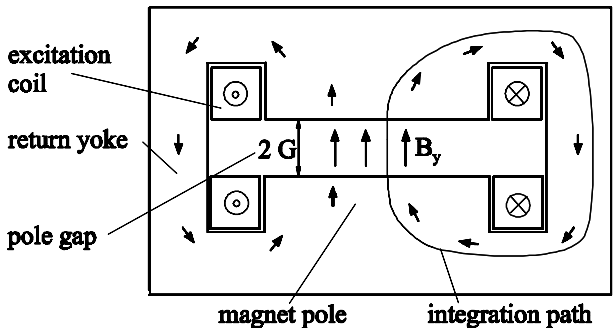

Fig. 6.1. Cross section of bending magnet

The magnetic field $\boldsymbol{B}$ is generated by an electrical current I in current carrying coils surrounding the magnet poles. A ferromagnetic return yoke provides an efficient return path for the magnetic flux. The magnetic field is determined by one of Maxwell's equations

$$\nabla \times \frac{\boldsymbol{B}}{\mu_{\mathrm{r}}} = \left[\frac{\mu_0\, c}{4\pi}\right] \frac{4\pi}{c} \boldsymbol{j}\,, \tag{6.2}$$

where μ_{r} is the relative permeability of the ferromagnetic material and $\boldsymbol{j}$ is the current density in the coils. We integrate (6.2) over an area enclosed by the integration path as shown in Fig. 6.1 and apply Stoke's theorem (B.29) to get

$$\frac{1}{\mu_{\mathrm{r}}} \int \nabla \times \boldsymbol{B}\, \mathrm{d}\boldsymbol{A} = \frac{1}{\mu_{\mathrm{r}}} \oint \boldsymbol{B}\, \mathrm{d}\boldsymbol{s} = \frac{4\pi}{c} \left[\frac{\mu_0 c}{4\pi}\right] \int \boldsymbol{j}\, \mathrm{d}\boldsymbol{A}\,. \tag{6.3}$$

The integration on the r.h.s. is just the total current in both excitation coils $2I_{\mathrm{tot}} = \int \boldsymbol{j}\, \mathrm{d}\boldsymbol{A}$. The l.h.s. must be evaluated along an integration path surrounding the excitation coils. We choose an integration path which is convenient for analytical evaluation. Starting in the middle of the lower magnet pole and integrating straight to the middle of the upper pole, we know from symmetry that the magnetic field along this path has only a vertical nonvanishing component $B_y \neq 0$, which is actually the desired field in the magnet gap and $\mu_{\mathrm{r}} = 1$. Within the iron the contribution to the integral vanishes since we assume no saturation effects and set $\mu_{\mathrm{r}} = \infty$. The total path integral becomes therefore

$$G\, B_y = \left[\frac{\mu_0\, c}{4\pi}\right] \frac{4\pi}{c}\, I_{\mathrm{tot}}\,, \tag{6.4}$$

where I_{tot} is the total current through one coil. Solving (6.4) for the total excitation current in each coil we get in more practical units

$$I_{\mathrm{tot}}\,(\mathrm{Amp}) = \frac{1}{\mu_0}\, B_y\,[\mathrm{T}]\; G[\mathrm{m}] = 795774\, B_y\,[\mathrm{T}]\; G[\mathrm{m}]\,. \tag{6.5}$$

The total required excitation current in each magnet coil is proportional to the desired magnetic field and proportional to half the gap between the magnet poles.

As a practical example, we consider a magnetic field of 1 Tesla in a dipole magnet with a gap of $2G = 10$ cm. From (6.5) we find a total electrical current of about 40,000 A is required in each of two excitation coils to generate this field. Since the coil in general is composed of many turns, the actual electrical current is usually much smaller by a factor equal to the number of turns and the total coil current I_{tot}, therefore, is often measured in units of Ampere-turns. For example two coils each composed of 40 windings with sufficient cross section to carry an electrical current of 1000 A would provide the total required current of 40,000 A-turns each to produce a magnetic field of 1 Tesla.

Beam deflection in a magnetic field is derived from the equilibrium of the centrifugal force and Lorentz force

$$\frac{\gamma m v^2}{\rho} \;=\; [c]\,\frac{e}{c}\,vB\,, \tag{6.6}$$

where we assumed that the direction of the particle velocity $\boldsymbol{v}$ is orthogonal to the magnetic field: $\boldsymbol{v}\perp\boldsymbol{B}$. A pure dipole field deflects a charged particle beam onto a circular path with a bending radius ρ given by

$$\frac{1}{\rho} \;=\; [c]\,\frac{eB}{\beta E} = \frac{B}{B\rho}\,, \tag{6.7}$$

where $\beta = v/c$, E the particle energy, and $B\rho$ is defined as the beam rigidity .

In practical units

$$\frac{1}{\rho}(m^{-1}) \;=\; C_\rho\,\frac{B(\mathrm{T})}{cp\,(\mathrm{GeV})}\,, \tag{6.8}$$

with

$$C_\rho = [c]\,e = 0.299792\;\frac{\mathrm{GeV}}{\mathrm{m\ T}}\,. \tag{6.9}$$

The beam rigidity is

$$B\rho\,(\mathrm{Tm}) = 3.3356\,cp\,(\mathrm{GeV})\;. \tag{6.10}$$

A magnet of length ℓ_b deflects a particle beam by the angle

$$\psi = \ell_\mathrm{b}/\rho\,. \tag{6.11}$$

Distributing a set of magnets bending the electron beam by appropriate deflection angles along a closed loop establishes the geometric shape of the storage ring.

6.2 Beam Focusing

A ring consisting only of bending magnets would not work since any particle beam has the tendency to spread out. Similar to a light beam, we require focusing elements to confine the particle beam to the vicinity of the orbit defined by the location of the bending magnets.

6.2.1 Principle of Focusing

We borrow much from light optics to describe the focusing of particle beams. To learn how to focus charged particles, we recall the principle of focusing in light optic (Fig. 6.2). The deflection of a light ray parallel to the optical axis by a focusing lens is proportional to the distance of the ray from the optical axis. The distance from the lens to the focal point, where all parallel rays are focused to a point, is called the focal length .

Applying this to the focusing of particle beams, we note from the discussion on bending magnets that in a focusing magnet the deflection angle α must increase linearly with x

$$\alpha = \frac{\ell}{\rho} = [c]\,\frac{eB\ell}{cp} \propto x\,. \tag{6.12}$$

To accomplish this, we consider now a field expressed by $B = B_0 + gx$ which gives two contributions to the deflection, one a constant deflection due to the uniform dipole field B_0 and the other is an x-dependent deflection

$$\alpha \;=\; [c]\,\frac{eg\ell}{cp}\,x \;=\; kl\,x\,, \tag{6.13}$$

as desired for focusing. The x-dependent field component gx can be created by a quadrupole magnet, which functions as the focusing element for charged particle beams. The quantity g is the field gradient , and k is defined as the quadrupole strength

$$k(\mathrm{m}^{-2}) \;=\; C_\rho\,\frac{g(\mathrm{T/m})}{cp\,(\mathrm{GeV})}\,. \tag{6.14}$$

The focal length of the quadrupole is $1/f = k\ell_{\mathrm{q}}$ where ℓ_{q} is the length of the quadrupole.

6.2.2 Quadrupol Magnet

How do we produce the desired field gradient or a field: $B_y = gx$ in a quadrupole magnet? Static magnetic fields can be derived from a magnetic potential

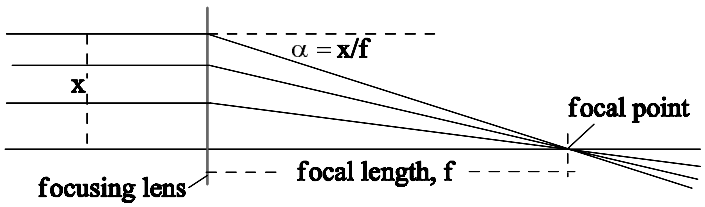

Fig. 6.2. Principle of focusing

and a field $B_y = gx$ can be derived from the potential $V = -gxy$ by simple differentiation giving the field-components

$$B_y = -\frac{\partial V}{\partial y} = gx\,, \qquad \text{and} \qquad B_x = -\frac{\partial V}{\partial x} = gy\,. \tag{6.15}$$

Because ferromagnetic surfaces are equipotential surfaces (just like metallic surfaces are equipotential surfaces for electric fields) we use magnetic poles shaped in the form of a hyperbola (Fig. 6.3) given by

$$x \cdot y = \pm\tfrac{1}{2}R^2\,, \tag{6.16}$$

where R is the aperture radius between the four hyperbolas. Along the z-axis the magnet cross section is assumed to be the same. A quadrupole is made of four hyperbolic poles with alternating magnetization producing the desired focusing field gradient.

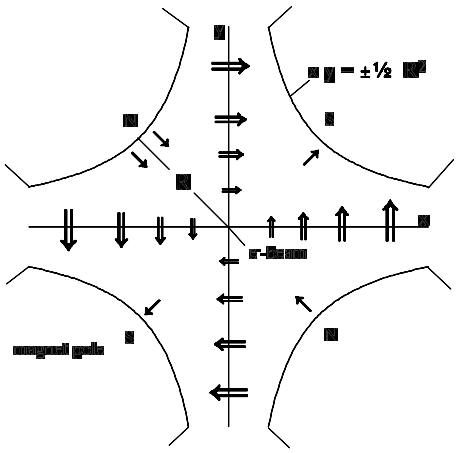

Fig. 6.3. Cross section of a quadrupole (schematic)

Each of the four poles is excited by electrically powered coils wound around it. Although quadrupoles function as focusing elements just like glass lenses function as focusing elements in light optics there is a fundamental difference. Quadrupoles focus in one plane but defocus in the other depending on the sign of the excitation current. An actual particle beam, however, requires focusing in both planes. To solve this problem, we borrow again from light optics the characteristics of focusing in a lens-doublet. The focal length of two lenses is $1/f^* = 1/f_1 + 1/f_2 - d/f_1 f_2$ where f_1 and f_2 are the focal lengths, and d is the distance between both lenses. If we choose, for example, $f_1 = -f_2 = f$ we get $1/f^* = d/f^2 > 0$ which is focusing in both

planes. By using combinations of focusing and defocusing quadrupoles, one can create overall focusing systems. The quadrupoles in a storage ring or a general beam transport line are therefore polarized alternately as focusing or defocusing quadrupoles. It is common in this regard to consider a quadrupole to be focusing if it focuses a particle beam in the horizontal plane. Tacitly, we know that this same quadrupole is defocusing in the vertical plane.

6.3 Equation of Motion

Bending magnets and quadrupoles are the main components to guide and focus a charged particle beam. Sextupole magnets are used to correct chromatic aberration introduced by quadrupole focusing. In the following discussion we will formulate mathematical equations to describe the path of individual particles along a beam transport line including any of theses magnet types.

The equation of motion in the presence of dipole (B_0), quadrupole (g) and sextupole (g') fields can be derived from the general expression for the curvature $1/\rho$ of paraxial beams. Here, we define the curvature very general to include all fields (dipole, quadrupole, sextupole...) although in any one magnet only one field type may be present. There are exceptions to this separation of fields in some special cases. Specifically, in some new synchrotron light sources, we find a combination of a dipole and gradient field in the same bending magnet. For paraxial beams ($x' \ll 1$) the curvature $1/\rho$ is

$$\frac{1}{\rho} \approx x'' = [c]\,\frac{eB}{cp}\,, \tag{6.17}$$

where

$$B = B_0 + gx + \tfrac{1}{2}\,g'\,x^2 + \ldots \qquad \text{or} \tag{6.18}$$

$$[c]\,\frac{eB}{cp} = \frac{1}{\rho_0} + kx + \tfrac{1}{2}mx^2 + \ldots\,.$$

Before we proceed to derive the equation of motion, we notice that the field term $\frac{1}{\rho_0}$ describes the ideal beam guidance through the bending magnets. The solution of the equations of motion would be a rather complicated expression describing the alternating straight and curved segments of the ideal orbit as defined by the location and strength of the bending magnets. We are not interested in this solution, because we already know from the placement of bending magnets where the beam should be. We rather concern ourselves with deviation of particle trajectories from this ideal orbit and redefine (6.17) by a transformation eliminating the geometric expression of the idea orbit and set

$$\frac{1}{\rho} - \frac{1}{\rho_0} \approx x'' = [c]\,\frac{e}{cp}\,(B - B_0)\,. \tag{6.19}$$

With the expansions (10.8) inserted into (6.19) the equation of motion becomes

$$\begin{aligned} x'' = \; & -kx \ldots\ldots\ldots\ldots\ldots \text{focusing term} \\ & + \frac{1}{\rho_0}\delta \ldots\ldots\ldots\ldots \text{dispersion} \\ & + kx\delta \ldots\ldots\ldots\ldots \text{chromatic aberration} \\ & - \tfrac{1}{2}\, mx^2 \ldots\ldots\ldots\ldots \text{chromatic and geometric aberration} \\ & + \mathcal{O}(3) \ldots\ldots\ldots\ldots \text{higher order terms,} \end{aligned} \tag{6.20}$$

where $\delta = \Delta E/E_0$ is the relative energy deviation of a particle from the ideal energy E_0 and m the sextupole strength defined in (10.8).

Each term in the equation of motion makes its specific (sometimes unwanted) contribution to beam dynamics. Deflection of the beam in a bending magnet depends on the particle energy. Particles with a slightly different energy are deflected differently and this difference cannot be neglected and is covered by the term $\frac{1}{\rho_0}\delta$. The same is true for focusing giving rise to the chromatic aberration term, $kx\delta$. Finally, to avoid beam instability, we must correct one of the most serious chromatic effects, the chromaticity, by the installation of sextupole magnets. Unfortunately, such sextupole magnets introduce nonlinear terms into the otherwise linear beam dynamics causing significant stability problems for particles at large amplitudes x. A similar equation exists for the vertical plane keeping in mind that the magnet parameters must change signs ($k \rightarrow -k$), etc.

In the approximation of linear beam optics, we keep only linear terms in (10.8) and get the differential equation of motion

$$x'' + k(s)x = \frac{1}{\rho_o}\,\delta\,. \tag{6.21}$$

This equation is similar to that of a perturbed harmonic oscillator although in this case we have a s-dependent rather than a constant restoring force.

The solution of this equation is composed of the solution of the homogeneous differential equation and a particular solution of the inhomogeneous differential equation. The physical significance of both solutions is the following. Solutions for the homogeneous equation represent oscillations about an equilibrium orbit. Such oscillations are called betatron oscillations. In this case, the equilibrium orbit is $x \equiv 0$ because it is the path we defined by the placement of the magnets and x represents only the deviation from this ideal orbit. For off-energy particles, we must consider the perturbation term on the right hand side of the equation. This perturbation is on average a constant generating a shift of the particle trajectory from the ideal orbit. For example, particles with a higher energy, $\delta > 0$, would oscillate about a path which is mostly outside ($x > 0$) of the ideal path. The solution of the inhomogeneous

equation of motion therefore defines the reference orbit for particles with energy $E = E_0(1+\delta)$. Such particles perform oscillations about this reference orbit. In the following we discuss both solutions in more detail.

6.3.1 Solutions of the Equations of Motion

First, we set $\delta = 0$ and solve the homogeneous equation: $x'' + k(s)x = 0$. We cannot solve this equation in general since $k = k(s)$ is a function of s describing the distribution of quadrupoles along the beam transport line. Within each individual quadrupole, however, the solution for k =const >0 is simply

$$x(s) = a\,\cos(\sqrt{k}s) + b\sin(\sqrt{k}s)\,, \tag{6.22a}$$

$$x'(s) = -a\sqrt{k}\sin(\sqrt{k}s) + b\sqrt{k}\cos(\sqrt{k}s)\,. \tag{6.22b}$$

The integration constants a, b are determined by initial conditions. With $x = x_0$ and $x' = x'_0$ at $s = 0$, we get at the location s the particle coordinates

$$x = x_0\cos(\sqrt{k}s) + x'_0\frac{1}{\sqrt{k}}\sin(\sqrt{k}s)\,, \tag{6.23a}$$

$$x' = -x_0\sqrt{k}\,\sin(\sqrt{k}s) + x'_0\,\cos(\sqrt{k}s)\,. \tag{6.23b}$$

For a particle with ideal energy, these two equations express the position and slope at point s as a function of initial particle coordinates at $s = 0$.

6.3.2 Matrix Formalism

Both equations can be expressed in matrix formulation

$$\begin{pmatrix} x \\ x' \end{pmatrix} = \begin{pmatrix} \cos(\sqrt{k}s) & \frac{1}{\sqrt{k}}\sin(\sqrt{k}s) \\ -\sqrt{k}\,\sin(\sqrt{k}s) & \cos(\sqrt{k}s) \end{pmatrix} \begin{pmatrix} x_0 \\ x'_0 \end{pmatrix}. \tag{6.24}$$

For the case of a defocusing quadrupole $k < 0$ we derive a similar transformation matrix

$$\begin{pmatrix} x \\ x' \end{pmatrix} = \begin{pmatrix} \cosh(\sqrt{|k|}s) & \frac{1}{\sqrt{|k|}}\sinh(\sqrt{|k|}s) \\ \sqrt{|k|}\,\sinh(\sqrt{|k|}s) & \cosh(\sqrt{|k|}s) \end{pmatrix} \begin{pmatrix} x_0 \\ x'_0 \end{pmatrix}. \tag{6.25}$$

A special case appears for $k \longrightarrow 0$ describing a drift space of length s for which the transformation matrix is

$$\begin{pmatrix} x \\ x' \end{pmatrix} = \begin{pmatrix} 1 & s \\ 0 & 1 \end{pmatrix} \begin{pmatrix} x_0 \\ x_0 \end{pmatrix}. \tag{6.26}$$

The transformations are expressed for quadrupoles of finite length. Sometimes it is desirable to perform quick calculations in which case we use the thin lens

approximation just like in light optics by setting $s \to 0$ while $1/f = ks =$ const and get a thin lens transformation matrix for a quadrupole

$$\begin{pmatrix} x \\ x' \end{pmatrix} = \begin{pmatrix} 1 & 0 \\ -\frac{1}{f} & 1 \end{pmatrix} \begin{pmatrix} x_0 \\ x_0 \end{pmatrix} . \tag{6.27}$$

Of course, in this case half the length of the actual quadrupole must be assigned to the drift space on either side.

Transformation of particle trajectories through complicated, multi-magnet arrangements, called lattice, with transformation matrices $M_1, M_2, \ldots$ are derived by simple matrix multiplication

$$M = M_n \cdot M_{n-1} \cdot \cdots \cdot M_2 \cdot M_1 . \tag{6.28}$$

This matrix formalism is quite powerful and well matched to the capabilities of computers.

6.3.3 FODO Lattice

As an example of a beam line appropriate to demonstrate the usefulness of the matrix formalism we use what is called the FODO structure. This magnet structure consist of an alternating series of focusing and defocusing quadrupoles, thence the name FODO lattice as shown in Fig. 6.4. This lattice has been used to construct large high energy physics storage rings by filling the space between the quadrupoles with bending magnets. The FODO lattice is a very stable magnet configuration and its simplicity lends itself to "back-of-an-envelope" calculations.

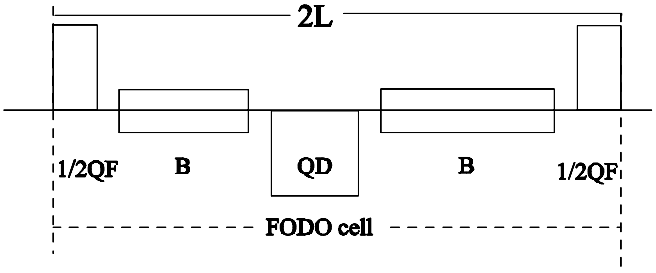

Fig. 6.4. FODO lattice

To formulate particle dynamics in a FODO-lattice we keep the formalism simple by starting in the middle of a quadrupole. The transformation through a half cell, 1/2 QF–DRIFT–1/2 QD, in thin lens approximation becomes

$$\begin{pmatrix} 1 & 0 \\ -\frac{1}{f_{\mathrm{d}}} & 1 \end{pmatrix} \begin{pmatrix} 1 & L \\ 0 & 1 \end{pmatrix} \begin{pmatrix} 1 & 0 \\ -\frac{1}{f_{\mathrm{f}}} & 1 \end{pmatrix} = \begin{pmatrix} 1-\frac{L}{f_{\mathrm{f}}} & L \\ -\frac{1}{f^*} & 1-\frac{L}{f_{\mathrm{d}}} \end{pmatrix} , \tag{6.29}$$

where $2L$ is the length of the FODO-cell, $1/f^* = 1/f_\mathrm{f} + 1/f_\mathrm{d} - L/(f_\mathrm{f} f_\mathrm{d})$. Bending magnets are ignored in (6.29) because they do not contribute to focusing in first approximation used here. For the second half cell we get the transformation matrix by replacing $f_\mathrm{f} \leftrightarrows f_\mathrm{d}$ and vice versa. For simplicity, we consider a symmetric FODO lattice by setting $f_\mathrm{f} = -f_\mathrm{d} = f$ and get from both half cell transformation matrices the transformation matrix of a full FODO-cell starting in the center of a QF and ending in the middle of the next QF

$$M_{\mathrm{cell,qf}} = \begin{pmatrix} 1 - \frac{2L^2}{f^2} & 2L\left(1 - \frac{L}{f}\right) \\ -\frac{2L}{f^2}\left(1 - \frac{L}{f}\right) & 1 - \frac{2L^2}{f^2} \end{pmatrix} . \tag{6.30}$$

This transformation matrix is valid for the horizontal plane. In the vertical plane, we have the same matrix except that the sign of the focal length must be changed, $f \rightarrow -f$.

We may combine the transformation in both planes into one 4×4 transformation matrix which we can use to transform a particle trajectory with initial coordinates x_0, x_0', y_0, y_0' to through a full FODO-cell

$$\begin{pmatrix} x \\ x' \\ y \\ y' \end{pmatrix} = \begin{pmatrix} 1 - \frac{2L^2}{f^2} & 2L\left(1 + \frac{2L^2}{f}\right) & 0 & 0 \\ -\frac{2L}{f^2}\left(1 - \frac{L}{f}\right) & 1 - \frac{2L^2}{f^2} & 0 & 0 \\ 0 & 0 & 1 - \frac{2L^2}{f^2} & 2L - \frac{2L^2}{f} \\ 0 & 0 & -\frac{2L}{f^2}\left(1 + \frac{L}{f}\right) & 1 - \frac{2L^2}{f^2} \end{pmatrix} \begin{pmatrix} x_0 \\ x_0' \\ y_0 \\ y_0' \end{pmatrix} . \tag{6.31}$$

For practical reasons, however, mostly only 2×2 matrices are used to describe beam dynamics in one plane only.

The matrix formalism is a very powerful tool to calculate the trajectories of single particles. Yet, in a storage ring there are of the order of 10^{11} or more particles circulating and it would be prohibitive to have to recalculate the trajectories of all particles whenever a quadrupole strength is changed. A more simple formalism has been developed which allows us to determine the overall behavior of a multi-particle beam.

6.4 Betatron Function

Although the quadrupole strength is a function of s, $k = k(s)$, the homogeneous part of the equation of motion(6.21) looks very much like that of a harmonic oscillator $x'' + k(s)x = 0$. As an analytical solution of the equation of motion we try the solution of a harmonic oscillator with variable amplitude and phase

$$x(s) = a_i \sqrt{\beta(s)} \cos\left[\psi(s) + \varphi_i\right] , \tag{6.32}$$

where a_i and φ_i are the integration constants for particle i and $\beta(s)$, $\psi(s)$ are so far unidentified functions of s. We insert this ansatz into the differential equation and get from the coefficients of both the sine-and cosine-terms two conditions for $\beta(s)$ and $\psi(s)$

$$\frac{\mathrm{d}^2\sqrt{\beta}}{\mathrm{d}s^2} + k(s)\sqrt{\beta} + \beta^{-\frac{3}{2}} = 0 , \tag{6.33}$$

$$\psi'(s) = \frac{1}{\beta(s)} , \tag{6.34}$$

where the primes $'$ are derivations with respect to s.

Equation (6.32) describes the oscillatory motion of particles about the ideal orbit leading through the center of all magnets. These oscillations are defined separately in both the horizontal and vertical plane and are called betatron oscillations. The function $\beta(s)$ is called the betatron function and is defined by the placement and strength of the quadrupole magnets. It is a periodic function of s resembling the periodic distribution of quadrupoles along the ring circumference. The periodicity is the circumference of the machine or shorter if quadrupoles are arranged around the ring in a higher periodicity.

Because of the nonlinearity of the differential equation for the betatron function (6.33) , there is only one periodic solution in each plane for a given lattice configuration. Matrix formalism is used to determine this one betatron function in each plane utilizing special computer programs. For each lattice configuration a tabulated list of the values of betatron functions exists which can be used to determine beam sizes. The betatron function is, however, of much higher importance in beam dynamics beyond the ability to calculate single particle trajectories as we will discuss in the next section.

6.4.1 Betatron Phase and Tune

The second equation (6.34) can be integrated immediately for

$$\psi(s) = \int_{s_0}^{s} \frac{\mathrm{d}\,\sigma}{\beta(\sigma)} \tag{6.35}$$

defining the phase of the betatron oscillation at point s and is measured from the starting point $s = s_0$. Integrating along the full orbit produces the betatron tune $\nu_{x,y}$ of the machine which is equal to the number of betatron oscillations per revolution. Again, tunes are defined separately in both planes.

$$\nu_{x,y} = \frac{\psi_{x,y}(C)}{2\pi} = \frac{1}{2\pi} \oint \frac{\mathrm{d}\,\sigma}{\beta_{x,y}(\sigma)} . \tag{6.36}$$

The significance of the tune is that it may not be an integer or a half integer value. If one or the other assumes such a value, beam dynamics becomes

instantly unstable leading to beam loss. This becomes obvious for an integer resonance ($\nu_{x,y} = n$) when considering a small dipole field perturbation at say one point along the orbit. This dipole field gives the beam a transverse kick at the same phase of its betatron oscillations after every turn building up larger and larger oscillation amplitudes until the beam gets lost on the vacuum chamber walls.

6.4.2 Beam Envelope

Solution (6.32) describes individual particle trajectories with different amplitudes a_i and phases φ_i. If we choose only particles with the largest amplitude $a_i = \hat{a}$ within a beam and further look among these particles for the one for which $\cos[\psi(s) + \varphi_i] = 1$, we have defined the beam envelope at point s by

$$E_{x,y}(s) \;=\; \pm\,\hat{a}_{x,y}\,\sqrt{\beta_{x,y}(s)}\,. \tag{6.37}$$

No other particle will have a greater amplitude at this point. Knowledge of the betatron functions in both the x and y-plane and knowledge of the quantity $\hat{a}$ in both planes will allow us to define the beam dimensions at any point along the ring orbit.

As important the knowledge of the beam width and height at some point s is, we do not yet have the tools to calculate either the numerical value of the betatron functions nor that of the beam emittances in both the horizontal and vertical plane.

6.5 Phase Ellipse

Particles perform oscillatory motion, called betatron oscillations, about the ideal reference orbit and its amplitude and slope is given by

$$x(s) = a\sqrt{\beta(s)}\,\cos\left[\psi(s) + \varphi\right]\,, \tag{6.38}$$

$$x'(s) = -a\,\frac{\alpha}{\sqrt{\beta(s)}}\,\cos\left[\psi(s) + \varphi\right] - a\sqrt{\beta(s)}\,\sin\left[\psi(s) + \varphi\right]\cdot\psi'(s)\,, \tag{6.39}$$

where $\alpha = -\frac{1}{2}\beta'$ and $\gamma = \frac{1+\alpha^2}{\beta}$. All functions $\alpha(s), \beta(s)$ and $\gamma(s)$ are defined separately in x and y and are known as betatron functions or lattice functions. Eliminating the phase $\psi(s) + \varphi$ from both equations results in a constant of motion or the Courant–Snyder invariant[42].

$$\gamma x^2 + 2\alpha x x' + \beta x'^2 \;=\; a^2\,. \tag{6.40}$$

This equation describes an ellipse with an area πa. While travelling around the storage ring and performing betatron oscillations, individual particles

move in phase space along the contour of an ellipse. Each particle i has a different amplitude a_i and travels therefore along a different phase ellipse. Again, there exist two different sets of phase ellipses for each particle, one in (x, x')-and the other in (y, y')-phase space.

6.6 Beam Emittance

Liouville's theorem states with respect to particle dynamics that in the presence of only external macroscopic fields the particle density in phase space is a constant of motion. That means, no particle can cross the phase ellipse of any other particle. We may therefore look for particles with the maximum amplitude $\hat{a}$ travelling along an ellipse which encloses all other particles. This phase ellipse then becomes representative for the whole beam (Fig. 6.5) because it encloses all other particles and due to Liouville no particle can cross this maximum phase ellipse. We have thereby succeeded in describing the dynamics of a many-particle beam by the dynamics of a single particle. Due to the variation of the betatron functions along the orbit, the phase ellipses also change their form and orientation but the area of the phase ellipses stay constant. At a particular point s along the closed orbital path in a storage ring the phase ellipse has always the same shape/orientation while the actual particle appears at different points on the ellipse after each revolution. The

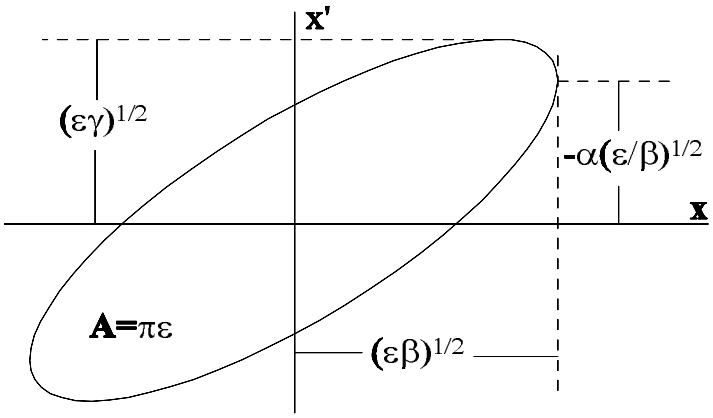

Fig. 6.5. Phase space ellipse with ellipse area A

constant $\pi\hat{a}$ is the area of the largest phase ellipse in a beam and we use this area to define the beam emittance. Because of synchrotron radiation, an electron beam in a storage ring has a Gaussian distribution and it is customary to define the beam emittance for a Gaussian particle distribution by the amplitude of the one-sigma particle

$$\epsilon_x = \frac{\langle x^2 \rangle}{\beta_x(s)} = \frac{\sigma_x^2}{\beta_x(s)} . \tag{6.41}$$

From (6.38) we find $\langle x^2 \rangle / \beta_x(s) = \frac{1}{2}\hat{a}_x^2$ or $\hat{a}_x^2 = 2\epsilon_x$.The standard beam size is then defined by

$$\sigma_x = \sqrt{\epsilon_x \beta_x} \qquad \text{and} \qquad \sigma_y = \sqrt{\epsilon_y \beta_y} \tag{6.42}$$

and the beam divergence by

$$\sigma_{x'} = \sqrt{\epsilon_x \gamma_x} \qquad \text{and} \qquad \sigma_{y'} = \sqrt{\epsilon_y \gamma_y} . \tag{6.43}$$

Ignoring for the moment effects due to the finite energy spread in the beam and diffraction, the photon source parameters in transverse phase space are equal to those of the electron beam.

electron beam parameter $\equiv$ photon beam parameter .

6.6.1 Variation of the Phase Ellipse

While the area of the phase ellipse is a constant of motion, the shape of the ellipse is not. The orientation and aspect ratio continuously change through the action of quadrupole focusing and even along a fieldfree drift space. In Fig. 6.6 the variation of the phase ellipse is shown for a beam in a drift space while converging to a minimum followed by divergence.

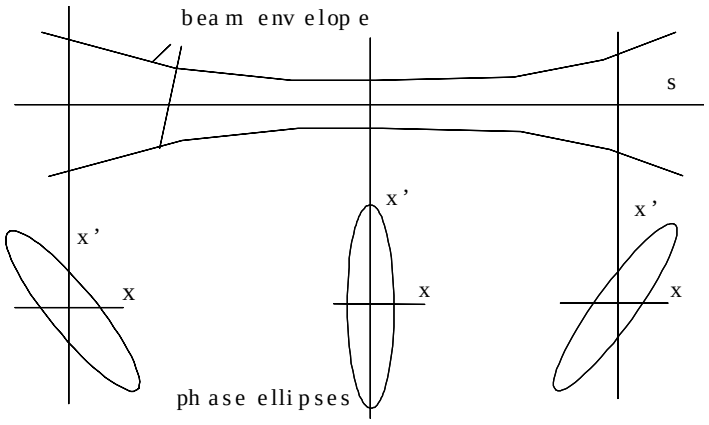

Fig. 6.6. Evolution of the phase ellipse along a drift space

The phase ellipse for a converging beam is tilted to the left while that for a diverging beam is tilted to the right. Of special interest is the upright ellipse which occurs at any symmetry point. At such a point $\alpha_{x,y} = 0$ and

$\gamma_{x,y} = 1/\beta_{x,y}$ and the beam emittance is simply $\epsilon = \hat{x} \cdot \hat{x}'$ or for a Gaussian beam $\epsilon = \sigma_x \cdot \sigma_{x'}$.

Fig. 6.7 shows the variation of the phase ellipse as the beam travels through a focusing quadrupole. We note the divergent nature of the beam before the quadrupole. Focusing turns the phase ellipse around resembling a convergent beam.

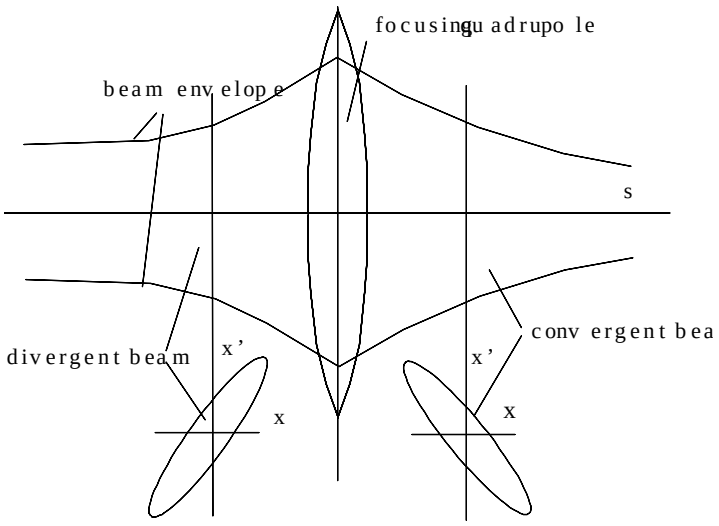

Fig. 6.7. Evolution of phase ellipse through a focusing quadrupole

6.6.2 Transformation of Phase Ellipse

The transformation matrix for a single particle can be used to determine the transformation of a phase ellipse from one point to another. Liouville's theorem requires that

$$\gamma x^2 + 2\alpha x x' + \beta x'^2 \;=\; \gamma_0 x_0^2 + 2\alpha_0 x_0 x_0' + \beta_0 x_0'^2 \;=\; a^2\,, \tag{6.44}$$

where the particle coordinates (x_0, x_0') and (x, x') are related by the transformation matrix $M = \begin{pmatrix} a & b \\ c & d \end{pmatrix}$. Replacing coordinates (x_0, x_0') by (x, x') and collecting all coefficients for x^2, x'^2 and xx', we obtain a relation of the betatron functions from one point to another. Noting that the coordinates are independent variables we expect all three coefficients to be equal to zero independently. These three conditions are sufficient to determine the three lattice functions β, α and γ. In matrix formulation the transformation of betatron functions is then given by

$$\begin{pmatrix} \beta \\ \alpha \\ \gamma \end{pmatrix} = \begin{pmatrix} a^2 & -2ab & b^2 \\ -ac & ad+bc & -bd \\ c^2 & -2cd & d^2 \end{pmatrix} \begin{pmatrix} \beta_0 \\ \alpha_0 \\ \gamma_0 \end{pmatrix} = M_\beta \cdot \begin{pmatrix} \beta_0 \\ \alpha_0 \\ \gamma_0 \end{pmatrix} . \tag{6.45}$$

The transformation of betatron functions can be expressed by the elements of single particle transformation matrices. We apply this transformation to a drift space to formulate the evolution of the betatron function and find from (6.45) for a drift space

$$\beta(s) = \beta_0 - 2\alpha_0 s + \gamma_0 s^2 . \tag{6.46}$$

Specifically, we look at a beam waist where $\alpha_0 = 0$ and get the betatron function a distance s away from the waist

$$\beta(s) = \beta_0 + \frac{s^2}{\beta_0} . \tag{6.47}$$

The betatron function increases quadratically with distance from the waist and the beam size evolves like

$$\sigma(s) = \sigma_0 \sqrt{1 + \frac{\epsilon^2 s^2}{\sigma_0^4}} , \tag{6.48}$$

where ϵ is the beam emittance.

6.7 Dispersion Function

So far, we have treated particle dynamics for a monochromatic beam only and the solutions for particle trajectories cover only those of the homogeneous differential equation of motion. This is not correct for a real beam and we must consider corrections due to effects related to energy errors. Chromatic effects are described by a particular solution of the inhomogeneous differential equation

$$x'' + \left(k + \frac{1}{\rho_0^2}\right) x = \frac{1}{\rho_0}\delta , \tag{6.49}$$

where $\delta = \Delta E/E_0$. On the left hand side, we have added the term $1/\rho_0^2$ which takes care of a second order focusing effect from a bending magnet. So far we have neglected this weak focusing term, but we need to include it now because we are about to determine a chromatic aberration due to the right hand term which is of the same order of magnitude. The general solution is $x = x_\beta + x_\delta$, where the betatron oscillation x_β is the solution of the homogeneous differential equation and x_δ the offset for off-momentum particles. Assuming a pure dipole field ($k = 0$) and $\delta = 1$ a special solution to (6.49) , called the dispersion function $D(s) = x/\delta$, is

$$D(s) = \rho_0 \left(1 - \cos \frac{s}{\rho_0}\right) . \tag{6.50}$$

This solution is nonvanishing only within a bending magnet of length L_b and for $0 \leq s \leq L_\mathrm{b}$. The 2×2-matrix formulation can be expanded to include off-energy particles by defining 3×3-transformation matrices

$$\begin{pmatrix} x \\ y \\ \delta \end{pmatrix} = \begin{pmatrix} a & b & D \\ c & d & D' \\ 0 & 0 & 1 \end{pmatrix} \begin{pmatrix} x_0 \\ y_0 \\ \delta \end{pmatrix} . \tag{6.51}$$

The matrix elements (D, D') are nonzero only for bending magnets. For drift spaces and quadrupoles $D \equiv 0$, and $D' \equiv 0$. This is not to say that the dispersion in drift spaces and quadrupoles is zero if there was a bending magnet upstream. The chromatic contribution to the particle trajectory starting at the first bending magnet will transform through the beam line just like a regular trajectory, but getting specially modified within each bending magnet.

Knowledge of the dispersion function allows the calculation of chromatic offsets for any value of the energy deviation δ. The dispersion function $\delta\, D(s)$ defines the reference path for particles with an energy deviation δ just like the ideal path ($x \equiv 0$) is the reference path for $\delta = 0$. Particles with energy $E_0(1+\delta)$ perform betatron oscillations about their respective reference paths defined by $\delta\, D(s)$.

6.8 Periodic Lattice Functions

In circular accelerators the betatron functions at any point s are the same from turn to turn and therefore $\boldsymbol{\beta} = M_\beta\, \boldsymbol{\beta}_0 = \boldsymbol{\beta}_0$. This periodic solution of the betatron functions can be derived from the eigenvalues of the eigenfunction equation

$$(M_\beta - I)\, \boldsymbol{\beta} = 0 , \tag{6.52}$$

where M_β is the transformation matrix from point s through a whole orbit to point $s + C$, C the ring circumference and I is the unit matrix.

Generally, storage rings are composed of a number of equal sections with equal magnet distributions. In this case, each section, called either cell or unit, is representative for all cells and we need to find the periodic solution for one cell only. This solution then repeats from cell to cell as we progress along the orbit.

6.8.1 Periodic Betatron Function in a FODO Lattice

As an example, we look for the periodic solution of the betatron function in a FODO lattice. With $\alpha_0 = 0$, and $\gamma_0 = 1/\beta_0$ in the middle of the QF, we solve

(6.52) with (6.30) for the periodic betatron function and get from (6.45) with (6.30) the periodic solution $\beta = \beta_0 = (1 - 2L^2/f^2)^2\beta_0 + 4L^2(1 + L/f)^2/\beta_0$. Similarly, we can go from the middle of the QD to the middle of the next QD and get the value of the periodic betatron function in the middle of the QD. Since a QF is a QD in the vertical plane and vice versa, the two solutions just described present the horizontal and vertical betatron functions in the middle of the QF and interchangeably those in the middle of the QD. With the FODO parameter $\kappa = f/L$, the betatron functions in the middle of the QF are

$$\beta_{x,0} = L\frac{\kappa(\kappa+1)}{\sqrt{\kappa^2-1}} \quad \text{and} \quad \beta_{y,0} = L\frac{\kappa(\kappa-1)}{\sqrt{\kappa^2-1}}\,. \tag{6.53}$$

For values of the betatron functions in the middle of the QD we merely interchange indices x with y. Obviously, a solution and therefore beam stability exists only if $\kappa > 1$ or if $f > L$. Knowing the betatron functions at one point is enough to allow the calculation of those functions at any other point in the lattice by virtue of (6.45). In Fig. 6.8 the betatron functions are shown for one cell of a FODO lattice. Note the similarity of the horizontal and vertical betatron functions being only one quadrupole distance shifted with respect to each other. The periodic nature of the solutions allows us to construct a circular accelerator made up of a series of equal FODO cells with periodic repetition of betatron functions and beam sizes.

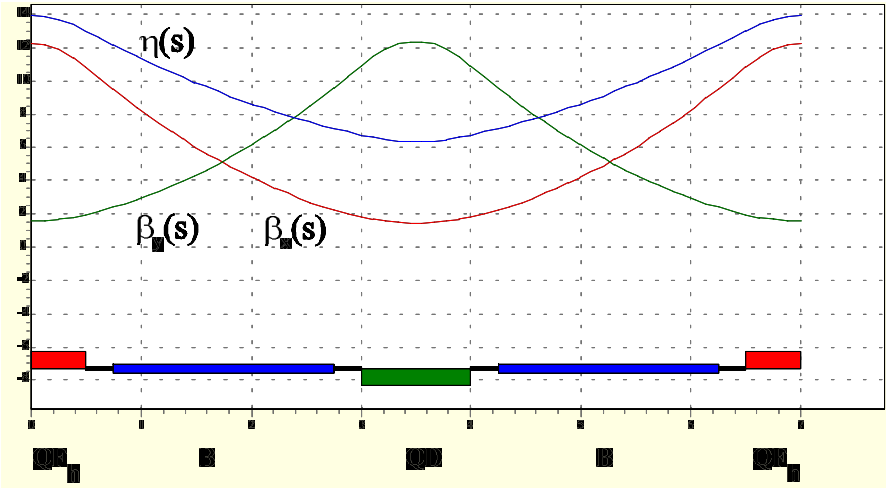

Fig. 6.8. Betatron functions in a FODO lattice

6.8.2 Periodic Dispersion or η-Function

In a circular accelerator there is also only one periodic solution for the dispersion function. Utilizing the 3×3 -transformation matrix for a cell or the whole circumference, the periodic dispersion function, called the η-function, is defined by

$$\begin{pmatrix} \eta_0 \\ \eta_0' \\ 1 \end{pmatrix} = \begin{pmatrix} a & b & D \\ c & d & D' \\ 0 & 0 & 1 \end{pmatrix} \begin{pmatrix} \eta_0 \\ \eta_0' \\ 1 \end{pmatrix} . \tag{6.54}$$

Again, knowledge of the η-function at one point permits the calculation of $\eta(s)$ at any point around the circular accelerator. The η-function defines the equilibrium orbit $\eta(s)\,\delta$ for off-energy particles about which they perform betatron oscillations. The ideal orbit, $x \equiv 0$, is the equilibrium orbit for particles with the design energy E_0 or $\delta = 0$. The η-function varies generally between zero and positive values. Particles with $\delta > 0$ follow therefore a path which is farther away from the ring center while lower energy particles follow a path closer to the ring center than the ideal orbit. The length of the closed path is also energy dependent which becomes of great significance later in connection with synchrotron oscillations as will be discussed in the next chapter.

Periodic dispersion or η-function in a FODO lattice. To illustrate the determination of the η-function, we take the FODO lattice as an example. A storage ring can be constructed from a series of FODO cells which include bending magnets between the quadrupoles. These bending magnets cause the appearance of a dispersion establishing a periodic η-function. Based on the transformation matrix through one FODO cell and assuming for simplicity that the bending magnets are as long as the thin-lens FODO cell we may calculate the 3×3 transformation matrix through one FODO cell. From that we get for the η-functions in the middle of the QF or QD

$$\eta_{\mathrm{qf}} = \frac{L^2}{2\rho}\kappa(2\kappa + 1) \qquad \text{and} \qquad \eta_{\mathrm{qd}} = \frac{L^2}{2\rho}\kappa(2\kappa - 1)\,, \tag{6.55}$$

respectively. Knowing the η-function at one point allows us to calculate its values at any other point around the storage ring. The result for a FODO lattice is shown in Fig. 6.8.

6.8.3 Beam Size

With the addition of these chromatic effects, the total beam sizes (6.42, 6.43) are modified to become

$$\sigma_{x_{\mathrm{tot}}} = \sqrt{\epsilon_x \beta_x + \eta^2 \delta^2} \qquad \text{and} \qquad \sigma_y = \sqrt{\epsilon_y \beta_y}\,, \tag{6.56}$$

where $\delta = \delta E/E_0$ is the relative energy spread in the beam. The total beam divergence is

$$\sigma_{x'_{\rm tot}} = \sqrt{\epsilon_x \gamma_x + \eta'^2 \delta^2} \qquad \text{and} \qquad \sigma_{y'} = \sqrt{\epsilon_y \gamma_y}\,. \tag{6.57}$$

There is no effect on the vertical beam parameters since we assume a storage ring with only horizontal bending magnets.

Exercises *

Exercise 6.1 (S). Consider a uniform static magnetic field B in the laboratory system. Determine the electromagnetic field in the restframe of a moving electron. Show that the Lorentz force in both reference systems point in the same direction. In the laboratory system, the static magnetic field causes a transverse deflection of the moving charge. Show, that the angular deflection is the same in both systems.

Exercise 6.2 (S). Consider a transverse electric field of 10 kV/cm and a transverse magnetic field of 1 Tesla. At what kinetic energy of an electron are the forces of both fields the same?

Exercise 6.3 (S). Construct a $E = 3$ GeV circular accelerator from a series of bending magnets. The magnet length shall be $\ell = 2$ m each and the magnetic field shall not exceed $B = 1.2$ T. Determine the number $n_{\rm b}$ of magnets needed and the exact field strength to complete the ring. What is the bending radius and the deflection angle per magnet?

Exercise 6.4 (S). Derive equation (6.16).

Exercise 6.5 (S). Focus a parallel 1.5 GeV beam to a point 5 m downstream from a thin quadrupole ($l = 0.2$ m). Determine the quadrupole strength k and field gradient g. For an aperture radius of $R = 5$ cm calculate the required excitation current to reach this field gradient g.

Exercise 6.6 (S). Consider a drift space of length L and a symmetric electron beam cross section along this drift space. Derive an expression for the value of the betatron function at the beginning of the drift space that results in the minimum beam size anywhere along this drift space. By how much does the beam size vary between the waist and ends of the drift space?

Exercise 6.7 (S). Use the bending magnets of Exercise 6.3 and add quadrupoles to form a FODO lattice. Choose the optimum quadrupole strength for minimal beam sizes and calculate the value of the horizontal and vertical betatron function in the middle of the defocusing quadrupole? What is the focal length of the quadrupole?

* The argument (S) indicates an exercise for which a solution is given in Appendix A.

Exercise 6.8 (S). For a FODO lattice derive an expression (thin lens approximation) for one betatron function between quadrupoles and calculate the phase advance for the full FODO cell.

Exercise 6.9. Construct a bending magnet with a length of 1.2 m which deflects a 1.5 GeV beam by 20 degrees. What is the required magnetic field. For a gap height between poles of $g = 7$ cm calculate the required excitation current per coil to reach the design field and how many turns must each coil have if the power supply can deliver a current of about 500 A?

Exercise 6.10. Derive (6.33) and (6.34) form (6.32).

Exercise 6.11. Consider an electron beam entering a magnetfree straight section with $(\beta_0, \alpha_0) = (5.0\text{ m}, 2.0)$. Plot the beam size $\sigma(s)$ for an emittance of $\epsilon = 10$ nm for 0 m$< s <$ 5.0 m. What is the value of the betatron function at the symmetry point $\alpha = 0$?

Exercise 6.12. The horizontal beam size reaches a maximum value in the middle of the focusing quadrupole (QF) in a FODO lattice. Plot the beam size in the middle of the QF as a function of the FODO parameter κ. For which value of κ becomes the beam size in a QF a minimum?

7. Radiation Effects

Particle dynamics is greatly influenced by the emission of radiation as well as by the restoration of the energy loss in accelerating cavities. These processes are both beneficial and perturbing while fundamentally determining the electron beam parameters and thereby the characteristics of the photon beam. We will briefly discuss these effects to illuminate the basic physics responsible for the photon beam characteristics in a synchrotron light source.

As electrons travel through magnetic fields, they experience a Lorentz force which deflects the beam orthogonal to the field and velocity vector. This force is the cause for the emission of electromagnetic radiation and the instantaneous radiation power is given by (3.12) or (3.20). This loss of energy into synchrotron radiation during each revolution, while small compared to the electron energy, is sufficiently strong to cause perturbations in beam dynamics which must be compensated.

7.1 Synchrotron Oscillations

One or more rf-cavities are located along the orbit of the ring. These cavities are excited by external microwave sources to generate electric fields parallel to the beam path providing the acceleration needed. Since the rf-fields oscillate very fast (order of 500 MHz) the particle arrival time at the cavity is very critical (Fig. 7.1). Ideally, particles should pass through the cavities exactly at a phase such that they gain the same energy from the accelerating field as they lost to synchrotron radiation. That phase or time is called the synchronous phase ψ_s or synchronous time t_s. Not all particles follow that ideal timing.

Observing orbiting particles, we notice that particles with a higher than ideal energy follow a path which is mostly outside the ideal orbit while particle with lower energies follow a path mostly inside of the ideal path. All particles are highly relativistic, travel close to the speed of light and the going around travel time depends therefore on the length of the path around the ring and therefore on the particle energy. In spite of variations in the revolution time or arrival time at the cavity, a stable beam is ensured by virtue of the principle of phase focusing [43][44], which forces particles to arrive at the cavity, if not exactly, then at least close to the synchronous phase or time. The way this works can be explained with the help of Fig. 7.1. A particle with the ideal

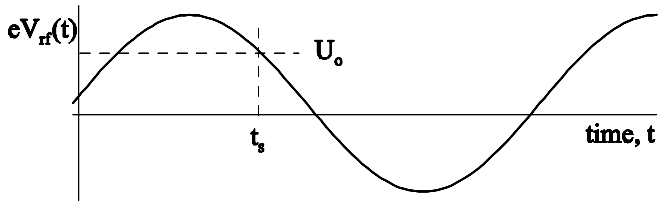

Fig. 7.1. Cavity acceleration voltage as a function of time

energy E_0 passing through the cavity at the synchronous time t_s will arrive again at the synchronous time after one turn. This synchronous particle will gain from the cavity fields the energy

$$U_0 = eV_\mathrm{rf} \sin \psi_\mathrm{s} \,, \tag{7.1}$$

where U_0 is the energy loss per turn of a particle with ideal energy E_0 to synchrotron radiation.. A particle with a higher than ideal energy starting, for example, at time t_s will take longer to orbit the storage ring and will arrive at the cavity after a time $t > t_\mathrm{s}$ to gain an energy $\Delta E < U_0$ thus reducing the positive energy deviation of this particle. The next time this same particle will arrive closer to the synchronous time t_s. A similar process occurs for lower energy particles. The energy dependent revolution time together with the time varying rf-voltage provide a restoring force for particles with a wrong energy. By this process, nonideal particles are made to oscillate about the synchronous time t_s similar to betatron oscillation due to the restoring forces from fields of quadrupole magnets. These oscillations are called synchrotron or phase oscillations.

To formulate this phase focusing, we consider the total energy change per turn $\mathrm{d}\varepsilon = eV_\mathrm{rf}(t) - U(E)$, where $eV_\mathrm{rf}(t)$ is the energy gained by a particle passing through a cavity at time t, and $U(E)$ the energy loss per turn at energy E. We have defined the ideal energy E_0 and synchronous time t_s such that the ideal particle would gain an energy exactly equal to its lost energy $U_0 = U(E_0)$. Expanding at $t = t_\mathrm{s} + \tau$ and $E = E_0 + \varepsilon$, keeping only linear terms and dividing by the revolution time T_0 we get the total energy gain per turn

$$\begin{aligned} \frac{\mathrm{d}\varepsilon}{\mathrm{d}t} &= \frac{1}{T_0} \left[eV_\mathrm{rf}(t_\mathrm{s}) + e\frac{\partial V_\mathrm{rf}}{\partial t}\bigg|_{t_\mathrm{s}} \tau - U(E_0) - \frac{\mathrm{d}U}{\mathrm{d}E}\bigg|_{E_0} \varepsilon \right] \\ &= \frac{1}{T_0} \left[e\,\frac{\partial V_\mathrm{rf}}{\partial t}\bigg|_{t_\mathrm{s}} \tau - \frac{\mathrm{d}U}{\mathrm{d}E}\bigg|_{E_0} \varepsilon \right] \,, \end{aligned} \tag{7.2}$$

where we made use of the fact that $eV_\mathrm{rf}(t_\mathrm{s}) = U(E_0)$. The revolution time depends on the particle velocity and momentum dependent path length (α_c

momentum compaction factor). The revolution time for a particle with energy deviation ε is different from the ideal revolution time T_0 and we find with $\Delta T/T_0 = \mathrm{d}\tau/\mathrm{d}t$

$$\frac{\mathrm{d}\tau}{\mathrm{d}t} \;=\; -(\gamma^{-2} - \alpha_\mathrm{c})\frac{\varepsilon}{E_0}\,. \tag{7.3}$$

The $1/\gamma^2$-term is due to the velocity variation with energy and the momentum compaction factor α_c is defined by the ratio of the relative change of the orbital path length to the relative energy error,

$$\frac{\Delta C}{C_0} = \alpha_\mathrm{c}\frac{\Delta E}{E_0} \tag{7.4}$$

and is

$$\alpha_\mathrm{c} = \left\langle \frac{\eta}{\rho} \right\rangle_\mathrm{s} \tag{7.5}$$

averaged over the circumference. Differentiation of (7.2) with respect to t and replacing $\dot{\tau}$ by (7.3) results in the equation of motion for synchrotron oscillations

$$\frac{\mathrm{d}^2\varepsilon}{\mathrm{d}t^2} + 2\alpha_\mathrm{s}\frac{\mathrm{d}\varepsilon}{\mathrm{d}t} + \Omega^2\varepsilon \;=\; 0\,, \tag{7.6}$$

where the damping decrement for synchrotron oscillations has been defined by

$$\alpha_\mathrm{s} \;=\; \frac{1}{2T_0}\,\frac{\mathrm{d}U}{\mathrm{d}E}\bigg|_{E_0} \;=\; \frac{1}{2}\frac{\mathrm{d}\,\langle P_\gamma\rangle}{\mathrm{d}E} \;=\; 2\frac{\langle P_\gamma\rangle}{E_0}\,, \tag{7.7}$$

where $\langle P_\gamma\rangle$ has been defined in (3.14). The synchrotron oscillation frequency Ω has been introduced with $\omega_0 = 2\pi/T_0$ by the definition

$$\Omega^2 \;=\; \frac{(\gamma^{-2} - \alpha_\mathrm{c})}{E_0 T_0}\,\frac{e\,\partial V_\mathrm{rf}(t)}{\partial t} \;=\; \omega_0^2\frac{h\,(\gamma^{-2} - \alpha_\mathrm{c})\,eV_\mathrm{rf}\,\cos\psi_\mathrm{s}}{2\pi E_0}\,. \tag{7.8}$$

A more detailed derivation of the damping decrement (7.9) reveals a correction, which is necessary to add for specific bending magnet types. The corrected expression reads like (see for example [45])

$$\alpha_\mathrm{s} \;=\; \frac{1}{2}\frac{\mathrm{d}\,\langle P_\gamma\rangle}{\mathrm{d}E} \;= J_s\,\frac{\langle P_\gamma\rangle}{E_0}\,, \tag{7.9}$$

where

$$J_s = 2 + \vartheta \tag{7.10}$$

is the synchrotron partition number with

$$\vartheta = \frac{\oint \frac{\eta}{\rho^3}\left(1+2k\rho^2\right)\,\mathrm{d}s}{\oint \frac{1}{\rho^2}\,\mathrm{d}s}\,. \tag{7.11}$$

The term ϑ is a correction to the damping resulting from specific properties in some bending magnets. The first term under the integral in the nominator occurs only in sector magnets and is zero in rectangular magnets. The second term becomes nonzero only in gradient magnets where $k \neq 0$ and $\rho \neq 0$.

The synchrotron radiation power $\langle P_\gamma \rangle = U(E_0)/T_0$ is the average radiation power along the circumference. We also made use of the fact that the integrated rf-field changes sinusoidally with time like $V_{\mathrm{rf}} = V_0 \sin(\omega_{\mathrm{rf}}\, t)$ and therefore $\dot{V} = \omega_{\mathrm{rf}} V_0 \cos\psi_{\mathrm{s}} = 2\pi h/T_0 V_0 \cos\psi_{\mathrm{s}}$, where h is the integer harmonic number defined by $h = C_0/\lambda_{\mathrm{rf}}$ and $\psi_{\mathrm{s}} = \omega_{\mathrm{rf}}\, t_{\mathrm{s}}$ the synchronous phase at which a particle with energy E_0 is accelerated to compensate exactly for the energy loss U_0 to radiation.

The differential equation of motion exhibits two significant terms. For one, we may expect stable synchrotron oscillations with frequency Ω only if the synchronous phase is chosen such that this frequency is real and not imaginary. Furthermore, the damping term tells us that any deviation ε_0 of a particle from the ideal parameters in longitudinal phase space is damped due to the emission of synchrotron radiation. Due to the fact that synchrotron radiation depends on the particle energy in such a way that higher/lower energy particles loose more/less energy, we observe an energy correcting effect of the emission of synchrotron radiation.

The solution to the differential equation of motion (7.6) is that of a damped harmonic oscillator

$$\varepsilon(t) \;=\; \varepsilon_0\, \mathrm{e}^{-\alpha_{\mathrm{s}} t}\, \cos\Omega t\,. \tag{7.12}$$

Generally, the damping time $\tau_{\mathrm{s}} = 1/\alpha_{\mathrm{s}}$ is of the order of milliseconds, while the synchrotron oscillation time is much shorter of the order of 10–50 μs and we can safely assume that $\tau_{\mathrm{s}} \gg 1/\Omega$. This different time scale allows us to treat synchrotron oscillations while ignoring damping.

Particles orbiting in the storage ring perform oscillations in energy about the ideal energy E_0. At the same time, there is also an oscillation about the synchronous time described by τ, which from (7.3) is 90° out of phase and described by

$$\tau(t) \;=\; \tau_0\, \mathrm{e}^{-\alpha_{\mathrm{s}} t}\, \sin\Omega t\,, \tag{7.13}$$

where from (7.3)

$$\tau_0 \;=\; \frac{\gamma^{-2} - \alpha_{\mathrm{c}}}{\Omega}\frac{\varepsilon_0}{E_0}\,, \tag{7.14}$$

while ignoring damping. This longitudinal oscillation about the synchronous time t_{s} leads to a longitudinal distribution of particles and defines the bunch length ℓ_{b}, which is from (7.14)

$$\ell_b = \beta c \tau_0 \,. \tag{7.15}$$

Later, we will quantify this bunch length in a storage ring in more detail. The energy spread in the beam is directly related to the bunch length and the bunch length or bunch duration eventually defines the pulse length of the photon pulse from each electron bunch.

7.1.1 Longitudinal Phase Space Motion

It is interesting at this point to discuss in some detail the particle motion in longitudinal phase space because it relates directly to the process of radiation production in a Free Electron Laser to be discussed in Chap. 11. We ignore damping and eliminate from (7.12, 7.13) the trigonometric functions to get the formulation for the phase ellipse

$$\frac{\varepsilon^2}{\varepsilon_0^2} + \frac{\tau^2}{\tau_0^2} = 1 \,. \tag{7.16}$$

While performing synchrotron oscillations, particles move along an ellipse in phase space. This is true, however, only for small deviations from the reference point because we used only the linear term in the expansion (7.2) of the rf-voltage in the vicinity of the synchronous time. For large synchrotron oscillation amplitudes, the actual sinusoidal voltage variation must be taken into account. In this case the typical phase space trajectories of particle motion under the influence of an electromagnetic field are shown in Fig. 7.2.

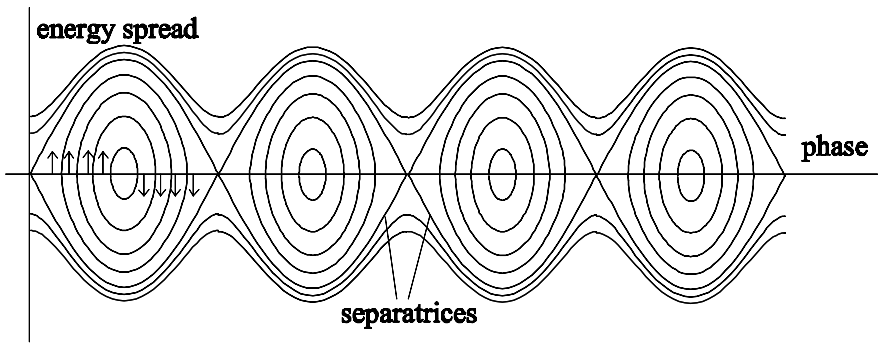

Fig. 7.2. Longitudinal phase space ellipses with separatrices

The phase space trajectories still look very much like ellipses for small amplitudes, which become somewhat distorted towards the shape of a lens as the oscillation amplitudes increase. The region of stable phase motion is

enclosed by two intertwined separatrices, which separate the region of oscillatory motion with that of libration (see Fig. 11.2). This is similar to the dynamics of a swing which performs oscillations at small amplitudes or energies and keeps rotating over the top in one direction for large energies. For a stable beam, we require that all particles are contained well within the separatrices. Observing an individual particle, we notice that it gains and looses energy as it interacts with the electromagnetic field in the accelerating cavity and travels along its phase space trajectory in a clockwise direction. This motion will become specifically significant for a free electron laser as we will discuss in more detail in Chapter 11.

7.2 Damping

Due to synchrotron radiation, all particle motion in 6-dim phase space becomes damped. As we have seen above, energy damping occurs at a rate proportional to the average synchrotron radiation power $\langle P_\gamma \rangle$. Damping occurs also in the transverse plane due to a geometric effect. While particles perform betatron oscillations, they emit radiation in the direction of travel which is generally at a finite angle with the beam axis. During this emission of radiation the particles loose longitudinal as well as transverse momentum. Yet in the rf-cavity, acceleration occurs only in the longitudinal direction. As a consequence, the combined process of emission and acceleration results in a net loss of transverse momentum which is equivalent to a reduction in the betatron amplitude or transverse damping.

To be more quantitative, we note that the direction of the particle motion does not change with the emission of radiation since radiation is emitted in the forward direction within a negligibly small angle of $1/\gamma$. The momentum vector of the particle before emission is for small values of x_0' in x,z-space $(cp_0 x_0', cp_0)$. Emission of a photon caries away the momentum $(-c\Delta p x_0', -c\Delta p)$ and the transverse particle momentum becomes $([cp_0 - c\Delta p]\, x_0', cp_0 - c\Delta p)$. To compensate for this loss of momentum, the particle gains energy in an accelerating cavity and its associated momentum gain in the cavity is $(0, \beta P_{\rm rf}\, {\rm d}t)$. Since the transverse momentum will not be changed by the acceleration, which for simplicity we assume to occur at the location of the radiation emission, we have

$$(cp_0 - c\Delta p)\, x_0' \;=\; (cp_0 - c\Delta p + \beta \langle P_\gamma \rangle \, {\rm d}t)\, x_1' \,, \tag{7.17}$$

where x_0', x_1' are the angles of the particle trajectories with respect to the beam axis before and after acceleration, respectively and the acceleration is equal to the energy loss, $P_{\rm rf}\, {\rm d}t = \langle P_\gamma \rangle \, {\rm d}t$. With $x' = \dot{x}/\beta c$ and the particle energy after emission of a photon but before acceleration $\beta E = cp$ the particle direction after acceleration is

$$\dot{x}_1 \;=\; \frac{E}{E + P_\gamma {\rm d}t}\, \dot{x}_0 \;\approx\; \left(1 - \frac{\langle P_\gamma \rangle \, {\rm d}t}{E}\right) \dot{x}_0 \,, \tag{7.18}$$

where we made use of the fact that $\langle P_\gamma \rangle \, \mathrm{d}t \ll E$ and $E_0 \approx E$. From this, the horizontal damping decrement becomes

$$\alpha_x = -\frac{1}{\dot{x}_0} \frac{\mathrm{d}\dot{x}}{\mathrm{d}t} = J_x \frac{\langle P_\gamma \rangle}{E_0} \,. \tag{7.19}$$

Similar to the synchrotron damping decrement, this expression also has to be corrected for second order effects in sector and gradient magnets, which is done by introducing the partition number

$$J_x = 1 - \vartheta \,, \tag{7.20}$$

where ϑ is defined in (7.11).

A similar expression is valid for the vertical plane:

$$\alpha_y = -\frac{1}{\dot{y}_0} \frac{\mathrm{d}\dot{y}}{\mathrm{d}t} = J_y \frac{\langle P_\gamma \rangle}{E_0} \,, \tag{7.21}$$

where the vertical partition number $J_y = 1$ for a flat storage ring without vertical bending. The amplitude of a betatron oscillation $x(t) = A(t)\sqrt{\beta}\cos\psi(t)$ scales then like

$$A(t) \;=\; A_0 \, \mathrm{e}^{-\alpha_s t} \tag{7.22}$$

because of damping. Under certain circumstances, one or more damping decrements may be modified, e.g. when we have a field gradient in a bending magnet. However, due to very general principles, the sum of all damping decrements is a constant

$$\alpha_s + \alpha_x + \alpha_y \;=\; 4 \frac{\langle P_\gamma \rangle}{E_0} \tag{7.23}$$

or

$$J_x + J_y + J_\mathrm{s} = 4 \,, \tag{7.24}$$

also called the Robinson criterion. Whenever one decrement is modified another one will be modified in the opposite direction. From here on we will ignore such details and point to related discussions on this point to available literature (for example [46]).

7.3 Quantum Effects

Damping of 6-dim phase-space coordinates is counterbalanced in a storage ring by quantum effects [14]. We evaluate the emission of radiation in terms of photon emission and discuss the effect of a single photon emission process on particle dynamics. Consider, for example, a particle performing synchrotron

oscillations, $A = A_0 \mathrm{e}^{\mathrm{i}\Omega(t-t_0)}$, where the last photon emission occurred at time t_0. A new photon of energy ε be emitted at time t_1 causing an energy jump in phase space which alters the synchrotron oscillation like

$$\begin{aligned} A &= A_0 \exp\left[\mathrm{i}\,\Omega(t-t_0)\right] - \varepsilon \exp\left[\mathrm{i}\,\Omega(t-t_1)\right] \\ &= A_1 \exp\left[\mathrm{i}\,\Omega(t-t_1)\right] . \end{aligned} \tag{7.25}$$

Solving for the new amplitude we get

$$A_1^2 = A_0^2 + \varepsilon^2 - 2\,\varepsilon A_0 \cos[\Omega(t_1 - t_0)] . \tag{7.26}$$

Radiation emission occurs many times during a synchrotron oscillation period and we may therefore average over all times to get the average change in the oscillation amplitude due to the emission of a photon with energy ε.

$$\langle \delta A^2 \rangle = \langle A_1^2 - A_0^2 \rangle = \langle \varepsilon^2 \rangle . \tag{7.27}$$

Furthermore, we average now over all photon energies in the radiation spectrum and get the rate of change of the synchrotron oscillation amplitude

$$\left\langle \frac{\mathrm{d}A^2}{\mathrm{d}t} \right\rangle_{s,\mathrm{excitation}} = \int_0^\infty \varepsilon^2 \dot{n}(\varepsilon)\,\mathrm{d}\varepsilon = \left\langle \dot{N}_{\mathrm{ph}} \langle \varepsilon^2 \rangle \right\rangle_s , \tag{7.28}$$

where $\dot{n}\,(\varepsilon)$ is the number of photons of energy ε emitted per unit time and unit energy bin $\mathrm{d}\epsilon$, and $\dot{N}_{\mathrm{ph}}$ is the total number of all photons emitted per unit time. The subscript $_s$ indicates that the integral be taken along the circumference of the ring. Since both photon energy and flux are positive we get from this effect a continuous increase of the oscillation amplitude.

7.4 Equilibrium Beam Parameters

Two radiation effects reflect on the particle beam, damping and quantum excitation which eventually determine the transverse beam sizes, beam divergencies, energy spread and bunch length. The geometric and temporal particle bunch parameters transform directly into those of the photon pulses. Equilibrium values for all of these quantities are determined by damping and quantum excitation.

7.4.1 Equilibrium Energy Spread

The equilibrium energy spread and bunch length can be derived by the requirement that the amplitudes do not change or with (7.28) that

$$\left\langle \frac{\mathrm{d}A^2}{\mathrm{d}t} \right\rangle_s = \left\langle \frac{\mathrm{d}A^2}{\mathrm{d}t} \right\rangle_{s,\mathrm{excitation}} + \left\langle \frac{\mathrm{d}A^2}{\mathrm{d}t} \right\rangle_{s,\mathrm{damping}} = 0 , \tag{7.29}$$

where $\left\langle \frac{\mathrm{d}A^2}{\mathrm{d}t} \right\rangle_s \Big|_{\text{damping}} = -2\alpha_s \langle A^2 \rangle$. With $\tau_s = 1/\alpha_s$ we get

$$\langle A^2 \rangle = \tfrac{1}{2}\tau_s \left\langle \dot{N}_{\text{ph}} \langle \varepsilon^2 \rangle \right\rangle_s , \tag{7.30}$$

where from the discussion in Section 9.7.1 (9.171)

$$\left\langle \dot{N}_{\text{ph}} \langle \varepsilon^2 \rangle \right\rangle_s = \frac{55}{24\sqrt{3}} r_{\text{e}} c\, mc^2\, \hbar c\, \gamma^7 \left\langle \frac{1}{\rho^3} \right\rangle_s . \tag{7.31}$$

The Gaussian energy spread is from $\varepsilon = A \sin \Omega t$ defined by $\sigma_\varepsilon^2 = \langle \varepsilon^2 \rangle = \frac{1}{2}\langle A^2 \rangle$ and the equilibrium energy spread becomes from (7.30) and (7.31)

$$\left(\frac{\sigma_\varepsilon}{E}\right)^2 = C_{\text{q}} \frac{\gamma^2 \langle 1/\rho^3 \rangle}{2\, J_{\text{s}} \langle 1/\rho^2 \rangle} , \tag{7.32}$$

where

$$C_{\text{q}} = \frac{55}{32\sqrt{3}} \frac{\hbar c}{mc^2} = 3.84\ 10^{-13}\ \text{m} . \tag{7.33}$$

It should be noted that the bending radius ρ is always taken to be positive independent of the direction of deflection. The emission of synchrotron radiation does not depend on the sign of deflection. For an isomagnetic ring, where all bending magnets are of the same strength, the energy spread is

$$\left(\frac{\sigma_\varepsilon}{E}\right)^2 = C_{\text{q}} \frac{\gamma^2}{2 J_{\text{s}} \rho} \tag{7.34}$$

depending only on the beam energy and magnet fields, $B \propto \gamma/\rho$.

7.4.2 Bunch Length

The energy oscillation is correlated with a longitudinal oscillation about the bunch center and a beam with a Gaussian energy spread will also have a Gaussian longitudinal particle distribution. From (7.3), and $\tau = \tau_0 \sin \Omega t$ we find for the bunch length $\sigma_\ell = c \frac{|(\gamma^{-2} - \alpha_{\text{c}})|}{\Omega} \frac{\sigma_\varepsilon}{E_0}$ noting that $\sigma_\ell = c\sigma_\tau$. Replacing the synchrotron oscillation frequency by its definition (7.8) we get finally for the equilibrium bunch length (7.3)

$$\sigma_\ell = \frac{\sqrt{2\pi} c}{\omega_{\text{rev}}} \sqrt{\frac{|(\gamma^{-2} - \alpha_{\text{c}})| E_0}{h\, e V_{\text{rf}} \cos \psi_s}} \frac{\sigma_\varepsilon}{E_0} . \tag{7.35}$$

The bunch length is proportional to the energy spread and can be reduced by increasing the rf-voltage although the reduction scales only like $1/\sqrt{V_{\text{rf}}}$.

7.4.3 Horizontal Beam Emittance

Similar to the beam energy spread, we find an excitation effect also in transverse phase space. The emission of a photon occurs in a time short compared to the damping time and therefore causes a sudden change in the particle energy and consequently a sudden change of its reference orbit. Since the electron cannot jump to the new reference orbit, it must oscillate about it with a new betatron amplitude. The particle position is the sum of the betatron amplitude and the offset due to its energy deviation. Emission of a photon with energy ε does not change the particle position $x = x_\beta + x_\eta$ directly but causes a variation of its components

$$\delta x = 0 = \delta x_\beta + \eta\frac{\varepsilon}{E_0} \rightarrow \delta x_\beta = -\eta\frac{\varepsilon}{E_0}\,, \tag{7.36a}$$

$$\delta x' = 0 = \delta x'_\beta + \eta'\frac{\varepsilon}{E_0} \rightarrow \delta x'_\beta = -\eta'\frac{\varepsilon}{E_0}\,. \tag{7.36b}$$

Particles orbiting the storage ring travel along their phase ellipses described by

$$\gamma {x_\beta}^2 + 2\alpha x_\beta {x'}_\beta + \beta {x'}_\beta^2 \;=\; a^2 \tag{7.37}$$

and its perturbation due to the emission of a photon is

$$\gamma\delta({x_\beta}^2) + 2\alpha\delta(x_\beta {x'}_\beta) + \beta\delta({x'}_\beta^2) \;=\; \delta a^2\,. \tag{7.38}$$

Expressing these variations by (7.36) , we get

$$\begin{aligned}
\delta(x_\beta^2) &= (x_{0,\beta} + \delta x_\beta)^2 - x_{0,\beta}^2 = 2x_{0,\beta}\delta x_\beta + \delta x_\beta^2\,,\\
\delta(x_\beta x'_\beta) &= (x_{0,\beta} + \delta x_\beta)(x'_{0,\beta} + \delta x'_\beta) - x_{0,\beta}x'_{0,\beta}\,,\\
&= x_{0,\beta}\delta x'_\beta + x'_{0,\beta}\delta x_\beta + \delta x_\beta \delta {x'}_\beta\;,\\
\delta(x'^2_\beta) &= (x'_{0,\beta} + \delta x'_\beta)^2 - x'^2_{0,\beta} = 2x'_{0,\beta}\delta x'_\beta + \delta x'^2_\beta\,.
\end{aligned} \tag{7.39}$$

Emission of a photon can happen at any phase of the betatron oscillation and we therefore average over all betatron phases which causes the terms linear in x_β and x'_β to vanish. Replacing the variations in (7.38) by their expressions from (7.39) we get

$$\delta a^2 \;=\; \frac{\langle\varepsilon^2\rangle}{E_0^2}\mathcal{H}(s)\,, \tag{7.40}$$

where we have averaged over all photon energies and have defined

$$\mathcal{H}(s) = \gamma\eta^2 + 2\alpha\eta\eta' + \beta{\eta'}^2\,. \tag{7.41}$$

This equation looks very similar to (7.27) and the rate of change of the betatron oscillation amplitude is analogous to (7.28)

$$\left\langle \frac{\mathrm{d}\,\langle a^2\rangle}{\mathrm{d}t} \right\rangle_{s,\mathrm{excitation}} = \frac{\langle \dot{N}_{\mathrm{ph}}\,\langle \varepsilon^2\rangle\,\mathcal{H}\rangle_s}{E_0^2}\,. \tag{7.42}$$

This excitation is again to be combined with damping to get an equilibrium beam emittance

$$\langle a^2\rangle_s \;=\; \tfrac{1}{2}\left\langle \dot{N}_{\mathrm{ph}}\,\langle \varepsilon^2\rangle \mathcal{H}(s)\right\rangle_s\,. \tag{7.43}$$

The rms beam size is $\sigma_x^2 = \frac{1}{2}\langle x^2\rangle = \frac{1}{2}a^2\beta_x$ and the equilibrium beam emittance

$$\epsilon_x \;=\; \frac{\sigma_x^2}{\beta_x} \;=\; C_{\mathrm{q}}\,\gamma^2 \frac{\langle \mathcal{H}(s)/\rho^3\rangle}{J_x\,\langle 1/\rho^2\rangle}\,. \tag{7.44}$$

The equilibrium beam emittance is proportional to the square of the particle energy and further depends on lattice parameters like the strength of the bending magnets and the function $\mathcal{H}(s)$. Depending on the design goal, the magnet lattice can be optimized for a large beam emittance as is desired, for example, in colliding beam storage rings for high energy physics. Many such rings were and are in use now for the production of synchrotron radiation and are known as first generation radiation sources. Another lattice design approach is to minimize the beam emittance, which is the preferred goal for synchrotron radiation sources to maximize photon beam brightness. Synchrotron light sources with intermediate beam emittances and few or no magnet-free straight sections for insertion devices are classified as second generation storage rings. Third generation storage rings have been designed for as small a beam emittance as feasible and include many magnet free sections to install insertion devices. Generally, the focusing power must be increased to minimize the beam emittance leading to significant chromatic and geometric aberrations which limit beam stability in a storage ring.

7.4.4 Vertical Beam Emittance

In most storage rings, there is no dispersion in the vertical plane, $\eta_y \equiv 0$, and it seems therefore that $\mathcal{H}_y(s) = 0$ resulting in a vanishing vertical beam emittance $\epsilon_y = 0$. In this situation we must reconsider the approximations made so far which include the transverse recoil a particle may receive if a photon is emitted not exactly in the forward direction but at a finite angle within $\pm 1/\gamma$. Due to this recoil $\Delta p_\perp \neq 0$ and the vertical equilibrium beam emittance due to the transverse recoil turns out to be

$$\epsilon_y \;=\; \frac{\sigma_y^2}{\beta_y} \;=\; C_{\mathrm{q}}\,\gamma^2 \frac{\langle \beta_y\rangle\,\langle 1/\rho^3\rangle}{2\,J_y\,\langle 1/\rho^2\rangle} \approx 10^{-13}\ \mathrm{rad\,m}\,, \tag{7.45}$$

indeed a very small emittance. This small value justifies the fact that we neglected this effect for the horizontal beam emittance. The smallest beam

emittance achieved so far in any electron storage ring operated in the world is of the order of 10^{-9} rad m, much higher than this fundamental lower limit (7.45).

This result is actually so small that still other effects must be considered. Coupling of horizontal betatron oscillations into the vertical plane due to magnet misalignments (rotational errors of quadrupole alignment) contribute much more to the vertical beam emittance. Actually, in existing storage rings this coupling dominates the vertical beam emittance. For a well aligned storage ring

$$\epsilon_y \lesssim 0.01\epsilon_x \,. \tag{7.46}$$

7.5 Transverse Beam Parameters

Beam parameters like width, height, length, divergence, beam emittances and energy spread are not all fixed independent quantities, but rather depend on lattice and rf parameters. These dependencies on technical design parameters allow the storage ring designer the adjustment of beam parameters, within limits, to be optimum for the intended application. In this section we will discuss such dependencies. A particle beam at any point along a beam trans-

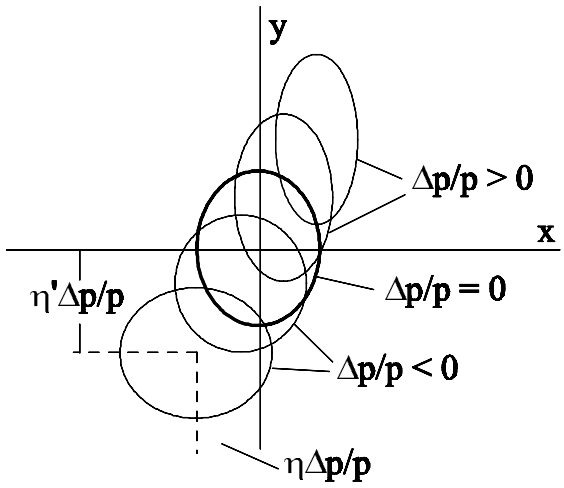

Fig. 7.3. Distribution of beam ellipses for a beam with finite emittance, dispersion and momentum spread (schematic). The variation in the shape of the phase ellipses for different energies reflects the effect of chromatic aberrations

port line may be represented by a few phase ellipses for different particle momenta as shown in Fig. 7.3. The phase ellipses for different momenta are

shifted proportional to the dispersion function at that point and its derivative. Generally, the form and orientation of the ellipses are slightly different too due to chromatic aberrations in the focusing properties of the beam line. For the definition of beam parameters we need therefore the knowledge of the lattice functions including chromatic aberrations and the beam emittance and momentum spread.

7.5.1 Beam Sizes

The particle beam width or beam height is determined by the beam emittance, the values of the betatron and dispersion functions, and the energy spread. The betatron and dispersion functions vary along a beam transport line and depend on the distribution of the beam focusing elements. The beam sizes are therefore also functions of the location along the beam line. From the magnet lattice these functions can be derived and the beam sizes be calculated.

The beam size of a particle beam is generally not well defined since the boundaries of a beam tends to become fuzzy. We may be interested in the beam size that defines all of a particle beam. In this case we look for that phase ellipse that encloses all particles and obtain the beam size in the form of the beam envelope. The beam half-width or half-height of this beam envelope is defined by

$$u_\beta(s) \;=\; \sqrt{\epsilon_u \beta_u(s)} \tag{7.47}$$

with $u = (x, y)$. If there is also a finite momentum spread the overall beam size or beam envelope is increased by the dispersion

$$u_\eta(s) \;=\; \eta_u(s)\,\frac{\Delta cp}{cp_0} \tag{7.48}$$

and the total beam size is

$$u_{\mathrm{tot}}(s) \;=\; u_\beta(s) + u_\eta(s) \;=\; \sqrt{\epsilon_u \beta_u(s)} + \eta_u(s)\,\frac{\Delta cp}{cp_0}\,. \tag{7.49}$$

This definition of the beam size assumes a uniform particle distribution within the beam and is used mostly to determine the acceptance or the beam stay clear of a beam transport system. The acceptance of a beam transport system is defined as the maximum emittance a beam may have and still pass through the vacuum chambers of a beam line. In Fig. 7.3 this would be the area of that ellipse that encloses the whole beam including off momentum particles. In practice, however, we would choose a larger acceptance to allow for errors in the beam path.

Since the lattice functions vary along a beam line the required aperture, to let a beam with the maximum allowable emittance pass, is not the same

everywhere along the system. To characterize the aperture variation consistent with the acceptance, a beam stay clear area, BSC, is defined as the required material free aperture of the beam line.

For a more precise description of the actual beam size, the particle distribution must be considered. In a storage ring, most particle beams assume a Gaussian or near Gaussian density distribution in all six dimensions of phase space and therefore the contributions to the beam parameters from different sources add in quadrature. The beam parameters for Gaussian particle distributions are defined as the standard values of the Gaussian distributions

$$\sigma_x, \sigma_{x'}, \sigma_y, \sigma_{y'}, \sigma_\delta, \sigma_\ell \,, \tag{7.50}$$

where most designations have been defined and used in previous chapters and where $\sigma_\delta = \sigma_\varepsilon / cp_0$ and σ_ℓ the bunch length. The beam size for Gaussian beams is for $u = x$ or $u = y$

$$\sigma_{\mathrm{u,tot}} \;=\; \sqrt{\epsilon_u \beta_u(s) + \eta_u^2(s)\sigma_\delta^2}\,. \tag{7.51}$$

Four parameters are required to determine the beam size in each plane although in most cases the vertical dispersion vanishes.

7.5.2 Beam Divergence

The angular distribution of particles within a beam depends on the rotation of the phase ellipse and we define analogous to the beam size an angular beam envelope by

$$\sigma_{\mathrm{u',tot}} \;=\; \sqrt{\epsilon_u \gamma_u(s) + \eta_u'^{\,2}(s)\,\sigma_\delta^2}\,. \tag{7.52}$$

Again, there is a contribution from the betatron motion, from a finite momentum spread and associated chromatic aberration. The horizontal and vertical beam divergencies are also determined by four parameters in each plane.

7.6 Beam Emittance and Wiggler Magnets

In circular electron accelerators, the beam emittance is determined by the emission of synchrotron radiation and the resulting emittance is not always as desired. In such situations methods to alter the equilibrium emittance are desired and we will discuss in the next sections methods which may be used to either increase or decrease the beam emittance.

The beam emittance in an electron storage ring can be greatly modified by the use of wiggler magnets both to increase [47] or to decrease the beam emittance. Manipulation of the beam emittance in electron storage rings has

become of great interest specifically, to obtain extremely small beam emittances, and we will therefore derive systematic scaling laws for the effect of wiggler magnets on the beam emittance as well as on the beam energy spread.

The particle beam emittance in a storage ring is the result of two competing effects, the quantum excitation caused by the quantized emission of photons and the damping effect. Both effects lead to an equilibrium beam emittance observed in electron storage rings. Independent of the value of the equilibrium beam emittance in a particular storage ring, it can be further reduced by increasing the damping without also increasing the quantum excitation. More damping can be established by causing additional synchrotron radiation through the installation of deflecting dipole magnets like strong wigglers magnets. In order to avoid quantum excitation of the beam emittance, however, the placement of wiggler magnets has to be chosen carefully. As discussed earlier, an increase of the beam emittance through quantum excitation is caused only when synchrotron radiation is emitted at a place in the storage ring where the dispersion function is finite.

Emittance reducing wiggler magnets must be placed in areas around the storage ring where the dispersion vanishes to minimize quantum excitation. To calculate the modified equilibrium beam emittance, we start from (7.42) and get with (7.31) an expression for the quantum excitation of the emittance which can be expanded to include wiggler magnets

$$\left.\frac{\mathrm{d}\epsilon_x}{\mathrm{d}t}\right|_{\mathrm{q_0}} = cC_{\mathrm{Q}}E^5\left\langle\frac{\mathcal{H}}{\rho^3}\right\rangle_0 , \tag{7.53}$$

where

$$C_{\mathrm{Q}} = \frac{55}{24\sqrt{3}}\frac{r_{\mathrm{e}}\hbar c}{(mc^2)^6} = 2.06\,10^{-11}\frac{\mathrm{m}^2}{\mathrm{GeV}^5} . \tag{7.54}$$

The quantity $\mathcal{H}$ is evaluated for the plane for which the emittance is to be determined, E is the particle energy, and ρ_0 the bending radius of the regular ring magnets. The average $\langle\rangle$ is to be taken for the whole ring and the index $_0$ indicates that the average $\langle\mathcal{H}/\rho^3\rangle_0$ be taken only for the ring magnets without wiggler magnets.

Since the contributions of different magnets, specifically, of regular storage ring magnets and wiggler magnets are independent of each other, we may use the results of the basic ring lattice and add to the regular quantum excitation and damping the appropriate additions due to the wiggler magnets,

$$\left.\frac{\mathrm{d}\epsilon_x}{\mathrm{d}t}\right|_{\mathrm{q_w}} = cC_{\mathrm{Q}}E^5\left[\left\langle\frac{\mathcal{H}}{\rho^3}\right\rangle_0 + \left\langle\frac{\mathcal{H}}{\rho^3}\right\rangle_{\mathrm{w}}\right] . \tag{7.55}$$

Both, ring magnets and wiggler magnets produce synchrotron radiation and contribute to damping of the transverse particle oscillations. Again, we may consider both contributions separately and adding the averages the combined rate of emittance damping is

$$\left.\frac{\mathrm{d}\epsilon_x}{\mathrm{d}t}\right|_{\mathrm{d_w}} = -2\,\epsilon_{x\mathrm{w}}\,C_\mathrm{d}\,\frac{E^3}{J_x}\left[\left\langle\frac{1}{\rho^2}\right\rangle_0 + \left\langle\frac{1}{\rho^2}\right\rangle_\mathrm{w}\right], \tag{7.56}$$

where ϵ_w is the beam emittance with wiggler magnets,

$$C_\mathrm{d} = \frac{c}{3}\frac{r_\mathrm{e}}{(mc^2)^3} = 2110\,\frac{\mathrm{m}^2}{\mathrm{GeV}^3\mathrm{s}}, \tag{7.57}$$

and J_x the horizontal damping partition number, assuming a flat storage ring in the horizontal plane. The equilibrium beam emittance is reached when the quantum excitation rate and the damping rates are of equal magnitude. We add therefore (7.55) and (7.56) and solve for the horizontal equilibrium beam emittance

$$\epsilon_{x\mathrm{w}} = C_\mathrm{q}\frac{\gamma^2}{J_u}\frac{\left\langle\frac{\mathcal{H}}{\rho^3}\right\rangle_0 + \left\langle\frac{\mathcal{H}}{\rho^3}\right\rangle_\mathrm{w}}{\left\langle\frac{1}{\rho^2}\right\rangle_0 + \left\langle\frac{1}{\rho^2}\right\rangle_\mathrm{w}}, \tag{7.58}$$

where C_q is defined in (7.33). With ϵ_{x0} being the original beam emittance for $\rho_\mathrm{w} \to \infty$, the relative emittance ratio due to the presence of wiggler magnets is

$$\frac{\epsilon_{x\mathrm{w}}}{\epsilon_{x0}} = \frac{1 + \left\langle\frac{\mathcal{H}}{\rho^3}\right\rangle_\mathrm{w} \Big/ \left\langle\frac{\mathcal{H}}{\rho^3}\right\rangle_0}{1 + \left\langle\frac{1}{\rho^2}\right\rangle_\mathrm{w} \Big/ \left\langle\frac{1}{\rho^2}\right\rangle_0}. \tag{7.59}$$

Making use of the definition of average parameter values and the circumference of the storage ring $C = 2\pi R$ we get

$$\left\langle\frac{\mathcal{H}}{\rho^3}\right\rangle_0 = \frac{1}{C}\oint\frac{\mathcal{H}}{\rho_0^3}\mathrm{d}s, \tag{7.60a}$$

$$\left\langle\frac{\mathcal{H}}{\rho^3}\right\rangle_\mathrm{w} = \frac{1}{C}\oint\frac{\mathcal{H}}{\rho_\mathrm{w}^3}\mathrm{d}s, \tag{7.60b}$$

$$\left\langle\frac{1}{\rho^2}\right\rangle_0 = \frac{1}{C}\oint\frac{1}{\rho_0^2}\mathrm{d}s, \tag{7.60c}$$

$$\left\langle\frac{1}{\rho^2}\right\rangle_\mathrm{w} = \frac{1}{C}\oint\frac{1}{\rho_\mathrm{w}^2}\mathrm{d}s. \tag{7.60d}$$

When evaluating these integrals, note, that the bending radii are always positive, $\rho_{0,\mathrm{w}} > 0$. Evaluation of these integrals for a particular storage ring and wiggler magnet employed gives from (7.59) the relative change in the equilibrium beam emittance. The quantum excitation term scales like the cube while the damping scales only quadratically with the wiggler curvature. This feature leads to the effect that the beam emittance is always reduced for small wiggler fields and increases only when the third power terms become significant.

Concurrent with a change in the beam emittance a change in the momentum spread occurs due to the wiggler radiation which can be derived in a similar way for

$$\frac{\sigma^2_{\epsilon_\mathrm{w}}}{\sigma^2_{\epsilon_0}} = \frac{1+\langle 1/\rho^3\rangle_\mathrm{w}/\langle 1/\rho^3\rangle_0}{1+\langle 1/\rho^2\rangle_\mathrm{w}/\langle 1/\rho^2\rangle_0}\,. \tag{7.61}$$

Closer inspection of (7.59,7.61) reveals basic rules and conditions for the manipulations of beam emittance and energy spread. If the ring dispersion function is finite in the wiggler section, we have $\langle \mathcal{H}_\mathrm{w}\rangle \neq 0$ which can lead to strong quantum excitation depending on the magnitude of the wiggler magnet bending radius ρ_w. This situation is desired if the beam emittance must be increased [47]. If wiggler magnets are placed into a storage ring lattice were the ring dispersion function vanishes, only the small dispersion function created by the wiggler magnets themselves must be considered for the calculation of $\langle \mathcal{H}_\mathrm{w}\rangle$ and therefore only little quantum excitation occurs. In this case the beam emittance can be reduced since the wiggler radiation contributes more strongly to damping and we call such magnets damping wigglers. Whenever wiggler magnets are used which are stronger than the ordinary ring magnets $\rho_\mathrm{w} < \rho_0$ the momentum spread in the beam is increased. This is true for virtually all cases of interest.

Conceptual methods to reduce the beam emittance in a storage ring have been derived which are based on increased synchrotron radiation damping while avoiding quantum excitation effects. Optimum lattice parameters necessary to achieve this will be derived in the next section.

7.6.1 Damping Wigglers

General effects of wiggler magnet radiation on beam emittance has been discussed and we found that the beam emittance can be reduced if the wiggler is placed where $\eta = 0$ to eliminate quantum excitation $\langle \mathcal{H}_\mathrm{w}\rangle = 0$. This latter assumption, however, is not quite correct. Even though we have chosen a place, where the storage ring dispersion function vanishes, we find the quantum excitation factor $\mathcal{H}_\mathrm{w}$ to be not exactly zero once the wiggler magnets are turned on because they, being bending magnets, create their own dispersion function. To calculate this dispersion function we assume a sinusoidal wiggler field

$$B(z) = B_\mathrm{w}\cos k_\mathrm{p} z\,, \tag{7.62}$$

where $k_\mathrm{p} = 2\pi/\lambda_\mathrm{p}$ and λ_p the wiggler period length as shown in Fig. 7.4. From (6.49) the differential equation for the dispersion function in a wiggler magnet

$$\eta'' = \frac{1}{\rho} = \frac{1}{\rho_\mathrm{w}}\cos k_\mathrm{p} z\,, \tag{7.63}$$

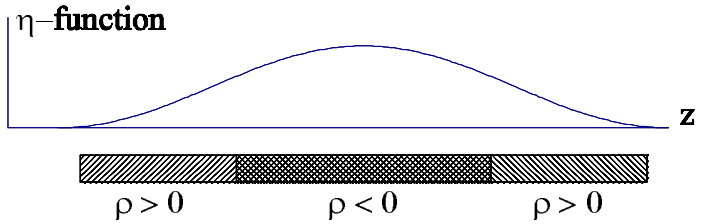

Fig. 7.4. Dispersion function in one period of a wiggler magnet

which can be solved by

$$\eta\left(z\right) = \frac{\theta_{\mathrm{w}}}{k_{\mathrm{p}}}\left(1 - \cos k_{\mathrm{p}} z\right) , \tag{7.64}$$

$$\eta'\left(z\right) = \theta_{\mathrm{w}} \sin k_{\mathrm{p}} z , \tag{7.65}$$

where we have assumed that the wiggler magnet is placed in a dispersion free location $\eta_0 = \eta_0' = 0$ and where from (4.3) $\theta_{\mathrm{w}} = 1/(\rho_{\mathrm{w}} k_{\mathrm{p}})$ is with the deflection angle per wiggler halfpole. With this solution, the first two equations (7.60) can be evaluated. To simplify the formalism, we ignore the z-dependence of the lattice functions within the wiggler magnet and set $\alpha_x = 0$ and $\beta_x = \mathrm{const}$. Evaluating the integrals (7.60), we note that the absolute value of the bending radius ρ must be used along the integration path because the synchrotron radiation does not depend on the sign of the deflection. With this in mind, we evaluate the integrals $\int_0^{\pi} (\eta^2/|\rho^3|)\,\mathrm{d}z$ and $\int_0^{\pi} (\eta'^2/|\rho^3|)\,\mathrm{d}z$. For each half period of the wiggler magnet, the contribution to the integral is with $\mathcal{H} = \eta^2/\beta_x + \eta'^2\beta_x$

$$\Delta \int_0^{\lambda_{\mathrm{p}}/2} \frac{\mathcal{H}}{\rho^3}\,\mathrm{d}z \;=\; \frac{36}{15}\frac{1}{\beta_x}\theta_{\mathrm{w}}^5 + \frac{4}{15}\frac{\beta_x \theta_{\mathrm{w}}^3}{\rho_{\mathrm{w}}^2} \;\approx\; \frac{4}{15}\frac{\beta_x \theta_{\mathrm{w}}^3}{\rho_{\mathrm{w}}^2} , \tag{7.66}$$

where the approximation $\lambda_{\mathrm{p}} \ll \beta_x$ was used. For the whole wiggler magnet with N_{w} periods, the total quantum excitation integral

$$\int_{\mathrm{w}} \frac{\mathcal{H}}{\rho^3}\,\mathrm{d}z \;\approx\; N_{\mathrm{w}}\,\frac{8}{15}\,\frac{\beta_x}{\rho_{\mathrm{w}}^2}\,\theta_{\mathrm{w}}^3 . \tag{7.67}$$

Similarly, the damping integral for the total wiggler magnet is

$$\int_{\mathrm{w}} \frac{1}{\rho^2}\,\mathrm{d}z \;=\; \pi\, N_{\mathrm{w}}\,\frac{\theta_{\mathrm{w}}}{\rho_{\mathrm{w}}} . \tag{7.68}$$

Inserting expressions (7.60,7.67,7.68) into equation (7.59) we get for the emittance ratio

$$\frac{\epsilon_{\mathrm{xw}}}{\epsilon_{x0}} \;=\; \frac{1 + \frac{8}{30\pi}\,\frac{\beta_x}{\langle \mathcal{H}_0 \rangle_\rho}\, N_{\mathrm{w}}\,\frac{\rho_0^2}{\rho_{\mathrm{w}}^2}\,\theta_{\mathrm{w}}^3}{1 + \frac{1}{2}\,N_{\mathrm{w}}\,\frac{\rho_0}{\rho_{\mathrm{w}}}\,\theta_{\mathrm{w}}} , \tag{7.69}$$

where $\langle \mathcal{H}_0 \rangle_\rho$ is the average value of $\mathcal{H}$ in the ring bending magnets excluding the wiggler magnets. We note from (7.69) that the beam emittance indeed can be reduced by wiggler magnets if θ_w is kept small. For easier numerical calculation we replace $\langle \mathcal{H}_0 \rangle_\rho$ by the unperturbed beam emittance which from (7.58) in the limit $\rho_\mathrm{w} \to \infty$ is

$$\langle \mathcal{H}_0 \rangle_\rho \;=\; \frac{J_x\, \rho_0\, \epsilon_{\mathrm{x}0}}{C_\mathrm{q}\, \gamma^2} \tag{7.70}$$

and get instead of (7.69) with the wiggler strength parameter $K = \gamma\theta_\mathrm{w}$

$$\frac{\epsilon_{\mathrm{x}\mathrm{w}}}{\epsilon_{x0}} \;=\; \frac{1 + \frac{8\,C_\mathrm{q}}{30\pi J_x}\,\frac{\beta_x}{\epsilon_{\mathrm{x}0}}\,\frac{K^2}{\rho_\mathrm{w}}\,N_\mathrm{w}\frac{\rho_0}{\rho_\mathrm{w}}\theta_\mathrm{w}}{1 + \frac{1}{2}\,N_\mathrm{w}\frac{\rho_0}{\rho_\mathrm{w}}\theta_\mathrm{w}}\,. \tag{7.71}$$

The beam emittance is reduced by wiggler magnets whenever the second term in the nominator is smaller than the second term in the denominator or when the condition

$$\frac{8}{15\pi}\,\frac{C_\mathrm{q}}{J_x}\,\frac{\beta_x}{\epsilon_{\mathrm{x}0}}\,\frac{K^2}{\rho_\mathrm{w}} \;\le\; 1 \tag{7.72}$$

is fulfilled. For large numbers of wiggler periods, $N_\mathrm{w} \to \infty$, the beam emittance reaches asymptotically a lower limit given by

$$\frac{\epsilon_{\mathrm{x}\mathrm{w}}}{\epsilon_{\mathrm{x}0}} \;\to\; \frac{8\,C_\mathrm{q}}{15\pi J_x}\,\frac{\beta_x}{\epsilon_{\mathrm{x}0}}\,\frac{K^2}{\rho_\mathrm{w}}\,. \tag{7.73}$$

For many wiggler periods the increase in momentum spread also reaches an asymptotic limit which is from (7.61)

$$\frac{\sigma^2_{\epsilon\mathrm{w}}}{\sigma^2_{\epsilon 0}} \;\to\; \frac{\rho_0}{\rho_\mathrm{w}} \;=\; \frac{B_\mathrm{w}}{B_0}\,, \tag{7.74}$$

where B_0 is the magnetic field strength in the ring magnets. Beam stability and acceptance problems may occur if the beam momentum spread is allowed to increase too much and therefore inclusion of damping wigglers must be planned with some caution.

7.6.2 Variation of the Damping Distribution

Robinson's criterion (7.23) provides an expression for the overall damping in six-dimensional phase space without specifying the distribution of damping in the three degrees of freedom. In accelerators, we make an effort to decouple the particle motion in the three degrees of freedom as much as possible and as a result we try to optimize the beam parameters in each plane separately from the other planes for our application. Part of this optimization is the

adjustment of damping and, as a consequence, of beam emittances to desired values. Robinson's criterion allows us to modify the damping in one plane at the expense of damping in another plane. This shifting of damping is done by varying damping partition numbers defined in Section 7.2.

From the definition of the ϑ parameter is is clear that damping partition numbers can be modified depending on whether the accelerator lattice is a combined function or a separated function lattice. By choosing a combination of gradient and separated function magnets we may generate virtually any distribution between partition numbers while staying within Robinson's criterion.

Damping partition and rf-frequency. Actually such "gradient magnets" can be introduced even in a separated function lattice. If the rf-frequency is varied, the beam will follow a path that meets the synchronicity condition. Increasing the rf-frequency corresponds to a shorter wavelength and therefore to a reduced orbit length to keep the harmonic number constant. As a consequence of the principle of phase stability, the beam energy is reduced and the beam follows a lower energy equilibrium orbit with the same harmonic number as the reference orbit for the reference energy. Decreasing the rf-frequency leads just to the opposite effect. Off momentum orbits pass systematically off center through quadrupoles which therefore function like combined function gradient magnets.

To quantify this effect, we use for ϑ only the second term in (7.11). The first term, coming from sector magnets, will stay unaffected. Displacement of the orbit in the quadrupoles will cause bending with a bending radius

$$\frac{1}{\rho_{\mathrm{q}}} \;=\; k\,\delta x\,. \tag{7.75}$$

An rf-frequency shift causes a momentum change of

$$\frac{\Delta p}{p_0} \;=\; -\,\frac{1}{\alpha_{\mathrm{c}}}\,\frac{\Delta f_{\mathrm{rf}}}{f_{\mathrm{rf}}}\,, \tag{7.76}$$

which in turn causes a shift in the equilibrium orbit of

$$\delta x \;=\; \eta\,\frac{\Delta p}{p_0} \;=\; -\,\frac{\eta}{\alpha_{\mathrm{c}}}\,\frac{\Delta f_{\mathrm{rf}}}{f_{\mathrm{rf}}} \tag{7.77}$$

and the bending radius of the shifted orbit in quadrupoles is

$$\frac{1}{\rho_{\mathrm{q}}} \;=\; k\delta x \;=\; k\,\eta\frac{\Delta p}{p_0} \;=\; -\;k\frac{\eta}{\alpha_{\mathrm{c}}}\frac{\Delta f_{\mathrm{rf}}}{f_{\mathrm{rf}}}\,. \tag{7.78}$$

Inserted into the second term of (7.11), where ρ_{a} is the actual bending radius of the ring bending magnets we get

$$\Delta\vartheta \;=\; -\,\frac{1}{\alpha_{\mathrm{c}}}\,\frac{\oint 2\,k^2\,\eta^2\,\mathrm{d}s}{\oint \mathrm{d}s/\rho_{\mathrm{a}}^2}\,\frac{\Delta f_{\mathrm{rf}}}{f_{\mathrm{rf}}}\,. \tag{7.79}$$

We see that all quantities in (7.79) are fixed properties of the lattice and changing the rf-frequency leads just to the effect we expected. Specifically, we note that all quadrupoles contribute additive irrespective of their polarity. We may apply this to a simple isomagnetic FODO lattice where all bending magnets and quadrupoles have the same absolute strength. Integration of the nominator in (7.79) leads to

$$\oint 2\,k^2\,\eta^2\,\mathrm{d}s \;=\; 2\,k^2(\eta^2_{\max}+\eta^2_{\min})\,l_{\mathrm{q}}2\,n_{\mathrm{c}}\,,$$

where $2l_{\mathrm{q}}$ is the quadrupole length in a FODO lattice, $\eta_{\max}$ and $\eta_{\min}$ the values of the η-function in the focusing QF and defocusing QD quadrupoles, respectively, and n_{c} the number of FODO cells in the ring. The denominator $\oint \mathrm{d}s/\rho^2 = 2\pi/\rho_{\mathrm{a}}$ and the variation of ϑ in a FODO lattice is

$$\Delta\vartheta \;=\; -\,n_{\mathrm{c}}\frac{2\,\rho_a}{\pi\,\alpha_{\mathrm{c}}\,l_{\mathrm{q}}}\frac{\eta^2_{\max}+\eta^2_{\min}}{f^2}\frac{\Delta f_{\mathrm{rf}}}{f_{\mathrm{rf}}}\,, \tag{7.80}$$

where we have used the focal length $f^{-1} \;=\; k\,l_{\mathrm{q}}$. We replace in (7.80) the η functions by the expressions (6.55) derived for a FODO lattice, recall the relation $f \;=\; \kappa\,L$ and get finally

$$\Delta\vartheta \;=\; -\,\frac{\rho_a}{\rho}\frac{1}{\alpha_{\mathrm{c}}}\frac{L}{l_{\mathrm{q}}}(4\kappa^2+1)\frac{\Delta f_{\mathrm{rf}}}{f_{\mathrm{rf}}}\,, \tag{7.81}$$

where ρ is the average bending radius in the FODO cell as defined in Chap. 6. The variation of the ϑ parameter in a FODO lattice is the more sensitive to rf-frequency variations the longer the cell compared to the quadrupole length and the weaker the focusing. For other lattices the expressions may not be as simple as for the FODO lattice but can always be computed by numerical evaluation of (7.79).

By varying the rf-frequency and thereby the horizontal and longitudinal damping partition number, we have found a way to either increase or decrease the horizontal beam emittance. To decrease the horizontal beam emittance we would increase the horizontal partition number and at the same time the longitudinal partition number would be reduced. The adjustments, however, are limited. The limit is reached when the longitudinal motion becomes unstable or in practical cases when the partition number becomes less than about 0.5. Other more practical limits may occur before stability limits are reached if the momentum change becomes too large to fit in the vacuum chamber aperture or within the dynamic aperture, whichever is smaller.

7.6.3 Can we Eliminate the Beam Energy Spread?

To conclude the discussions on beam manipulation, we try to eliminate the energy spread in a particle beam. From beam dynamics, we know that the beam

particles can be sorted according to their energy by introducing a dispersion function. The distance of a particle from the reference axis is proportional to its energy and given by

$$x_\delta \;=\; D\,\delta\,, \tag{7.82}$$

where D is the value of the dispersion at the location under consideration and $\delta = \Delta E/E_0$ the energy error. For simplicity, we make no difference between energy and momentum during this discussion. We consider now a cavity excited in a mode (TM_{011}-mode) such that the accelerating field is zero at the axis, but varies linearly with the distance from the axis. If now the accelerating field, or after integration through the cavity, the accelerating voltage off axis scales like

$$eV_{\mathrm{rf}}(x_\delta) \;=\; -\frac{x_\delta}{D}\,E_0\,, \tag{7.83}$$

we have just compensated the energy spread in the beam. The particle beam has become monochromatic, at least to the accuracy assumed here. In this process Liouville's theorem is violated because this scheme does not change the bunch length and the longitudinal emittance has been indeed reduced by application of macroscopic fields.

The problem is that we are by now used to consider transverse and longitudinal phase space separate. While this separation is desirable to manage the mathematics of beam dynamics, we must not forget, that ultimately beam dynamics occurs in 6-dimensional phase space. Since Liouville's theorem must be true, its apparent violation warns us to observe changes in other phase space dimensions. In the case of beam monochromatization, we notice that the transverse beam emittance has been increased by virtue of Maxwell's equations. The transverse variation of the longitudinal electric field causes the appearance of transverse magnetic fields which deflect the particles trajectories transversely thus increasing the transverse phase space at the expense of the longitudinal phase space.

This is a general feature of electromagnetic fields known as the Panofsky–Wenzel Theorem [48] . The Lorentz force due to electromagnetic fields causes a change in the particle momentum which in the transverse direction is given by

$$c\boldsymbol{p}_\perp \;=\; \frac{e}{\beta}\int_0^d [\boldsymbol{E}_\perp + (\boldsymbol{\beta}\times\boldsymbol{B})_\perp]\;\mathrm{d}z\,. \tag{7.84}$$

Expressing the fields by the vector potential $\boldsymbol{E}_\perp = -\partial\boldsymbol{A}_\perp/\partial t$ and $\boldsymbol{B}_\perp = (\nabla\times\boldsymbol{A})_\perp$ the change in the transverse momentum can be expressed by

$$c\boldsymbol{p}_\perp \;=\; -e\nabla_\perp\int_0^d \boldsymbol{E}\mathrm{d}z\,, \tag{7.85}$$

where the integration is taken over the length d of the cavity. This is the Panofsky–Wenzel theorem which states in our case that transverse acceleration occurs whenever there is a transverse variation of the accelerating field. In conclusion, we find that indeed a particle beam can be monochromatized with the use of, for example, a TM_{110}–mode cavity, but only at the expense of transverse beam emittance.

7.7 Photon Source Parameters

With the knowledge of betatron functions, beam emittances and energy spread we are in a position to define the particle beam cross sections and photon source parameters. The total beam width or height is defined by the contribution of the betatron phase space $\sigma_{\beta,x,y}$ and the energy phase space $\sigma_{\eta,x,y}$ and is

$$\sigma_{\mathrm{tot},x,y} = \sqrt{\sigma^2_{\beta,x,y} + \sigma^2_{\eta}} = \sqrt{\epsilon_{x,y}\beta,x,y + \eta^2_x \frac{\sigma_\varepsilon}{E_0}} \tag{7.86}$$

with $\sigma^2_{\beta,x,y} = \epsilon_{x,y}\beta_{x,y}$ and $\sigma_{\eta,x} = \eta_x \frac{\sigma_\varepsilon}{E_0}$, $\gamma_{x,y} = \frac{1+\alpha^2_{x,y}}{\beta_{x,y}}$ and $\alpha_{x,y} = -\frac{1}{2}\beta'_{x,y}$. Similarly, we get for the beam divergence

$$\sigma_{\mathrm{tot},x',y'} = \sqrt{\sigma^2_{\beta,x',y'} + \sigma^2_{\eta'}} = \sqrt{\epsilon_{x,y}\gamma_{x,y} + \eta'^2 \frac{\sigma_\varepsilon}{E_0}}\,. \tag{7.87}$$

These beam parameters resemble in general the source parameters of the photon beam. Deviations occur when the beam emittance becomes very small, comparable to the photon wavelength of interest. In this case, the photon source parameters may be modified by diffraction effects which limit the apparent source size and divergence to some minimum values even if the electron beam cross section should be much smaller. For radiation at a wavelength λ, the diffraction limited, radial photon source parameters are [1]

$$\sigma_r = \frac{1}{2\pi}\sqrt{\lambda L} \qquad \text{and} \qquad \sigma'_r = \sqrt{\frac{\lambda}{L}}\,. \tag{7.88}$$

Projection onto the horizontal or vertical plane gives $\sigma_{x,y} = \sigma_r/\sqrt{2}$ etc. Due to diffraction, it is not useful to push the electron beam emittance to values much smaller than

$$\epsilon_{x,y} = \frac{\lambda}{4\pi}\,. \tag{7.89}$$

[1] Many authors use a different definition $\sigma_{\mathrm{r}} = \sigma_r/\sqrt{2}$. The difference is mainly that the subscript $_{\mathrm{r}}$ refers to radiation and the related beam parameters are already projected to the x or y-plane. In this text we use the subscript $_r$ from the radial coordinate since we derive the diffraction effects from a round beam.

For an arbitrary electron beam cross section the photon source parameters are the quadratic sums of both contributions

$$\sigma^2_{\mathrm{ph},x,y} = \sigma^2_{\mathrm{tot},x,y} + \tfrac{1}{2}\,\sigma^2_r\,, \tag{7.90}$$

$$\sigma'^2_{\mathrm{tot},x,y} = \sigma'^2_{\mathrm{tot},x,y} + \tfrac{1}{2}\,\sigma'^2_r\,. \tag{7.91}$$

The contribution from diffraction can be ignored if

$$\epsilon_{x,y} \gg \frac{\lambda}{4\pi}\,. \tag{7.92}$$

Exercises *

Exercise 7.1 (S). Derive the equation of motion for synchrotron oscillations with large amplitudes and for a sinusoidal variation of the rf–voltage.

Exercise 7.2 (S). Calculate the synchrotron damping time for the storage ring in Exercise 6.3 or 4.1 and rectangular pure dipole magnets. What are the damping times in that ring? Calculate the equilibrium energy spread.

Exercise 7.3 (S). What is the probability for a 6 GeV electron to emit a photon with an energy of $\varepsilon = \sigma_\varepsilon$ per unit time travelling on a circle with radius $\rho = 25$ m. How likely is it that this particle emits another such photon within a damping time? In evaluating quantum excitation and equilibrium emittances, do we need to consider multiple photon emissions? (use isomagnetic ring)

Exercise 7.4 (S). How many photons are emitted by an electron of energy E on average per turn.

Exercise 7.5. Consider an electron beam in a 6 GeV storage ring with a bending radius of $\rho = 20$ m . Calculate the rms energy spread σ_ε/E_0 and the damping time τ_s.

Exercise 7.6. For the storage ring design in Exercise 6.3 estimate the average value $\langle\mathcal{H}\rangle$ and calculate the beam emittance.

Exercise 7.7. An electron beam circulating in a 1.5 GeV storage ring emits synchrotron radiation. The rms emission angle of photons is $1/\gamma$ about the forward direction of the particle trajectory. Determine the photon phase space distribution at the source point and at a distance of 10 m away while ignoring the finite particle beam emittance. Now assume a Gaussian particle distribution with a horizontal beam emittance of $\epsilon_x = 0.15 \times 10^{-6}$ rad–m. Fold both the photon and particle distributions and determine the photon phase

* The argument (S) indicates an exercise for which a solution is given in Appendix A.

space distribution 10 m away from the source point if the electron beam size is $\sigma_x = 1.225$ mm, the electron beam divergence $\sigma_{x'} = 0.1225$ mrad and the source point is a symmetry point of the storage ring. Assume the dispersion function to vanish at the source point. For what minimum photon wavelength would the vertical electron beam size appear diffraction limited if the emittance coupling is 10% ?

8. Storage Ring Design as a Synchrotron Light Source

Synchrotron radiation sources have undergone significant transitions and modifications over past years. Originally, most experiments with synchrotron radiation were performed parasitically on high energy physics colliding beam storage rings. Much larger photon fluxes could be obtained from such sources compared to any other source available. The community of synchrotron radiation users grew rapidly and so did the variety of applications and fields. By the time the usefulness storage rings for high energy physics was exhausted some of these facilities were turned over to the synchrotron radiation community as fully dedicated radiation sources. Those are called first generation synchrotron radiation sources. They were not optimized for minimum beam emittance and maximum photon beam brightness. Actually, the optimization for high energy physics called for a maximum beam emittance to maximize collision rates for elementary particle events. The radiation sources were mostly bending magnets although the development and use of insertion devices started in these rings. Typically, the beam emittance is in the 100's nm.

As the synchrotron radiation community further grew, funds became available to construct dedicated radiation facilities. Generally, these rings were designed as bending magnet sources but with reduced beam emittance ($\leq$ 100 nm) to increase photon brightness. The design emittances were much smaller than those in first generation rings but still large by present day standards. The use of insertion devices did not significantly affect the storage ring designs yet. These rings are called second generation rings.

Third generation synchrotron radiation sources have been designed and constructed during the second half of the eighties and into the nineties. These rings were specifically designed for insertion device radiation and minimum beam emittance ($4 \leq \epsilon_x \leq 20$ nm) or maximum photon beam brightness. As such, they exhibit a large number of magnet-free insertion straight sections.

Finally, fourth generation synchrotron radiation sources are so far only under discussion. A consensus seems to emerge within the community that such sources may be based more on linear accelerators. For example, great efforts are underway in a number of laboratories to design x-ray lasers. Such a source would be based on the principle of a single pass FEL where a high energy and high quality electron beam passing through a long undulator

produces coherent undulator radiation in the x-ray regime. A storage ring based alternative has been proposed which uses the ring structure only as a distributor of radiation to individual beam lines. An electron beam is injected continuously from a high performance electron linear accelerator. Such a linac beam can have a very low beam emittance which is preserved in the storage ring for some number of turns before quantum excitation takes over. To compensate for the high energy cost the spent electron beam is ejected from the storage ring again and its energy is recovered.

8.1 Storage Ring Lattices

To achieve a small particle beam emittance for maximum photon beam brightness a number of different magnet lattices for storage rings are available. All lattices can basically be used to achieve as small a beam emittance as desired, limited only by diffraction effects of the photon beams. Other, more practical considerations, however, limit the minimum beam emittance achievable in a particular lattice. A variety of magnet lattices have been used in the designs of existing storage ring based synchrotron radiation sources. In this section three basic types and some variations thereof will be discussed:

- the FODO lattice
- the double bend achromat lattice (dba)
- the triple bend achromat lattice (tba)

All lattice types can provide long magnet free sections for the installation of insertion devices, accelerating cavities and injection components. For insertion devices one would prefer to have dispersion free sections available which is easy to achieve in a dba-or tba-lattice but more complicated in a FODO lattice. On the other hand, a FODO lattice is very compact and is therefore mostly suitable for generating low emittance beams in so-called damping rings for applications in high energy accelerator systems. The dba-and tba-lattices are more open and provide easily magnetfree straight sections, a desired feature for high brightness synchrotron radiation sources. More recently, the demand for dispersionfree insertion straight sections has been relaxed in favor of an even lower beam emittance achievable this way. Quantum excitation is kept very low by using short period undulator and wiggler magnets.

8.1.1 FODO Lattice

We consider here briefly the FODO lattice because of its simplicity and its ability to give us a quick feeling for the scaling of beam emittance with lattice parameters. The beam emittance can be manipulated at design time by adjusting $\langle \mathcal{H} \rangle$ to the desired value. To calculate the average value $\langle \mathcal{H} \rangle$ in a FODO lattice is somewhat elaborate. Here, we are interested primarily in the

scaling of the beam emittance with FODO lattice parameters. Recollecting the results for the symmetric solutions of the lattice functions in a FODO lattice (6.53,6.55) we notice the following scaling laws

$$\beta \propto L\,, \tag{8.1}$$
$$\beta' \propto L^0\,, \tag{8.2}$$
$$\eta \propto L^2/\rho\,, \tag{8.3}$$
$$\eta' \propto L/\rho\,, \tag{8.4}$$

where L is the distance between the centers of adjacent quadrupoles. All three terms in the function $\mathcal{H}(s) = \gamma(s)\,\eta^2 + 2\alpha(s)\,\eta\eta' + \beta(s)\,\eta'^2$scale in a similar fashion like

$$\{\mathcal{H}(s)\} = \left\{\frac{1}{L}\frac{L^4}{\rho};\; L^0\frac{L^2}{\rho}\frac{L}{\rho};\; L\frac{L^2}{\rho}\right\} \propto \frac{L^3}{\rho^2} \tag{8.5}$$

and the equilibrium emittance for a FODO lattice scales then like

$$\epsilon_x = C_\mathrm{q}\gamma^2\frac{\langle\mathcal{H}/\rho\rangle}{\langle 1/\rho^2\rangle} \propto \gamma^2\frac{L^3}{\rho^3} \propto \gamma^2\varphi^3\,, \tag{8.6}$$

where $\varphi = \ell_\mathrm{b}/\rho$ is the deflection angle in each bending magnet. The proportionality factor depends on the strengths of the quadrupoles and is large for very weak or very strong quadrupoles. A minimum can be reached for a focal length of $|\,f\,| \approx 1.06\,L$ in each half-quadrupole resulting in a minimum beam emittance achievable in a FODO lattice given in practical units by

$$\epsilon\,(\mathrm{radm}) \;\approx\; 10^{-11}\,E^{\,2}(\mathrm{GeV})\,\varphi^3\,(\mathrm{deg}^3)\,, \tag{8.7}$$

where $\varphi = 2\pi/N_\mathrm{M}$, N_M the number of bending magnets in the ring and $N_\mathrm{M}\,/\,2$ the total number of FODO cells in the ring. This result is significant because it exhibits a general scaling law of the beam emittance proportional to the square of the beam energy and the cube of the deflecting angle in each bending magnet, which is valid for all lattice types. The coefficients, though, vary for different lattices. While the beam energy is primarily driven by the desired photon spectrum, we find that high brightness photon beams from low emittance electron beams require a storage ring design composed of many lattice cells with a small deflection angle per magnet. Of course, there are some limits on how far one can go with this concept due to other limitations, not the least being size and cost of the ring which both grow with the number of lattice cells.

8.2 Optimization of a Storage Ring Lattice

While the cubic dependence of the beam emittance on the bending angle is a significant design criterion we discuss here a more detailed optimization

strategy. The emittance is determined by the beam energy, the bending radius and the $\mathcal{H}$-function. Generally, we have no choice on the beam energy which is mostly determined by the desired critical photon energy of bending magnet and insertion device radiation or cost. Similarly, the bending radius is defined by the ring geometry, desired spectrum etc. Interestingly, it is not the bending radius but rather the bending angle which influences the equilibrium beam emittance. The main process to minimize the beam emittance is to adjust the focusing such that the lattice functions in the bending magnets generate a minimum value for $\langle \mathcal{H} \rangle$.

8.2.1 Minimum Beam Emittance

The equilibrium beam emittance (7.44)

$$\epsilon_x = \frac{\sigma_x^2}{\beta_x} = C_\mathrm{q}\,\gamma^2 \frac{\langle \mathcal{H}(s)/\rho^3 \rangle}{\langle 1/\rho^2 \rangle} \tag{8.8}$$

depends only on the lattice function $\mathcal{H}(s)$ inside bending magnets where $1/\rho \neq 0$. We may therefore, independent of any lattice type, consider this function only within bending magnets. For the purpose of this discussion we assume a regular periodic lattice, where all lattice functions within each bending magnet are the same, and concentrate therefore our discussion just on one bending magnet. The average value $\langle \mathcal{H}/\rho^3 \rangle$ for the whole ring will then be the same as that for one magnet.

The contribution of any individual bending magnet with bending radius ρ to the beam emittance can be determined by calculation of the average

$$\langle \mathcal{H} \rangle = \frac{1}{\ell_\mathrm{b}} \int_o^{\ell_\mathrm{b}} \mathcal{H}\,(s)\,\mathrm{d}s\,, \tag{8.9}$$

where L is the length of the bending magnet and the bending radius is assumed to be constant within a magnet. From here on, we ignore the index $_x$ since we assume a flat storage ring in the horizontal plane. All lattice functions are therefore to be taken in the horizontal plane.

Since in first approximation there is no focusing within bending magnets we may treat such magnets as drift spaces. The lattice functions, starting at the entrance to the magnet (Fig. 8.1) with values $(\beta_0, \alpha_0, \gamma_0, \eta_0, \eta_0')$vary within the bending magnet like

$$\begin{aligned}
\beta(s) &= \beta_0 - 2\alpha_0\, s + \gamma_0\, s^2, \\
\alpha(s) &= \alpha_0 - \gamma_0\, s\,, \\
\gamma(s) &= \gamma_0\,, \\
\eta(s) &= \eta_0 + \eta_0'\, s + \rho\,(1 - \cos\psi)\,, \\
\eta'(s) &= \eta_0' + \sin\psi\,,
\end{aligned} \tag{8.10}$$

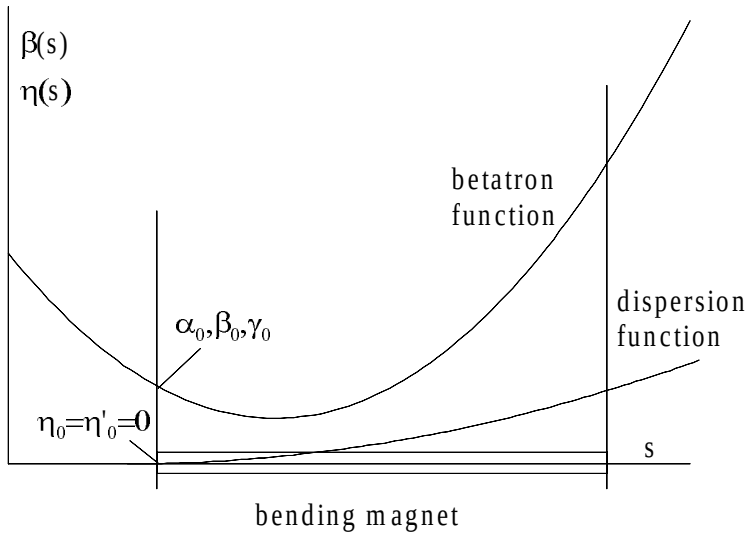

Fig. 8.1. Lattice functions in a bending magnet

where $0 \leq s \leq \ell_\mathrm{b}$ and the deflection angle $\psi = \frac{s}{\rho}$. Before we use these equations, we assume lattices where $\eta_0 = \eta_0' = 0$. The consequences of this assumption will be discussed later. Using (8.9) and (8.10) we get

$$\langle \mathcal{H} \rangle = \beta_0 \, B + \alpha_0 \rho \, A + \gamma_o \, \rho^2 \, C \, . \tag{8.11}$$

The coefficients A, B, and C are functions of the total deflection angle $\varphi = \ell_\mathrm{b}/\rho$ defined by

$$B = \tfrac{1}{2} \left(1 \, - \, \frac{\sin 2\varphi}{2\varphi} \right) , \tag{8.12}$$

$$A = 2 \, \frac{1 - \cos\varphi}{\varphi} - \, \frac{3 \sin^2 \varphi}{2\varphi} - \tfrac{1}{2} \, \varphi \, + \, \tfrac{1}{2} \, \sin 2\varphi \, , \tag{8.13}$$

$$C = \tfrac{3}{4} \, + \, 2 \cos\varphi + \, \frac{5 \sin \, 2\varphi}{8\varphi} - 4 \, \frac{\sin \, \varphi}{\varphi} + \tfrac{1}{6} \, \varphi^2 \, . \tag{8.14}$$

For small bending angles and an isomagnetic ring, where all bending magnets are the same, we have:

$$B \approx \tfrac{1}{3} \, \varphi^2 \, (1 - \tfrac{1}{5} \, \varphi^2 \,) \, , \tag{8.15}$$

$$A \approx -\tfrac{1}{4} \, \varphi^3 \, (1 - \tfrac{5}{18} \, \varphi^2 \,) \, , \tag{8.16}$$

$$C \approx \tfrac{1}{20} \, \varphi^4 \, (1 - \tfrac{5}{14} \, \varphi^2 \,) \, , \tag{8.17}$$

and the beam emittance (8.6) in the lowest order of approximation becomes

$$\epsilon = C_\mathrm{q}\,\gamma^2\,\varphi^3\,\left[\tfrac{1}{3}\,\frac{\beta_0}{\ell_\mathrm{b}} - \tfrac{1}{4}\,\alpha_0 + \tfrac{1}{20}\gamma_0\,\ell_\mathrm{b}\right]\,, \tag{8.18}$$

where C_q is defined in (7.33).

This equation shows clearly the cubic dependence of the beam emittance on the deflection angle φ per bending magnet, which is a general property of all lattices since we have not yet made any assumption on a particular lattice. Equation (8.18) has a minimum for both α_0 and β_0. From the derivative $\partial\,\langle\mathcal{H}\rangle\,/\,\partial\alpha_0 = 0$ we extract the optimum value for α_0

$$\alpha_{0\,\mathrm{opt}} = -\frac{1}{2}\,\frac{A}{C}\,\frac{\beta_0}{\rho}\,. \tag{8.19}$$

Inserting this result into (8.18), and evaluating the derivative $\partial\langle\mathcal{H}\rangle\,/\,\partial\,\beta_0 = 0$ the optimum value for β_0 becomes

$$\beta_0^* \;=\; \frac{2\,C\,\rho}{\sqrt{4BC\;-\;A^2}}\,. \tag{8.20}$$

With β_0^* the quantity α_0^* is

$$\alpha_0^* \;=\; \frac{-A}{\sqrt{4BC\;-\;A^2}} \tag{8.21}$$

and the minimum possible value for $\mathcal{H}$ is finally

$$\langle\mathcal{H}\rangle_\mathrm{min} \;=\; \sqrt{4BC\;-\;A^2}\,\rho\,. \tag{8.22}$$

For small deflection angles $\varphi \ll 1$, and neglecting second and higher order terms in φ, the optimum lattice functions at the entrance to the bending magnets are with $\eta_0 = \eta_0' = 0$

$$\alpha_0^* \approx \frac{(1-\frac{5}{18}\,\varphi^2)\sqrt{15}}{\sqrt{1-\frac{61}{105}\varphi^2}} \approx \sqrt{15}\,, \tag{8.23a}$$

$$\beta_0^* \approx \frac{\sqrt{12}\,(1-\frac{5}{14}\,\varphi^2)\,\ell_\mathrm{b}}{\sqrt{5}\,\sqrt{1-\frac{61}{105}\,\varphi^2}} \approx \sqrt{\tfrac{12}{5}}\,\ell_\mathrm{b}\,, \tag{8.23b}$$

$$\langle\mathcal{H}\rangle_\mathrm{min} \approx \frac{\varphi^3\,\rho}{4\,\sqrt{15}}\,\sqrt{1-\tfrac{61}{105}\,\varphi^2} \approx \frac{\rho}{4\,\sqrt{15}}\,\varphi^3\,. \tag{8.23c}$$

With this, the minimum obtainable beam emittance in any lattice is from (7.44)

$$\epsilon_\mathrm{dba,min} = C_\mathrm{q}\,\gamma^2\,\frac{\langle\mathcal{H}(s)/\rho^3\rangle}{\langle 1/\rho^2\rangle} \approx C_\mathrm{q}\,\gamma^2\,\frac{\varphi^3}{4\sqrt{15}}\,. \tag{8.24}$$

The results are very simple for small deflection angles but for angles larger than about 33° per bending magnet the error for $\langle\mathcal{H}\rangle_\mathrm{min}$ exceeds 10% at which

point higher order terms must be included. It is interesting to note that the next order correction due to larger bending angles gives a reduction in beam emittance compared to the lowest order approximation. Higher order terms, however, quickly stop and reverse this reduction.

For simplicity, we assumed that the dispersion functions $\eta_0 = 0$ and $\eta_0 = 0$. Numerical methods must be used to find the optimum solutions for finite dispersion functions. In the following we consider only very small values $\eta_0 \ll 1$ and $\eta_0' \ll 1$ to evaluate the impact of the correction for a finite dispersion on the beam emittance. Retaining only linear terms in η_0, η_0', and φ, the expression for $\langle \mathcal{H} \rangle$ becomes

$$\langle \mathcal{H} \rangle_{\eta\,\mathrm{min}} = \langle \mathcal{H} \rangle_{\mathrm{min}} + \tfrac{1}{\sqrt{5}} \left(\tfrac{5}{3}\,\eta_0 + 6\,\eta_0'\,\ell_\mathrm{b} \right) \varphi\,. \tag{8.25}$$

Obviously, the beam emittance can be further reduced for negative values of η_0 and η_0'. This has been exploited in recent storage ring designs. Nonlinear terms, however, quickly cause an increase in the beam emittance again, thus limiting the gain.

In summary, it has been demonstrated that there are certain optimum conditions for lattice functions in bending magnets to minimize the equilibrium beam emittance. No assumption about a particular lattice has been made yet. Another observation is that the beam emittance is proportional to the third power of the magnet deflection angle suggesting to use small deflection angles in order to achieve a small beam emittance. Low emittance storage rings therefore are characterized by many short magnet and lattice periods.

8.2.2 The Double Bend Achromat (dba) Lattice

The dba-lattice is designed such as to make full use of the minimization possibilities for the beam emittance as just discussed and to provide dispersionfree insertion straight sections. Fig. 8.2 shows two renditions of the basic layout for a dba-lattice. Other slightly different modifications have been used but the basic design features are the same. Starting from the middle of an insertion straight section a set of two or more quadrupoles provide the proper focusing of the lattice functions into the bending magnet to achieve the minimum beam emittance. The insertions are kept dispersion free which is the main function of the focusing between the dipole magnets. The section between and including the bending magnets is called an achromat because the dispersion is zero outside of the achromat. The ideal minimum beam emittance in this lattice type is from (8.24)

$$\epsilon_{\mathrm{dba,min}} = \frac{C_\mathrm{q}}{4\sqrt{15}}\,\gamma^2\,\varphi^3\,, \tag{8.26}$$

or in more practical units:

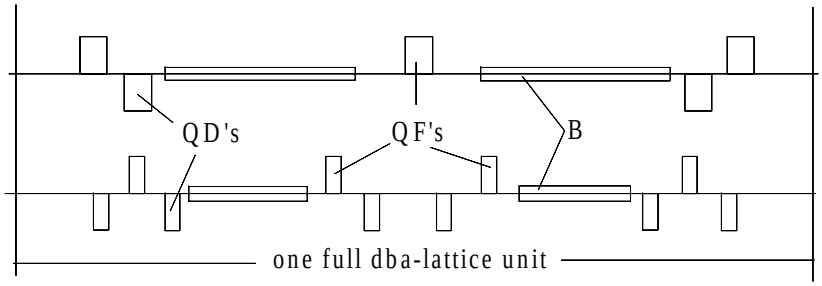

Fig. 8.2. dba Lattice

$$\epsilon_{\mathrm{dba}}\,(\mathrm{rad\,m}) \;=\; 5.036\times 10^{-13}\,E^{\,2}(\mathrm{GeV}^2)\,\varphi^3\,(\mathrm{deg}^3)\,. \tag{8.27}$$

To achieve this minimum beam emittance, we must provide specific values for the lattice functions at the entrance to the bending magnets. Specifically, the initial horizontal betatron function must be strongly convergent reaching a minimum about one third through the bending magnet. At the end of the bending magnet the ideal betatron function, however, becomes quite large. Note, that the vertical lattice functions can be chosen freely since they do not affect the beam emittance as long as there is no vertical dispersion.

In an actual lattice design it appears difficult to achieve sufficient beam stability if the lattice parameters at the entrance to the bending magnets are set to the optimum values. A compromise between optimum lattice parameters and beam stability must be reached resulting in a somewhat increased beam emittance compared to the theoretical minimum. The source of the problem are the large value of the betatron function at the exit of the bending magnet causing strong chromatic aberrations which must be corrected by sextupole magnets. This correction, while essential for beam stability, also generates geometric aberrations and a compromise between correction of chromatic and generating geometric aberrations must be made. The result of this compromise in a well designed storage ring must be a sufficiently large aperture within which the beam can travel for many hours without losses. Outside of this aperture, called the dynamic aperture, particles are lost due to geometric aberrations. Generally, a sufficiently large dynamic aperture cannot be obtained for the ideal solution of minimum beam emittance. On the other hand, the dynamic aperture grows rapidly as the optimum conditions on the lattice functions are relaxed.

An example of an actual dba-lattice is shown in Fig. 8.3 for the 1.3GeV storage ring at the Laboratorio National de Luz Sincrotron (LNLS) in Campinas, Brazil. The central part of the lattice between the bending magnets may consist of one to four quadrupoles and its only function is to focus the dispersion function so that all insertions are dispersion free.

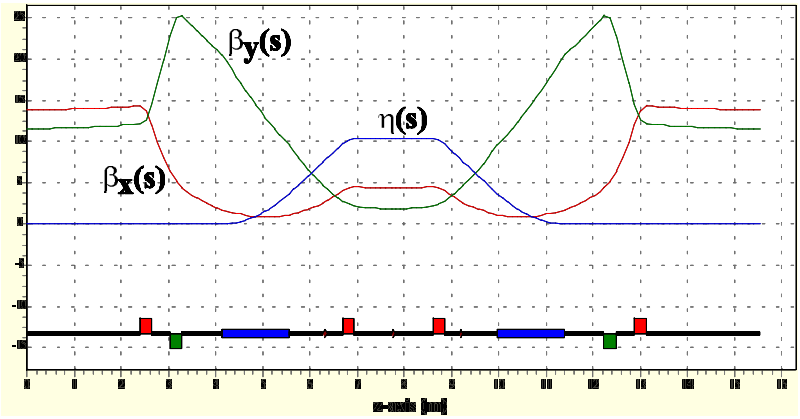

Fig. 8.3. dba Lattice of the Laboratorio National de Luz Sincrotron, LNLS in Campinas, Brazil

The choice of the optimum value for $\alpha_0^* = \sqrt{15}$ causes the betatron function to reach a sharp minimum at about one third into the bending magnet, $s_{\min} = \frac{\alpha_0^*}{\gamma_0^*} = \frac{3}{8}\,\ell_\mathrm{b}$, and to increase from there on to large values causing problems with nonlinear aberrations. We remove the minimum condition on α_0 and express the beam emittance in terms of the minimum emittance

$$\frac{\epsilon_\mathrm{dba}}{\epsilon_\mathrm{dba,min}} = 8\frac{\beta_0}{\beta_0^*} - \sqrt{15}\,\alpha_0 + \frac{1}{2}\left(1+\alpha_0^2\right)\,\frac{\beta_0^*}{\beta_0}\,. \tag{8.28}$$

In Fig. 8.4 this ratio of emittances is shown for different values of α_0 as a function of β_0/β_0^*. It is apparent from Fig. 8.4 that the minimum emittance changes only little even for big variations of α_0 about its optimum value allowing us to choose much more forgiving values for α_0 without significant loss in beam emittance. This weak dependence can be used to lessen the problems caused by nonlinear aberrations.

For arbitrary values of α_0 still an optimum value for β_0 exists. We evaluate the derivative $\partial\langle\,\mathcal{H}\,\rangle\,/\,\partial\beta_0 = 0$ only and get for the optimum betatron function at the entrance to the bending magnet

$$\beta_0 = \ell_\mathrm{b}\,\sqrt{\frac{3}{20}\,(1\,+\,\alpha_0^2)}\,. \tag{8.29}$$

The beam emittance in this case becomes

$$\frac{\epsilon_\mathrm{dba}}{\epsilon_\mathrm{dba,min}} = 4\sqrt{1+\alpha_0^2} - \sqrt{15}\,\alpha_0\,. \tag{8.30}$$

For the condition (8.29) the value of the betatron function $\beta(\ell_\mathrm{b})$ at the end of the bending magnet reaches a minimum for $\alpha_0 = \frac{4\sqrt{15}}{17} \approx 0.911$ at the expense of a loss in beam emittance by a factor of two. In this case

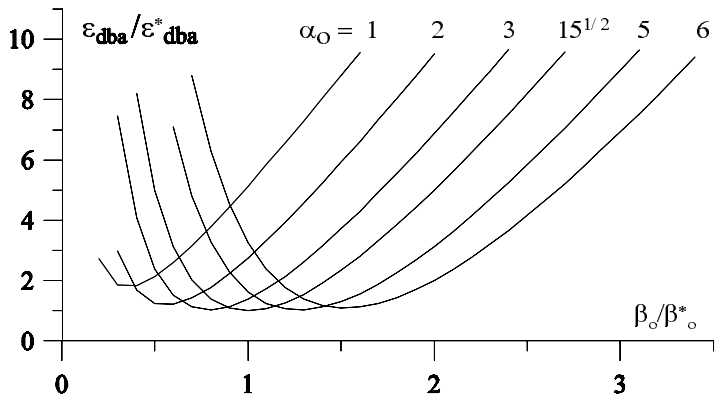

Fig. 8.4. Emittance and betatron functions in a dba-lattice

$$\frac{\alpha_0}{\alpha_0^*} = \frac{4}{17}\,, \tag{8.31}$$

$$\frac{\beta_0}{\beta_0^*} = \frac{23}{68}\,, \tag{8.32}$$

$$\frac{\beta(\ell_\mathrm{b})}{\beta^*(\ell_\mathrm{b})} = \frac{17}{32}\,, \tag{8.33}$$

$$\frac{\epsilon_\mathrm{dba}}{\epsilon_\mathrm{dba,min}} = \frac{32}{17}\,. \tag{8.34}$$

The betatron function at the end of the bending magnet has been reduced by almost a factor of two or by a factor of 17/32 which is a great improvement with respect to instabilities. In a particular storage ring design one would therefore reduce the value of α_0 although by not more than necessary for beam stability.

8.2.3 The Triple Bend Achromat (tba) Lattice

As a variation of the dba lattice a triple bend achromat lattice has become popular in recent synchrotron radiation source designs. In this case, three bending magnets are placed between each pair of insertion straight sections (Fig. 8.5). That results in a reduction of the circumference although at the expense of a similar reduction in available insertion straight sections. This lattice type serves well for smaller facilities and lower energies.

8.2.4 Limiting Effects

Given the usefulness of maximum photon beam brightness for experimenters one might wonder why don't we just design storage rings with a beam emittance below the diffraction limit. The answer has to do with limitations of

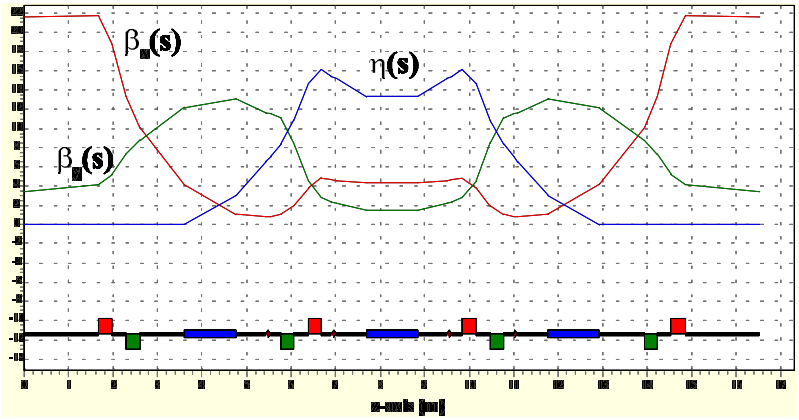

Fig. 8.5. Implementation of a tba-lattice at the National Synchrotron Laboratory, NSRL in Hefei, China

beam stability due to nonlinear betatron oscillations. To reduce the beam emittance, we require stronger and/or more quadrupole focusing. The energy spread in the beam causes a variation of focusing with lower energy particles being focused too much and higher energy particles focused too little as indicated in Fig. 8.6. The total amount of focusing in a storage ring is a measure for these chromatic aberrations, which can cause beam instability if not corrected. For this reason, we must compensate the chromatic aberrations which we call the storage ring chromaticity. Because the chromaticity derives from focusing and we have different focusing in both planes, there are two chromaticities, one for the horizontal and the other for the vertical plane.

Correction of the chromaticities can be accomplished by installing sextupole magnets into the storage ring at locations where the dispersion is not zero. The dispersion causes some degree of segregation between higher and lower energy particles with higher energy particles gathering more outside of the ideal orbit and lower energy particles more on the inside. Sextupoles can be considered as quadrupoles with varying focal strength across the horizontal aperture. A sextupole therefore can add some focusing for higher energy particles being outside of the ideal orbit ($x > 0$) and subtract some focusing for lower energy particles at $x < 0$ (Fig. 8.6). That compensates the under and over focusing these particles experience in the regular quadrupoles. Distributing sextupoles around the ring is therefore the preferred way to compensate the storage ring chromaticity.

Every coin has two sides, however. The sextupole field increases quadratically with x and while we compensate the chromaticities, these same sextupoles generate nonlinear, quadratic perturbations especially for particles with large betatron oscillation amplitudes. These perturbations are known as geometric aberrations generating pillowcase perturbations in the images as is well known from light optics. The art of storage ring design is then to

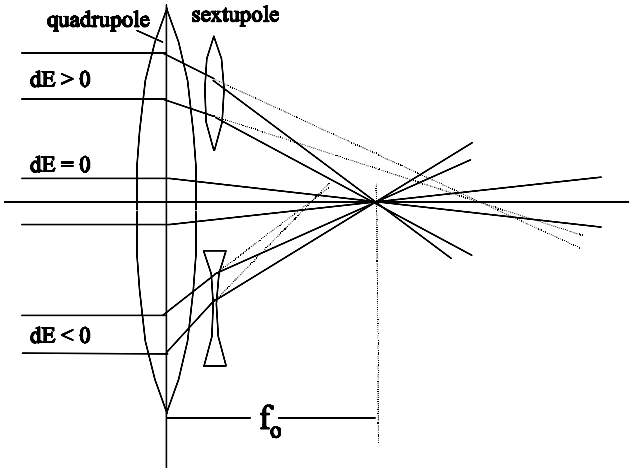

Fig. 8.6. Origin and correction of chromatic effects and chromaticity

correct the chromatic aberrations while keeping the geometric aberrations at a minimum. This can be achieved up to a certain degree by distributing sextupoles along the orbit at properly selected locations. It would therefore be wrong to use just two sextupoles to correct the two chromaticities. The sextupole strengths would be too high generating serious geometric aberrations. However, even with carefully distributing the sextupoles around the ring lattice, we still deal with a nonlinear problem and we cannot expect to get perfect compensation. There will always be a limit on the maximum stable betatron oscillation amplitude in the storage ring. The design objective is to expand the limit for large amplitude betatron oscillations. This limit is called the dynamic aperture in contrast to the physical aperture defined by the vacuum chamber. There is no analytical solution for the dynamic aperture and it is determined by numerical particle tracking programs which follow individual particles for some thousands of turns through all nonlinear fields to probe stability limits.

For a stable beam with a long beam lifetime, we must have a minimum dynamic aperture to accommodate not only the beam proper but also a halo of particles around the beam. This halo is made-up of particles which have been deflected by a small angle during elastic collisions with a residual gas atom. Such collisions occur quite frequently, constantly populating the halo with new particles. By damping, these particles loose betatron oscillation amplitudes and leave slowly the halo again to join the beam proper. While there are only few particles in the halo at any one time, we cannot scrape off this halo by lack of sufficient dynamic aperture. The beam lifetime could be reduced considerable since there is a constant flow of particles into the halo and back to the beam. This flow cannot be interrupted.